

AUTOMATIC STRATEGIES  
TO MODEL TRANSPORTATION FUEL SURROGATES

A DISSERTATION  
SUBMITTED TO THE DEPARTMENT OF MECHANICAL ENGINEERING  
AND THE COMMITTEE ON GRADUATE STUDIES  
OF STANFORD UNIVERSITY  
IN PARTIAL FULFILLMENT OF THE REQUIREMENTS  
FOR THE DEGREE OF  
DOCTOR OF PHILOSOPHY

Perrine Pepiot

June 2008

© Copyright by Perrine Pepiot 2008  
All Rights Reserved

I certify that I have read this dissertation and that, in my opinion, it is fully adequate in scope and quality as a dissertation for the degree of Doctor of Philosophy.

---

(Heinz Pitsch) Principal Adviser

I certify that I have read this dissertation and that, in my opinion, it is fully adequate in scope and quality as a dissertation for the degree of Doctor of Philosophy.

---

(Craig T. Bowman)

I certify that I have read this dissertation and that, in my opinion, it is fully adequate in scope and quality as a dissertation for the degree of Doctor of Philosophy.

---

(Eric S. G. Shaqfeh)

Approved for the University Committee on Graduate Studies.



# Acknowledgements

I would like to thank my advisor Prof. Heinz Pitsch for his constant support and invaluable help, and the members of my reading committee Prof. Craig T. Bowman and Prof. Eric S. G. Shaqfeh for their time and interest in my work.

Funding by the Air Force Office of Scientific Research under the technical supervision of Dr. Julian M. Tishkoff is very gratefully acknowledged.

# Abstract

Cost and efficiency drive the design of combustion devices to rely more and more on numerical simulations. As the methods for computational fluid dynamics (CFD) progress, complex problems such as the simulation of chemically reactive flows in engines become tractable. Of interest for instance, is the capability to accurately predict pollutant emissions from engines, for which the understanding and the accurate modeling of chemistry is tremendously important. The inherent complexity and high non-linearity of the combustion processes, modeled by chemical kinetic reaction mechanisms, and the broad spectrum of fossil fuel compositions render a detailed chemical representation of these fuels unachievable. Instead, simpler surrogate fuels can be formulated that reproduce adequately some desirable properties of real fuels. This work focuses on the design and implementation of automatic methods to generate reduced models for these surrogates.

A component library approach has been developed, in which the reduced model is assembled from small chemical modules specifically designed to simulate a certain chemical process, such as high temperature decomposition of a hydrocarbon molecule or pollutant formation. Each module is built by extracting from detailed kinetic mechanisms available in the literature the minimal amount of information needed to accurately reproduce the chemical process of interest. Several systematic and automated techniques have been developed, which are used throughout this simplification procedure. These methods include the Directed Relation Graph with Error Propagation method, a chemical lumping strategy, and the introduction of quasi-steady state assumptions.

In this study, a component library is created that includes individual constituents from

the major chemical groups present in hydrocarbon fuels, namely linear and branched paraffins, cyclo-paraffins and aromatics. Available detailed mechanisms are validated against a broad experimental database of different configurations such as homogeneous reactors and one-dimensional flames. Modules of various controlled accuracies and sizes are obtained and combined to form surrogate models for gasoline and jet fuel. These reduced mechanisms are shown to reproduce the behavior of real and surrogate fuels satisfactorily.

# Contents

<b>Acknowledgements</b>	<b>v</b>
<b>Abstract</b>	<b>vi</b>
<b>1 Introduction</b>	<b>1</b>
1.1 Motivation and Objectives . . . . .	1
1.2 Accomplishments . . . . .	3
<b>2 Reduction Techniques</b>	<b>4</b>
2.1 General Description . . . . .	4
2.1.1 Detailed Kinetic Modeling of Hydrocarbon Oxidation . . . . .	4
2.1.2 Overview of Chemistry Reduction . . . . .	9
2.2 DRGEP . . . . .	23
2.2.1 Graph-Based Methods . . . . .	23
2.2.2 DRGEP Methodology . . . . .	24
2.2.3 Species Reduction Algorithm . . . . .	32
2.2.4 Reaction Reduction Algorithm . . . . .	37
2.2.5 Practical Examples . . . . .	39
2.3 Chemical Lumping . . . . .	46
2.3.1 Background on Lumping Techniques . . . . .	46
2.3.2 Proposed Modeling Approach . . . . .	50
2.3.3 Technical Description . . . . .	56

2.3.4	Results and Validation . . . . .	58
2.4	Quasi-Steady State Assumptions . . . . .	63
2.4.1	Selection of Suitable QSS Species . . . . .	63
2.4.2	Decoupling QSS Algebraic Equations . . . . .	67
2.5	Multi-Stage Reduction Strategy . . . . .	69
2.5.1	Influence of the Ordering of the Reduction Techniques . . . . .	69
2.5.2	Full Reduction of an Iso-Octane Detailed Mechanism . . . . .	72
2.6	Summary . . . . .	77
<b>3</b>	<b>Transportation Fuel Modeling</b>	<b>79</b>
3.1	From Real Fuels to Surrogate Fuels . . . . .	79
3.2	Selection of Surrogate Components and Composition . . . . .	85
3.3	Component Library Approach . . . . .	92
3.3.1	Motivation and General Description . . . . .	92
3.3.2	Assumptions and Challenges . . . . .	95
<b>4</b>	<b>Applications</b>	<b>98</b>
4.1	Gasoline Surrogate . . . . .	98
4.2	Jet Fuel Surrogate . . . . .	113
4.2.1	Surrogate Formulation . . . . .	113
4.2.2	Validation of Individual Components . . . . .	116
4.2.3	Comparison with Jet Fuel Experimental Data . . . . .	124
<b>5</b>	<b>Conclusion and Perspectives</b>	<b>131</b>
	<b>Bibliography</b>	<b>133</b>

# List of Tables

2.1	Maximum and average errors introduced by the elimination stage of reduction, for initial conditions with pressures between 1 and 40 bar, equivalence ratios between 0.5 and 2, and temperatures between 600 K and 1500 K. . . .	45
2.2	Comparison of global parameters between skeletal and lumped iso-octane mechanisms. . . . .	61
2.3	Ignition delay times of <i>n</i> -heptane. Comparison between two different reduction strategies that differ in the order in which the individual reduction techniques are applied. The “Reference Mechanism” column defines the mechanism against which the reduced schemes are compared. . . . .	71
2.4	Relative computational cost for homogeneous simulations of the intermediate skeletal and final reduced mechanisms produced during the integrated multi-stage reduction of a detailed mechanism for iso-octane. . . . .	75
2.5	Relative computational cost for propagating flame simulations of the intermediate skeletal and final reduced mechanisms produced during the integrated multi-stage reduction of a detailed mechanism for iso-octane. . . . .	76
3.1	Average properties of petroleum-based transportation fuels (data have been compiled from several sources [38, 40, 39, 36]). . . . .	83
3.2	Example of a three component jet fuel surrogate. . . . .	92
4.1	Respective sizes of the mechanisms developed in this work. . . . .	104

4.2	Sizes of the various detailed mechanisms used in the component library approach for the development of a jet fuel surrogate kinetic model. . . . .	114
4.3	Compositions for jet fuel surrogate used in comparison with experimental measurements. . . . .	115

# List of Figures

2.1	Major reaction pathways of alkane oxidation and relevant temperature ranges (reproduced from Curran et al. [25]). . . . .	5
2.2	Example of a $\beta$ -scission reaction. Through a unimolecular reaction that consists in the scission of the C-C bond connected to an atom adjacent to the atom bearing the radical, the heptyl radical decomposes to form a smaller alkyl radical and an unsaturated compound. . . . .	6
2.3	Intermediate chemical molecules and radicals appearing during the oxidation of <i>n</i> -heptane. . . . .	6
2.4	Effect of the number of species and reactions on the computational cost of a homogeneous auto-ignition simulation. . . . .	12
2.5	Profiles of methane and methoxy radical during the ignition of a methane/air mixture. . . . .	20
2.6	Typical species profiles obtained in counter-flow configurations. . . . .	22
2.7	Comparison of the direct interaction coefficients computed using Eq. 2.13 ( $r_{AB}$ , solid line) and using Eq. 2.10, ( $r_{AB}^{\text{DRG}}$ , dashed line), in the case of a species <i>A</i> being consumed exclusively through reactions containing species <i>B</i> . <i>B</i> is not involved in any production reaction for <i>A</i> . Also shown is the normalized source term of the evolution equation for species <i>A</i> , including (dotted, solid line) and neglecting (dotted, dashed line) species <i>B</i> . . . . .	27

2.8	Part of a directed relation graph involving four species. Although the link between species $B$ and $C$ is not the weakest in the graph, removing $C$ should introduce the smallest error in the prediction of the target $A$ . . . . .	31
2.9	Direct interaction coefficients between species involved in Mechanism 2.33. .	37
2.10	Correlation between the error introduced in the fuel prediction and the species coefficients $R_{IC_s}$ obtained with or without error propagation during the isochor, adiabatic auto-ignition of a stoichiometric mixture of iso-octane and air at 13 bar and 1000 K. . . . .	40
2.11	Validation of the error propagation assumption. . . . .	41
2.12	Iso-octane auto-ignition at low temperature. Evolution of the error in ignition delay time (lines with symbols) and final mass fraction of CO (plain lines) when the group-based coefficients and the integrity check algorithm are used (open symbols, dashed lines) or not (filled symbols, solid lines). . . . .	43
2.13	Iso-octane auto-ignition. Evolution of the maximum (symbols) and average (lines) errors on ignition delay time (bold line, filled circles), first stage ignition delay time (thin line, open circles) and fuel profile (dashed line, plus signs) as function of the number of species during the reduction of the iso-octane mechanism. The dash-dotted line represents the error of the final value of the progress variable $Y_C$ . Dotted vertical bars indicate the sizes of the skeletal mechanisms used in the comparison shown in Fig. 2.14 . . . . .	44
2.14	Comparison of ignition times obtained with the detailed iso-octane mechanism and skeletal mechanisms of various sizes. . . . .	45
2.15	Quadratic error $\epsilon_i = \langle (\alpha_i - \langle \alpha_i   \Pi \rangle)^2 \rangle$ in the representation of the relative contributions $\alpha_i$ for iso-octyl radicals in homogeneous reactors for different sets of parameters $\Pi$ . $P_v$ is a progress variable defined as the sum of CO, CO <sub>2</sub> , H <sub>2</sub> O and H <sub>2</sub> . . . . .	53
2.16	Iso-octyl radical distribution as function of the temperature for homogeneous and flame configurations. Darker colors mean higher DRGEP coefficients. Dashed lines correspond to thermodynamic equilibrium ratios. . . . .	55

2.17	Ignition delay times obtained using different explicit methods. Comparison between the skeletal mechanism (solid lines), and lumped mechanisms obtained using fitted ratios (dashed lines), constant ratios (circles), thermodynamic equilibrium (filled squares) and equi-repartition (dash-dotted lines).	59
2.18	Error in ignition delay times. Comparison between the skeletal mechanism (solid lines), and lumped mechanisms obtained using fitted ratios (dashed lines), constant ratios (circles), thermodynamic equilibrium (filled squares) and equi-repartition (dash-dotted lines).	60
2.19	Comparison of iso-octyl isomers and lumped representative species concentrations in selected configurations.	62
2.20	Sensitivities of the most important classes of reactions. Comparison between the skeletal (dark bars) and the lumped (light grey bars) iso-octane mechanisms.	64
2.21	Maximum error in ignition delay time against the steady state parameter $Q$ of each species when set in steady state over the specified range of initial conditions used for the reduction of the iso-octane mechanism.	66
2.22	Example of QSS graph and coupling between species.	68
2.23	Linear system of equations corresponding to the coupled system shown in Fig. 2.22. Black squares represents a non-zero entry in the matrix.	69
2.24	Re-ordered linear system of equations corresponding to the coupled system shown in Fig. 2.22. The system is now block-triangular and will require fewer operations to be explicitly inverted.	69
2.25	Example of $\text{RO}_2$ isomerization reaction.	71
2.26	Lumped group of QOOH isomers. In $\text{C}_7\text{H}_{14}\text{OOHX-Y}$ , X denotes the site of $\text{O}_2$ addition, Y denotes the radical site.	71
2.27	Ignition delay times for $n$ -heptane. Comparison between experiments [21, 86, 49] (symbols), detailed mechanism (solid lines), mechanism lumped at the detailed level (dashed lines), and at the skeletal level (dotted lines with circles).	72

2.28	Very lean iso-octane oxidation in an atmospheric plug-flow reactor at 945 K. Comparison between experiments [18] (symbols), detailed (solid lines), 195 species skeletal (dashed lines), and 57 species reduced mechanism (dotted line with circles). . . . .	73
2.29	Ignition delay times for iso-octane. Comparison between experiments [31, 44, 16] (filled symbols), detailed (solid lines), 195 species skeletal (dashed lines), and 57 species reduced (open circles) mechanisms. Maximum error in ignition delay time is 34.94 %, average error is 10.86 %. Errors in the final concentration of the major products H <sub>2</sub> O and CO <sub>2</sub> do not exceed 0.5 %. . .	74
2.30	Atmospheric laminar burning velocity for iso-octane and air mixtures at 298 K. Comparison between experiments [32, 68, 58] (symbols), 195 species skeletal mechanism (solid line), 134 species lumped (dashed line), and 57 species reduced mechanisms (dash-dotted line). Maximum error with respect to the skeletal mechanism is 5.45 %, average error is 2.81 %. . . . .	75
2.31	Relative computational cost versus the number of variables kept in the kinetic system, for both homogeneous and propagating flame simulations using the intermediate skeletal and final reduced mechanisms produced during the integrated multi-stage reduction of a detailed mechanism for iso-octane. . .	76
2.32	Effect of reduction on key consumption pathways of the alkyl radical $\dot{R}$ and alkyperoxy radical $\dot{Q}OOH$ as function of the temperature in auto-ignition of iso-octane: Comparison between detailed mechanism (solid lines) and reduced mechanism (dashed line). Corresponding ignition delay times are added for reference. . . . .	77
3.1	Typical boiling curves of the three main transportation fuels. . . . .	81
3.2	Correlation between parameters describing the energy content of a fuel and its hydrogen-to-carbon ratio for petroleum-based transportation fuels and a few relevant components present in Fig. 3.3. . . . .	86

3.3	Potential components and their relevance to gasoline, diesel and jet fuels as determined by the surrogate fuels working groups [110, 22, 43] . . . . .	91
3.4	Layout and features of the component library approach. . . . .	94
3.5	Combination of a skeletal mechanism for <i>n</i> -heptane and the GRI3.0 mechanism for methane oxidation: some reactions in the basis chemistry of both mechanisms are not directly compatible. . . . .	97
4.1	Ignition delay times for stoichiometric <i>n</i> -heptane/air and iso-octane/air mixtures. Comparison between experimental data (filled symbols) and numerical results obtained using the detailed LLNL mechanisms (solid lines), the reduced combined high and low temperature mechanism (open circles), and the reduced high temperature mechanism (plus symbols, dashed lines). . . .	105
4.2	Ignition delay times for stoichiometric fuel/air mixtures. Comparison between experimental data for gasoline (symbols) and numerical results for PRF 87 obtained using the detailed LLNL mechanism for PRF [27] (solid lines) and the reduced combined high and low temperature mechanism (open circles). . . . .	106
4.3	Small alkane laminar burning velocities for $T_0 = 298$ K. Comparison between experimental data (symbols) and numerical results obtained using the reduced high temperature mechanism (lines). Figure 4.3(a) illustrates the sensitivity of $S_u^0$ to H <sub>2</sub> O third body efficiency in reaction H69f (= 1: dashed line, = 12: dash-dotted line, = 6: solid line). . . . .	107
4.4	Large alkane laminar burning velocities at $p = 1$ atm and $T_0 = 298$ K. Comparison between experimental data (symbols) and numerical results obtained using the reduced high temperature mechanism (lines). The dashed line in Fig 4.4(a) is obtained using the combined high and low temperature mechanism, and illustrates the negligible role of the low temperature chemistry in flames. . . . .	108

4.5	Laminar burning velocities of <i>n</i> -heptane/air ( $X_{O_2}^{\text{air}} = 0.205$ ) mixtures at high pressures and $T_0 = 373$ K. Comparison between experimental data by Jerzembeck et al. [60] (symbols) and numerical results obtained using the reduced high temperature mechanism (solid lines) . . . . .	109
4.6	Laminar burning velocities of iso-octane/air ( $X_{O_2}^{\text{air}} = 0.205$ ) mixtures at high pressures. Comparison between experimental data at $T_0 = 373$ K by Jerzembeck et al. [60] (circles), numerical results obtained using the reduced high temperature mechanism (solid lines), data from Bradley et al. [11] at $T_0 = 358$ K (filled diamonds), data extrapolated at $p = 10$ and 20 bar and $T_0 = 373$ K from Metghalchi et al. [85] (triangles), and data by Gülder [54] at $T_0 = 373$ K (crosses). . . . .	110
4.7	Laminar burning velocities of PRF/air ( $X_{O_2}^{\text{air}} = 0.205$ ) mixtures at high pressures and $T_0 = 373$ K. Comparison between experimental data by Jerzembeck et al. [60] for PRF 87 (open circles) and gasoline (filled diamonds), and numerical results obtained using the reduced high temperature mechanism for PRF87 (solid lines). . . . .	111
4.8	Pressure dependence of laminar burning velocities. Comparison between experimental data by Jerzembeck et al. [60] (symbols) and numerical results obtained using the reduced high temperature mechanism for PRF87 (lines). Data at 1 bar are obtained with $T_0 = 298$ K (simulation: dashed line), data at higher pressures are obtained with $T_0 = 373$ K (simulation: solid line) . . . . .	111
4.9	Laminar burning velocities of diluted fuel/air mixtures at high pressures and $T_0 = 373$ K. Comparison between experimental data for gasoline by Jerzembeck et al. [60] ( $X_{O_2}^{\text{air}} = 0.17$ : open circles, $X_{O_2}^{\text{air}} = 0.15$ : filled diamonds) and numerical results obtained using the reduced high temperature mechanism for PRF 87 ( $X_{O_2}^{\text{air}} = 0.17$ : solid lines, $X_{O_2}^{\text{air}} = 0.15$ : dashed lines) . . . . .	112

4.10	Validation of benzene component for auto-ignition (Figs. 4.10(a), 4.10(b) and 4.10(c)) and laminar burning velocity (Fig. 4.10(d)). Comparison between experimental data (filled squares, [13, 32]), detailed mechanism (solid line, [9]), single component skeletal mechanism (dashed line) and surrogate skeletal mechanism (dotted line with circles). . . . .	116
4.11	Validation of toluene component for auto-ignition (Figs. 4.11(a), 4.11(b) and 4.11(c)) and laminar burning velocity (Fig. 4.11(d)). Comparison between experimental data (filled squares, [13, 102, 32]), detailed mechanism (solid line, [9]), single component skeletal mechanism (dashed line) and surrogate skeletal mechanism (dotted line with circles). . . . .	117
4.12	Validation of acetylene component for auto-ignition (Figs. 4.12(a), 4.12(b) and 4.12(c)). Comparison between experimental data (filled squares, [56, 118]), detailed mechanism (solid line, [9]), single component skeletal mechanism (dashed line) and surrogate skeletal mechanism (dotted line with circles).	118
4.13	Validation of acetylene component in a counter-flow diffusion flame. Comparison between experimental data (symbols, [101, 100]), detailed mechanism (solid line, [9]), single component skeletal mechanism (dashed line) and surrogate skeletal mechanism (dotted line with circles). Thick lines correspond to filled symbols. . . . .	119
4.14	Validation of <i>n</i> -heptane component for auto-ignition (Figs. 4.14(a), 4.14(b) and 4.14(c)). Comparison between experimental data (filled squares, [21, 49]), detailed mechanism (solid line, [9]), single component skeletal mechanism (dashed line) and surrogate skeletal mechanism (dotted line with circles).	120
4.15	Validation of iso-octane component for auto-ignition (Figs. 4.15(a), 4.15(b) and 4.15(c)). Comparison between experimental data (filled squares, [31, 44]), detailed mechanism (solid line, [9]), single component skeletal mechanism (dashed line) and surrogate skeletal mechanism (dotted line with circles). . . . .	120

4.16	Validation of methyl-cyclohexane component for auto-ignition (Fig. 4.16(a)) and fuel decomposition rate in near-pyrolysis conditions (Fig. 4.16(b)). Comparison between experimental data (symbols, [154, 98, 111]), detailed mechanism (solid line, [111]), single component skeletal mechanism (dashed line) and surrogate skeletal mechanism (dotted line with circles). . . . .	121
4.17	Oxidation of methyl-cyclohexane in a plug flow reactor. Comparison between experimental data (symbols, [154]), detailed mechanism (solid line, [111]), single component skeletal mechanism (dashed line) and surrogate skeletal mechanism (dotted line with circles). Thick lines correspond to filled symbols.	121
4.18	Validation of <i>n</i> -dodecane component for auto-ignition (Figs. 4.18(a), 4.18(b) and 4.18(c)) and laminar burning velocity (Fig. 4.18(d)). Comparison between experimental data (symbols), detailed mechanism (solid line, [151]), single component skeletal mechanism (dashed line) and surrogate skeletal mechanism (dotted line with circles). Experimental data for auto-ignition are for mixtures of <i>n</i> -heptane and air [21, 49], and are shown for reference only. Experimental data for <i>n</i> -dodecane laminar burning velocities are taken from Kumar et al. [66]. . . . .	123
4.19	Auto-ignition of JetA/JP-8. Comparison between experimental data (squares, [142]), and simulation results obtained with pure dodecane (dash-dotted lines), surrogate #1 (dashed lines) and surrogate #2 (solid lines). . . . .	125
4.20	Jet fuel ignition delay times. Comparison between experimental data ([142], symbols), simulations using the jet fuel surrogate mechanism with the original constant U-V model (thin lines) and with modified constant U-V model including a background pressure gradient (thick lines). Solid lines correspond to the 3-component surrogate composition, dashed lines to the 5-component surrogate composition and dash-dotted line to pure <i>n</i> -dodecane. . . . .	127
4.21	Premixed burner-stabilized kerosene flame. Comparison between experimental data (squares, [34]), and simulation results obtained with pure dodecane (dash-dotted lines), surrogate #1 (dashed lines) and surrogate #2 (solid lines).	128



# Chapter 1

## Introduction

### 1.1 Motivation and Objectives

Cost and efficiency drive the design of combustion devices to rely more and more on numerical simulations. As the methods for computational fluid dynamics (CFD) progress, complex problems such as the simulation of chemically reactive flows in engines become tractable. Of interest, for instance, is the capability to accurately predict pollutant emissions from engines, such as particulate matter, carbon monoxide CO, or oxides of nitrogen NO<sub>x</sub>, all contributing at different levels to the greenhouse effect and global warming, smog, ground level ozone, stratospheric ozone depletion, and a myriad of related health problems. To predict and control these emissions, the understanding and the accurate modeling of chemistry is tremendously important. Currently, petroleum-derived fuels make up a very large portion of our energy resources, and their combustion proceeds through complex highly non-linear processes involving hundreds of different chemical compounds. A detailed chemical modeling of real hydrocarbon fuels is therefore excluded, and the fuel representation needs to be simplified drastically to be included in numerical simulations of combustion devices.

A first stage of simplification consists of approximating the fuel by a well-defined mixture of a few components that will match some physical or chemical properties of the real fuel. Using surrogate fuels in lieu of real fuels presents numerous advantages, among which

are the reproducibility of experiments and the possibility of formulating chemical models suitable for CFD. But even with this simplification, deriving chemical models for surrogate fuels that can actually be used in CFD simulations remains a real challenge for many reasons. First, hydrocarbon fuels obtained through crude oil refining processes are only required to satisfy a number of physical or chemical criteria, sometimes loosely formulated. Therefore, their composition can vary significantly among feed-stocks, and at best, only average fuel properties are known. Then comes the question of how to define the surrogate compositions. Guidelines and targets have to be developed to select appropriate individual components and their respective contribution to the surrogate mixture. Chemical modeling for these surrogates is a major challenge, too. State-of-the-art detailed kinetic models can comprise of the order of a thousand different species and several thousand reactions, even for single components. Uncertainties in kinetic data mean that chemical mechanisms from different sources will likely represent similar reaction pathways differently, rendering the merging of detailed mechanisms to create multi-component mechanisms extremely difficult. Additional complications come from the fact that chemistry modeling of single components and fuel surrogate compositions will likely evolve, and previously derived models will become obsolete. Finally, current computational resources and numerical combustion models put severe restriction of the size and amount of detail they can allow for the chemistry. Detailed chemical models must be considerably reduced in size before their implementation in CFD code can be considered.

This work aims to provide some solutions to the issues raised above. It is organized around two major axes, an efficient chemical reduction strategy and a systematic, modular approach to derive surrogate chemical models. The former is crucial to incorporate a certain level of detail in the combustion models of CFD codes, while flexibility and consistency appear as essential to go beyond the current empirical stage of the surrogate fuel approach.

## 1.2 Accomplishments

The most significant contribution of this thesis work concerns the development of systematic and efficient strategies for the reduction of large-scale chemical kinetic reaction mechanisms. Three different techniques have been proposed, that complement each other to provide very high degrees of reduction. These are an elimination method called Directed Relation Graph with Error Propagation [105], a chemical lumping method [104] and the automatic introduction of simplifying assumptions such as quasi-steady states. The next major achievement is the development of a modular framework, called component library approach, to automatically formulate surrogate compositions optimized for a given application and specific hydrocarbon fuel, and generate validated multi-component reduced models for these surrogates. These tools were used in the development of a multi-component mechanism for soot formation [9] and a reduced chemical model for primary reference fuels (PRF) that were used as gasoline surrogate components to validate new high pressure experimental measurements of laminar burning velocities [60]. Finally, the viability of the overall surrogate modeling strategy was assessed through the development of a reduced jet fuel surrogate model.

The thesis is organized in five chapters: the current introduction, a chapter describing the progress made in chemical kinetic mechanism reduction, a thorough discussion of the component library approach that enables the automatic generation of reduced models to represent real fuel combustion, an application chapter that illustrates the use and performance of the developed tools, and a conclusion and perspectives section. Relevant background information and existing literature are included in the beginning of each chapter.

## Chapter 2

# Automatic Reduction of Detailed Chemical Kinetic Mechanisms

### 2.1 General Description

#### 2.1.1 Detailed Kinetic Modeling of Hydrocarbon Oxidation: Characteristics and Validation

Hydrocarbon oxidation is a challenging process to model, as it presents some particular features that distinguish it from other chemical processes. Cool flame and two-stage ignition at low temperature, and negative temperature coefficient (NTC) behavior at medium temperature are the manifestation of complex and highly temperature-dependent competing chemical processes. Alkane oxidation [25, 3] is chosen here as an example to illustrate the complexity of these processes, and an overview of the corresponding main reaction channels is shown in Fig. 2.1. The oxidation process starts with direct decomposition of the fuel through unimolecular reactions, important mostly at high temperatures, and H-abstraction from the fuel molecule. The resulting alkyl radical can either decompose through  $\beta$ -scission to produce smaller olefin and radical species, as described in Fig. 2.2, or undergo a molecular oxygen addition to form  $\text{R}\dot{\text{O}}_2$ . Because of its high activation energy barrier, the  $\beta$ -scission pathway is important only at high temperatures, whereas the barrier-less oxygen addition

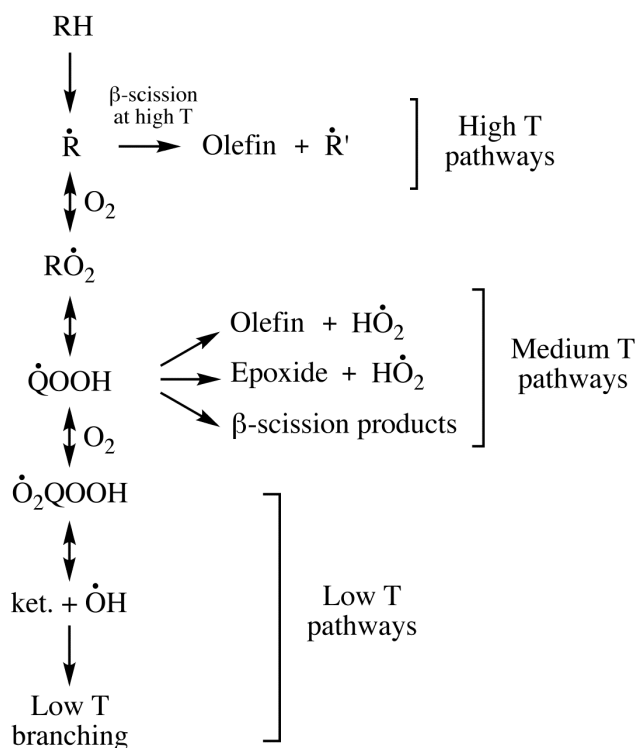


Figure 2.1: Major reaction pathways of alkane oxidation and relevant temperature ranges (reproduced from Curran et al. [25]).

is favored at lower temperatures. The  $\text{RO}_2$  radical isomerizes to form an alkylperoxy radical  $\dot{\text{QOOH}}$ , that either decomposes to  $\beta$ -scission products, cyclic ethers, and unsaturated compounds or undergoes a second oxygen addition, H-atom abstraction and subsequent decomposition to form ketohydroperoxides, and then smaller products. To illustrate these successive reactions, examples of some of the chemical molecules appearing in the oxidation of *n*-heptane are shown in Fig. 2.3. The decomposition of  $\dot{\text{O}}_2\text{QOOH}$ , that produces successively two hydroxyl and a carbonyl radicals, constitutes the chain branching reaction pathway responsible for two-stage ignition at low temperature. As the temperature increases however, the energy barrier of the reactions of decomposition of  $\dot{\text{QOOH}}$  are more easily overcome. These reactions that are chain-propagating and not chain-branching contribute significantly to the consumption of the  $\dot{\text{QOOH}}$  radical and play an important role

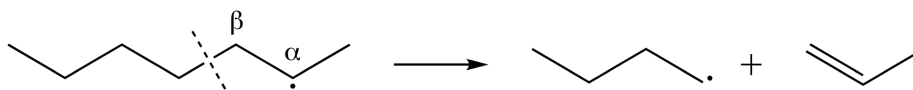


Figure 2.2: Example of a  $\beta$ -scission reaction. Through a unimolecular reaction that consists in the scission of the C-C bond connected to an atom adjacent to the atom bearing the radical, the heptyl radical decomposes to form a smaller alkyl radical and an unsaturated compound.

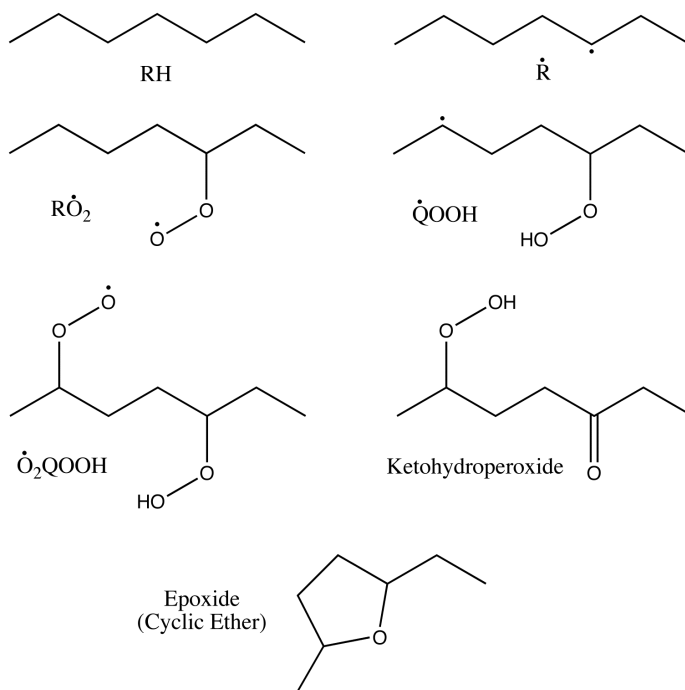


Figure 2.3: Intermediate chemical molecules and radicals appearing during the oxidation of *n*-heptane.

in the NTC behavior of the chemical system at intermediate temperatures. At high temperature,  $\beta$ -scission of the fuel radicals is the major oxidation path and chain branching is mainly due to the  $\dot{\text{H}} + \text{O}_2 = \dot{\text{O}} + \dot{\text{O}}\text{H}$  reaction.

The above description of alkane oxidation shows that high and low temperature combustion proceeds through very different chemical pathways. The low temperature channels involve a large number of oxygenated intermediate species that do not otherwise appear at high temperature and these oxygenated species contribute significantly to the very large size of kinetic mechanisms.

The development and validation of detailed kinetic mechanisms describing hydrocarbon combustion is guided by a number of experimental setups in simple physical configurations that provide information ranging from very detailed data, such as kinetic rates of elementary chemical processes, to more global characteristics such as laminar burning velocities. Since the present work aims to validate reduced mechanisms at the macroscopic level, a restricted set of relevant physical configurations, experimental validation data, and numerical models has been considered and is presented next.

Suppose a mixture of  $n$  chemically reacting species. Using mass conservation principles and the first law of thermodynamics, the general balance equations for the mass fraction of a species  $i$  and for energy can be written as [107, 148]:

$$\rho \frac{\partial Y_i}{\partial t} + \rho \mathbf{v} \cdot \nabla Y_i = -\nabla \cdot \mathbf{j}_i + \omega_i \quad (2.1)$$

and

$$\rho \frac{\partial h}{\partial t} + \rho \mathbf{v} \cdot \nabla h = \frac{\partial p}{\partial t} + \mathbf{v} \cdot \nabla p - \nabla \cdot \mathbf{j}_q + q_R. \quad (2.2)$$

In both equations, the first term corresponds to the local rate of change and the second term represents convection.  $\omega_i$  is the chemical source term,  $\mathbf{j}_i$  and  $\mathbf{j}_q$  are the diffusive and heat fluxes respectively, and  $q_R$  stands for the heat transfer due to radiation. These equations typically have to be implemented by a set of momentum equations. Due to the complexity of detailed kinetic reaction mechanisms, these equations usually require major simplifications to be solved.

The simplest configurations neglect both diffusion and convection terms in Eqs. 2.1 and 2.2. Among the experimental setups designed to approximate the resulting homogeneous conditions, steady reactors such as perfectly stirred reactors (PSR) [29] give access to the steady state composition of spatially homogeneous mixtures of fuel and oxidizer, while unsteady reactors allow to study the time evolution of these mixtures. Shock tubes [51, 49] and rapid compression machines (RCM) [87] can be used to study isochoric auto-ignition of mixtures over a wide range of temperatures and pressures. The measurement of ignition

delay times,  $\tau_{ig}$ , is a typical output of these experiments, and this global parameter which quantifies the reactivity of a mixture is extensively used in the validation of kinetic models. At constant pressure, plug flow reactors (PFR) [144, 63] provide a convenient setting to record the homogeneous evolution of species concentrations for diluted or lean fuel/oxidizer mixtures. Such experimental data that decouple kinetics from fluid mechanics effects, are very valuable to identify the main reaction pathways and intermediate species appearing during combustion.

The next step toward more realistic configurations is to consider one-dimensional laminar flames that include convection and diffusion of species. Two major modes of combustion can be identified in typical combustion devices, whose characteristics can be studied in these simple one-dimensional laminar flames: premixed and diffusion modes. Premixed mixtures can be studied in two slightly different settings: freely propagating or burner-stabilized flames. Propagating flames are generated, for example, in combustion bombs in which the unburned mixture filling a spherical cavity is ignited in the center and then propagates outward [60]. From these experiments is extracted the laminar burning velocity, that quantifies how fast the flame front propagates into the unburned gases. Burner-stabilized premixed flames, on the other hand, allow detailed measurements of temperature or species concentrations. Finally, one-dimensional diffusion flames can be generated in a counter-flow geometry, in which gaseous fuel is injected on one side, oxidizer on the other side, and a stagnation plane is created between the two nozzles. Several numerical methods exist to solve this problem, including the introduction of a similarity variable. In this work, the numerical equations solved are chosen to model as closely as possible the available experimental measurements. The sizes of detailed mechanisms most often prevent them to be used in more complex configurations than those just mentioned.

We have now an illustration of the complexity of the chemical processes occurring during combustion and a list of physical configurations in which these processes can be studied experimentally and numerically. The next section describes the rationale behind kinetic reduction, the challenges involved and a brief overview of the existing reduction techniques.

### 2.1.2 Overview of Chemistry Reduction

The typical size of detailed chemical kinetic reaction mechanisms has been increasing dramatically in the last two decades. This increase results from the combination of a number of factors, including the expansion of the database of elementary reaction rates, the exponential growth of computational power and the extension of kinetic modeling to fuel molecules relevant to engine combustion, that is, longer, heavier hydrocarbons. With single component mechanisms involving hundreds of species and thousands of reactions, chemistry reduction is essential from a fundamental point of view, to understand the combustion processes, and from a practical point of view, to allow these mechanisms to be embedded in computational fluid dynamic (CFD) codes to simulate more complex configurations and to enable the combination of single component mechanisms to model multi-component mixtures. Powerful short mechanisms [109, 91] have been derived manually, often by combining chemical intuition with tools such as sensitivity and flux analysis. However, the growing size of the mechanisms does not allow for such approaches anymore. Thus, developing reliable systematic reduction methods that require minimum user input is a necessity, and major advancements have been made on this topic recently. The issue at hand is to extract from the detailed mechanism the information needed to model with a given accuracy the physical phenomena of interest. Several reviews of the existing reduction methods can be found in the literature [138, 127, 48]. The methods referenced there can be classified on the basis of their action on the detailed chemistry into elimination methods that explicitly remove elementary steps from the detailed scheme, compacting methods that express information using fewer variables, and techniques introducing modeling assumptions, such as separation of time scales. A brief summary of the advantages and shortcomings of these methods is given next, motivating the introduction of the new techniques developed in this work. In the following, the term skeletal mechanism will apply to a mechanism that has been reduced through elimination or compacting methods, while a reduced mechanism contains some modeling assumptions such as separation of time scales.

An important tool on which numerous reduction techniques are based is sensitivity

analysis [131], that investigates the effect of parameter changes on the solution of a system of dynamic equations. In the context of kinetic modeling, the parameters may include the rate coefficients of the reactions, and the physical conditions such as pressure and temperature. In local sensitivity analysis, the sensitivity coefficients are estimated from a Taylor series expansion of the solution in the parameter space:

$$c_i(t, \mathbf{k} + \Delta\mathbf{k}) = c_i(t, \mathbf{k}) + \sum_{j=1}^m \frac{\partial c_i}{\partial k_j} \Delta k_j + \dots \quad (2.3)$$

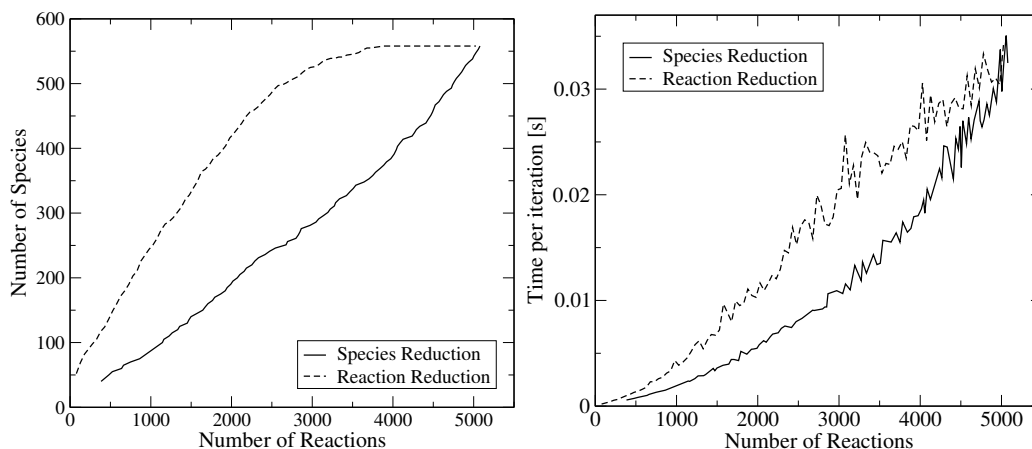
where  $c_i$  is the local concentration of species  $i$  and  $\mathbf{k}$  is a  $m$ -vector of system parameters. The normalized sensitivity coefficients

$$S_{i,j} = \frac{k_j}{c_i} \frac{\partial c_i}{\partial k_j} \quad (2.4)$$

then represent the fractional change of concentration  $c_i$  caused by a fractional change of parameter  $k_j$  [127]. Obtaining these local sensitivity coefficients requires solving additional specific differential equations. Also, sensitivity of global outputs of a chemical systems such as ignition delay times or laminar burning velocities can be obtained through brute-force analysis, where the solution is computed once with the original kinetic mechanism, and the results are compared to a second computation that includes the modified parameter. Several reduction strategies employing sensitivity coefficients have been developed. Turányi [130] classified the species into three categories: important species, whose accurate prediction is the very goal of the investigation, necessary species, for which a realistic representation is needed to get accurate prediction of the important species, and redundant species, that can be neglected without compromising the reduction objectives. He proposed several systematic methods to identify in which category each species present in the mechanism fell, along with a method to identify redundant reactions. These methods were applied to the reduction of mechanism for the low-temperature pyrolysis of propane. Principal component analysis (PCA), first introduced by Vajda et al. [135], allows to extract from the local sensitivity coefficients information pertinent to groups of species and reactions,

and not only single elementary reactions. PCA was successfully used to reduce kinetic systems for hydrogen/air [159] and methane/air [12] combustion. The major limitation of sensitivity-based methods to reduce large-scale kinetic mechanisms is their cost. Indeed, a number of additional differential equations at least equal to the number of parameters included in the analysis (usually the number of elementary reactions) need to be solved, which is impractical for large mechanisms over a wide range of initial conditions. Another issue is that the local sensitivity coefficients are applicable only locally in the parameter space, that is, for small changes of the parameters. Therefore, using them to evaluate the effect of completely removing a species from a mechanism may lead to unexpected behavior if no additional verification step is taken [130].

There are two ways to reduce the size of a detailed mechanism through elimination methods: removing reactions and removing species, and each acts differently to reduce the computational cost. When implicit solvers are used, which is most often the case, the computational cost comes from the evaluation of the Jacobian and its decomposition or inversion. The cost of building the Jacobian scales linearly with the number of reactions, the cost of the inversion scales with the number of species squared. The relative costs of these processes depend on the chemical mechanism that is used. This simple view can be complicated by evaluations of transport coefficients. Therefore, the scaling depends on the particular code and problem. Figure 2.4 shows the benefits of species and reaction reductions to the computational time needed to simulate the homogeneous ignition of an *n*-heptane/air stoichiometric mixture starting with the detailed mechanism of Curran et al. [25]. The order in which the reactions are removed is determined by their importance with respect to the major products and reactants. As shown in Fig. 2.4(a), removing reactions also removes species from the mechanism, but not until far into the reduction process, whereas elimination of species and reactions is more balanced in the species reduction case. For homogeneous cases, Fig. 2.4(b) shows that the intuitive behavior of linear dependence of the computational time with the number of reactions, and quadratic dependence with the number of species is obtained. Clearly, it is specifically important to remove species, as the reduction of the number of differential equations being solved translates into more



(a) Number of species and reactions included in the skeletal mechanisms when gradually reducing the size of a detailed mechanism for  $n$ -heptane. (b) Time per iteration needed to integrate the differential equations describing the homogeneous auto-ignition of a stoichiometric mixture of  $n$ -heptane and air depending on the number of reactions included in the mechanism.

Figure 2.4: Effect of the number of species and reactions on the computational cost of a homogeneous auto-ignition simulation.

time savings. But removing reactions also has two beneficial effects. First, there is a significant impact on computational time through a faster computation of the right-hand side and building of the Jacobian. Second, removing reactions decreases the complexity of the couplings between species, therefore rendering subsequent reduction techniques easier and more efficient.

Some methods are designed specifically to identify negligible reactions, such as the minimization technique introduced first by Frenklach et al. [146], and used to reduce mechanisms for the primary reference fuels  $n$ -heptane and iso-octane by Chaos et al. [17] and Ohashi et al. [95]. In this technique, a reaction has to be kept if it satisfies at least one of the following criteria:

$$|R_{f,i}| > \epsilon_R |R_{\text{ref}}| \quad (2.5)$$

$$|R_{b,i}| > \epsilon_R |R_{\text{ref}}| \quad (2.6)$$

$$|R_{\text{net},i}| > \epsilon_R |R_{\text{net,ref}}| \quad (2.7)$$

$$\left| \dot{Q}_i \right| > \epsilon_Q \dot{Q}_{\text{ref}} \quad (2.8)$$

where  $R_{f,i}$  and  $R_{b,i}$  are the forward and backward rates of reaction  $i$ , respectively,  $R_{\text{net},i} = R_{f,i} - R_{b,i}$  is the net rate of reaction  $i$ ,  $\dot{Q}_i$  is the heat release rate of reaction  $i$ ,  $R_{\text{ref}}$ ,  $R_{\text{net,ref}}$  and  $\dot{Q}_{\text{ref}}$  are some reference reaction and heat release rates, that can be taken, for example, as the maximum values over all reactions at a given time step.  $\epsilon_R$  and  $\epsilon_Q$  are user-defined cut-off parameters. This method is straightforward to implement and fast. However, although the higher the values for  $\epsilon_R$  and  $\epsilon_Q$  are, the smaller the resulting mechanism will be, these values are case-dependent and are not directly related to the accuracy of the skeletal mechanism. To gain control of the error introduced during the reaction reduction, Oluwole et al. [97, 96] developed a method based on Taylor model expansion providing rigorous ranges of validity for a skeletal mechanism, and coupled it with an integer programming optimization method by Bhattacharjee et al. [7]. The validity of the algorithm was demonstrated in the case of a 2D, laminar, steady, premixed flame. Although very good accuracy was observed, rather small computational savings were obtained, with a reduction of the computational time by a factor of 3 maximum.

These results illustrate that it is essential to be able to correctly identify species that do not play an important role during the chemical processes to reduce the computational cost most efficiently. To gain insight into the complex chemical dynamics, Bendtsen et al. [5] introduced a reaction matrix  $\mathbf{P}$  defined at any time  $t$ , whose elements  $P_{ij}$  correspond to the production of species  $j$  from all reactions involving species  $i$  as reactant at that time  $t$ . This matrix quantifies the interactions existing between species and was used to iteratively select important species. The selection process started with a set of major products or reactants. Species that contributed more than a certain percentage to the overall removal or production of any of these important species were included in the set. This procedure was repeated until no more species was included. The results were used to generate pathway plots at several times showing graphically the conversion of fuel into main intermediates, and then main products. Tham et al. [126] used the same reaction matrix to select an initial pool of species: for each of the major products or reactants, an additional set of important species was selected by going through the reaction matrix following the path that connects one species to another one that is most strongly coupled with it. A second step selected

for each of those species a subset of reactions such that a certain percentage of the total formation or destruction of that species was kept in the skeletal mechanism. Any additional species appearing in the kept reactions were then added to the list of important species and this last step was repeated until no more species were added. Reactions involving large heat release were also added to the mechanism. This method was shown to be efficient in selecting important reactions, but tended to retain a large number of species for a given accuracy. Soyhan et al. [125] also used an iterative procedure based on sensitivity analysis and reaction flow analysis to select a reduced set of important and necessary species. In their method, the transfer rate of C, H, and O atoms between the reacting molecules are computed and combined with sensitivity coefficients to iteratively evaluate the relative importance of each species. In addition, species with the smallest life time are set in steady-state. The method was applied to reduce a mechanism for mixtures of *n*-heptane and iso-octane originally containing 74 species and 510 reactions. Because of the extensive use of sensitivity coefficients, this algorithm cannot be applied to much larger mechanisms. Luche et al. [82] combined several techniques: an atomic flux analysis similar to that of Soyhan et al. [125] to select important species, a principal component analysis method to identify negligible reactions, and the introduction of quasi-steady state approximations based on a measure of the life time of each species. Using this combination of methods, a mechanism modeling kerosene oxidation in perfectly stirred reactors (PSR) containing 225 species and 3493 reactions was reduced to 134 species and 1220 reactions, among which 33 to 44 species could be set in steady-state. A shortcoming of the method is that at each stage, cut-off parameters must be specified, that are not a direct measure of the expected accuracy of the resulting small mechanisms. It is also worth noting that most PSR simulations are less demanding in terms of chemistry complexity than auto-ignition simulations, as was demonstrated for instance by Lu and Law [81]. Two other methods utilize the concept of directed relation graphs to identify important species, namely the DRG method by Lu and Law [77] and a technique based on computational singular perturbation method [69] by Valorani et al. [138]. These techniques will be described in more detailed in subsequent sections, along with a proper literature review of compacting methods such as lumping

techniques.

Skeletal mechanisms obtained through elimination and compacting techniques are expected to be of a size suitable for other techniques introducing model assumptions to further accelerate the computation. These techniques are usually based on time-scale analysis, the most intuitive ones being the partial-equilibrium (PE) and quasi-steady state (QSS) assumptions. Partial-equilibrium applies when some reversible reactions occur very fast compared to the controlling time scale of the kinetic system [124]. For such reactions, forward and backward reaction rates are large and nearly balance each other, hence providing algebraic relations between reactants and products involved in the PE reactions. On the other hand, quasi-steady state approximations are obtained by neglecting the substantial derivative of a species in its governing equation. In homogeneous systems, this corresponds to setting the time derivative of the species to zero. Such an approximation is physically justified for species whose consumption rate is very fast compared to its production rate. In such a case, the concentration of the species remains small compared to the others, and so does its time (or substantial) derivative [108]. Again, this assumption provides for each QSS species an algebraic equation that expresses its concentration as function of the other species in the system. As algebraic equations are usually much cheaper to solve than differential equations, applying PE and QSS assumptions may result in substantial computational savings. Several methods have been developed to identify suitable QSS species candidates, most of them rely on an estimate of the lifetime of the species, as short lifetime is often associated with fast consumption [19, 88]. Montgomery et al. [89] proposed an optimal way of selecting QSS species using a genetic algorithm. Lovas et al. [76, 75] exploited the fact that species with long lifetime (therefore not likely candidate for QSS), but low sensitivity coefficients, might still be set in steady state, as the error introduced through the QSS assumption would not influence the rest of the system much. Reduction methods based only on PE and QSS assumptions face challenging numerical problems to reach significant reduction ratios and computational time savings, as the complexity and non-linearity of the resulting system of algebraic equations increases dramatically when the number of steady state species or reactions in partial equilibrium increases [2, 20].

An additional benefit of introducing QSS assumptions is found in the fact that it removes from the system of differential equations some of the fast time scales that are responsible for the stiffness often observed in kinetic systems. A typical combustion system usually exhibits a wide range of chemical time scales, with orders of magnitude difference between the slowest and the fastest time scales. The solution can then be decomposed into fast and slow subspaces, or manifolds. The long-time behavior of such systems is governed by the dynamics on the slow manifold, and any trajectory in the state space is quickly constrained to this slow manifold by the fastest time scales. Because the dimensions of the slow manifolds are generally much less than the original number of variables, complexity is reduced considerably. Several techniques are based on the existence of this invariant, attractive subspace in composition space, including the method of intrinsic low-dimensional manifold (ILDm) by Maas and Pope [83, 120], an iterative method by Fraser [46] and Roussel and Fraser [119], the computational singular perturbation method by Lam and Goussis [69] and Valorani et al. [140]. An alternative formulation of reduction based on time-scale separation is the rate-controlled constrained equilibrium (RCCE) method [62]. In this method, the evolution of the system is guided by the kinetics of the kinetically-controlled species, while the remaining ones are calculated through a minimization of the Gibbs free energy of the system subject to the constraint that the kinetically-controlled species retain their current values, resulting in a system of differential-algebraic equations more efficient to solve than the original full equations.

The reduction techniques outlined above can be complemented by algorithms specifically designed to optimize the computational time required to treat chemistry during the simulation of complex reacting flows. One such method is the *in situ* adaptive tabulation (ISAT) technique developed by Pope [112]. ISAT is a storage/retrieval procedure in which the mixture composition corresponding to a previously accessed composition space region is not computed using the non-linear coupled equations, but obtained from linear approximations of previously stored data. Coupled with an efficient error control, this powerful technique allows to incorporate kinetic mechanisms of a few dozen species in numerical simulations of reactive flows [122]. Also, methods based on time-scale analysis usually involve

the computation of the eigenvalues/eigenvectors of the Jacobian of the system, which is a very expensive operation. Therefore, these methods are most efficient when applied to chemical systems that have been reduced already to a skeletal level through elimination and compacting techniques. It is judicious to be able to combine several different techniques when reducing a large-scale detailed kinetic mechanism, and to apply each of them at the most adequate stage of reduction, to exploit the full potential of the individual techniques. Hence the proposed objectives of this section on mechanism reduction: present a fully integrated reduction scheme, that automates and optimizes as much as possible each reduction step, tailored to the problem at hand, namely the combustion of hydrocarbon fuels, and that produces a reduced mechanism that is chemically consistent and thus, can be used for both quantitative and qualitative applications.

**Pre-Reduction Considerations** Several steps are involved in the development of a skeletal or reduced mechanism that are common to all reduction techniques. The first is the development of a detailed chemical kinetic reaction mechanism, which can in principle be considered as independent of the reduction procedure. However, the validation of the detailed mechanism has a very strong connection to the subsequent reduction procedure. First of all, the validation sets a range of validity and applicability for the detailed mechanism. Any reduced mechanism will also be applicable in the same range of parameters and configurations. Secondly, the validation procedure of the detailed mechanism will reveal a certain error when compared with experiments. This error might influence the choice of the accuracy requirements in the reduction procedure. For example, if the detailed mechanism reproduces the experimental data with very good accuracy, the reduced scheme should retain this desirable property, and the error tolerances in those regions could be more stringent than in regions in which experimental data are not well reproduced by the detailed model.

The range of applicability of the reduced mechanism must be defined next and the corresponding domain in parameter space on which the validation of the reduction procedure will be done, must be adequately sampled. The validity range of the reduced mechanism is either equal to or a subset of that of the detailed mechanism, but it cannot be larger. It is not

clear how to exactly define the range of validity of a mechanism, but one possible standpoint could be to define it just as the set of conditions for which the mechanism has been validated with experimental data. Then also, the reduced mechanism is valid only at the same distinct locations in parameter space, which can easily be sampled. However, the sample size used here for the reduction process should be expanded. We will assume that the detailed chemical mechanism is valid in the vicinity of the data points included in the validation data set, such that it defines a domain. In a similar way, the reduced mechanism will be assumed also to be valid in that domain. A sample of states is chosen in the parameter space such that it can be reasonably assumed that the accuracy of the reduced mechanism between the sample points is represented by the accuracy of the scheme at the sample points. Ideally, this validity should be ensured by the method itself. Oluwole et al. [97, 96], for instance, have developed a reduction technique based on constrained optimization that guarantees the range of validity of the reduced scheme. However, this approach is not applicable directly to the DRGEP method. Techniques that guarantee the validity of the reduced mechanism should be developed in the future. As a further condition, all sample points should be easily computable. This implies that these are restricted to steady and unsteady homogeneous reactor type configurations, such as those representing perfectly stirred reactors, shock tube and flow reactor experiments, or one-dimensional configurations, such as laminar premixed or counter-flow non-premixed flames. This condition could be relaxed, but it would render the reduction procedure more costly. The computed states at the sample points are then characterized by the chosen set of values for the pertinent parameters and additionally are functions of time or space. In the following, the equations given are often written for time as the independent variable, but the time can simply be replaced by a spatial coordinate for one-dimensional steady configurations. In practice, the numerical solutions for all sample points are computed and the solutions are stored for further analysis.

The next step in the reduction procedure is the choice of a set of targets. The targets are some desirable chemical features that the reduced mechanism is expected to reproduce over a pre-defined range of physical conditions. The targets can be as diverse as ignition properties, burning velocities, or levels of soot precursors. The choice of these targets has

to be done carefully, as it will determine in part the possible extent of the reduction. For example, including the prediction of some small intermediate in the targets requires to keep in the reduced mechanism reactions pathways that would have been discarded if only an accurate prediction of the major products and reactants was desired. Finally, the user needs to define the error level that can be tolerated in the reduced mechanism. A procedure to evaluate this error is described next.

**Assessment of the Quality of a Reduced Kinetic Scheme** It may seem easy to intuitively decide if a reduced mechanism is a sufficiently good approximation of the detailed scheme for a given configuration, by comparing species profiles. However, in the context of automatic reduction, a more rigorous and systematic way of evaluating the quality of a reduced mechanism is needed. As Valorani et al. [136] noticed, a meaningful error measure is a crucial, yet often ill-defined quantity for temporally or spatially unbounded problems, which include all homogeneous and propagating flames configurations. For instance, in the case of homogeneous ignition, the relative error on ignition delay time is not a monotonic function of the size of the skeletal mechanism, and a negligible error in ignition timing does not mean that the skeletal mechanism reproduces the dynamics of the detailed mechanism accurately. Moreover, evaluating the error made on intermediate species is non-trivial. To illustrate this problem, Fig. 2.5(a) shows the time dependent profiles of methane and methoxy radical during the ignition of a methane/air mixture, simulated using the GRI 3.0 mechanism [123], for different reduction levels: the detailed mechanism, a 35 species, and an 18 species skeletal mechanisms. The differences between the detailed and 35 species models are barely visible, while the solution for the 18 species mechanism stands far away from the others due to an error in ignition delay time, making it difficult to compare profiles or to evaluate how accurately the production and consumption paths of the methoxy radical are represented in the reduced mechanism.

The most commonly used approach to deal with this issue is to shift the skeletal solution so that some important parameter, such as ignition delay time, matches before computing a normalized integral of the difference between both solutions. For temporally or spatially

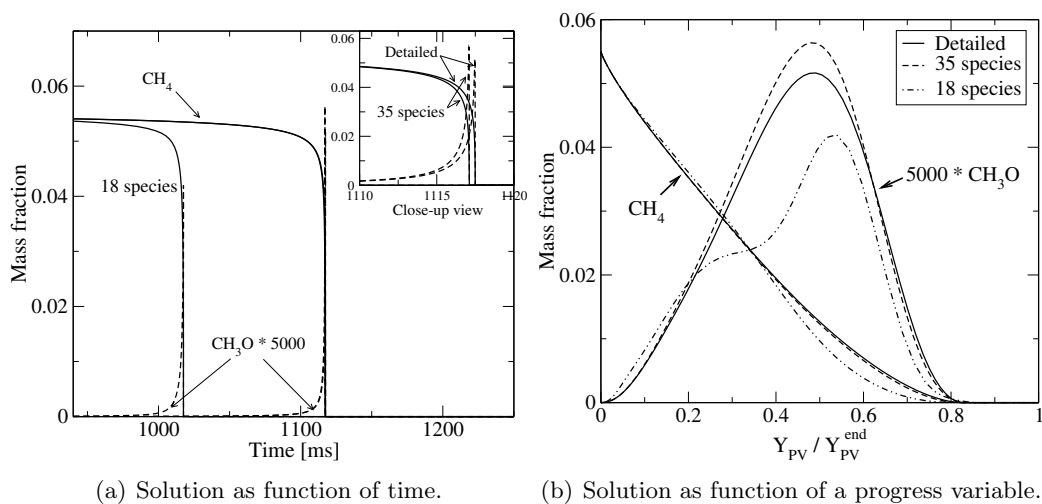


Figure 2.5: Profiles of methane and methoxy radical during the ignition of a methane/air mixture.

unbounded cases, however, this integral depends on the length of the domain, which can vary when the mechanism is reduced.

To remedy these problems, a more efficient approach has been proposed by Valorani et al. [136] that consists in computing this error in phase space. This implies finding a well-behaved mapping variable that uniquely parameterizes both detailed and skeletal solutions. To get meaningful measures, this variable needs to be independent of the quantities whose error is needed, vary smoothly between two fixed values, and be non-constant over the domain of interest. In [136], the fuel is used as independent coordinate. This transformation is adequate as long as the fuel is actively consumed, but is singular elsewhere. As a result, in ignition simulations for example, intermediate species, or even products whose production occurs later in the ignition process, are not well represented in phase space, and a major contribution of the error is missing. Moreover, this mapping cannot be used to evaluate the error made in fuel concentration itself.

In this work, a systematic way of measuring errors for temporally or spatially unbounded cases, such as homogeneous reactors or freely propagating flames, has been designed that adapts the error measure to the characteristics of the variables for which an error has to be computed. Global parameters such as burning velocities or ignition delay times are

compared using relative differences:

$$E_G = \left| \frac{G_{\text{det}} - G_{\text{red}}}{G_{\text{det}}} \right|. \quad (2.9)$$

Species are divided into two distinct subsets. The first subset includes any species whose contribution to the mixture at chemical equilibrium is negligible, namely most of the reactants and intermediate species. For this type of variables, the integrated error with respect to a common progress variable  $Y_C$  is applicable. The progress variable is formed based on the major products obtained in the simulation. When this progress variable is well chosen, it stretches the ignition zone, where most of the changes occur, and is well-defined during the early stages thanks to the early release of some of the combustion products such as  $\text{H}_2\text{O}$ . Figure 2.5(b) shows the same methane and methoxy radical profiles as Fig. 2.5(a), but plotted as function of a progress variable defined as the sum of  $\text{CO}_2$  and  $\text{H}_2\text{O}$  mass fractions. Clearly, the effect of the reduction procedure on the production and consumption pathways of species is more easily quantified when decoupled from the time shift due to changes in ignition delay time. The species used to define the progress variable and the minor products form the second subset.

A major issue of the error estimation based on a change of coordinate is that the error of species used for the progress variable, or even products that behave like the progress variable, cannot be estimated in the same way as the intermediates, as the mapping coordinate cannot be assumed to be independent anymore. A first meaningful quantity to compare between the detailed and reduced mechanisms is the value of the variable at chemical equilibrium. To appraise the differences in the formation of the products, the integrated error between detailed and reduced solution in terms of the spatial or temporal coordinate is used. In an effort to remove any ambiguity however, the reduced solution is rescaled twice: in amplitude, to recover the same chemical equilibrium, and in time, to get the same characteristic time scale  $\tau$ , ignition time or 95% of total fuel consumption for instance. Combined with the relative error in the chemical equilibrium, this error measure provides direct information on the amount of changes introduced in the skeletal model. In this work, any relative error

larger than 100%, indicating a very bad agreement between detailed and reduced solutions, is clipped to 100%. For ignition delay time, for example, 100% error means that either the relative difference between the detailed and reduced solution is larger than 100%, or that no ignition occurs when using the reduced scheme.

For bounded configurations such as counter-flow flames, for which typical species profiles are shown in Fig. 2.6, no distinction between species is necessary, and the error is defined as the integrated differences of the profiles over the domain.

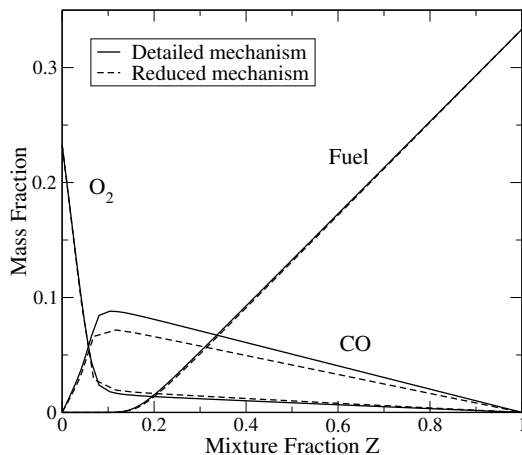


Figure 2.6: Typical species profiles obtained in counter-flow configurations.

In the next section, three reduction techniques will be presented, each of them addressing a different aspect of kinetic reduction. The first one, called Directed Relation Graph with Error Propagation (DRGEP) method, eliminates species and reactions, the second one compacts information through chemical isomer lumping, and the third one introduces quasi-steady state assumptions using a criterion based on lifetime analysis and DRGEP. The different techniques are combined into an integrated approach that is shown to reduce drastically the size of large-scale kinetic mechanisms.

## 2.2 Elimination Stage: the Directed Relation Graph with Error Propagation Method

### 2.2.1 Graph-Based Methods

As outlined above, the reduction procedure starts with the selection of a detailed mechanism, a range of applicability for the reduced scheme, and a set of targets. Then, a reference database can be obtained by computing the solutions for a number of sample cases pertaining to the applicability domain using the detailed mechanism. As the goal of this reduction stage is to identify negligible species and reactions, the database is analyzed to quantify couplings between species. Two existing methods are emphasized next, which are similar in structure but differ in the type of analysis that is done using the detailed or reference solution: the Directed Relation Graph (DRG) method [77, 78], which is based on production rate analysis, and a method that relies on time scale analysis using the CSP theory [138, 139, 137, 136]. The latter uses a decomposition of the solution into fast and slow subspaces. The solution vector is assumed to evolve along the slow subspace or manifold according to the slow time scales and to be constrained on this surface by the faster processes. In both DRG and CSP methods, the results of the analysis can be represented by a directed relation graph whose nodes are the species. In the DRG method, the strength of the directed edge linking a species  $A$  to another species  $B$  is proportional to the contribution of  $B$  in the production rate of  $A$ . In the CSP method on the other hand, the strength of this edge depends on the contribution to the slow and the fast subspaces of the elementary reactions involving both  $A$  and  $B$ , so that the rapid evolution toward the slow manifold and the slow evolution on this manifold are represented correctly.

For a given value of a user-defined parameter representing the desired degree of reduction, the graph is simplified to include only those edges whose strength is larger than this parameter, and all species reachable from the targets through this graph are included in the resulting skeletal mechanism. Variations of this selection process have been designed and tested for the CSP method by Valorani et al. [136]. The procedure is applied for each

sample point and the resulting sets are concatenated into one single global set. Both methods require only a single evaluation of the solution using the detailed mechanism, and once the initial graph has been constructed, the selection process is fast for both approaches.

However, in both the selection procedures of DRG and that of CSP, it is assumed that every species selected to be kept in the mechanism is equally important and that the set of strongly coupled species to which it belongs has to be kept entirely, which may not be necessary. To apply a finer selection, the Directed Relation Graph with Error Propagation (DRGEP) method is presented here, which postulates that the influence of an error introduced by the change of the concentration of a species, or by discarding the species entirely, is damped as it propagates along the graph to reach the targets. As pointed out by Lu and Law [79], the geometric damping we proposed in [103] using the DRG coupling coefficients failed to identify long chemical paths involving fast processes and quasi-steady state intermediate species. A new definition of the coupling coefficient is described here that addresses this issue. Also, the selection procedure is designed to avoid any truncated chemical path in the skeletal mechanism that would introduce mass accumulation in intermediate species, thus creating large discrepancies in the concentration of products. The methodology will be presented mostly in the context of species reduction, but similar procedures are employed to reduce both the number of species and the number of reactions.

### 2.2.2 DRGEP Methodology

The goal of the reduction procedure is to identify, for any number of species in the skeletal mechanism,  $N_{\text{skel}}$ , a group of species of size  $N_{\text{rm}} = N_{\text{det}} - N_{\text{skel}}$  that can be removed with minimal impact on the targets. This is done here by defining appropriate importance coefficients for each species based on the production and consumption rates, which are evaluated using results obtained from the detailed mechanism. The species with the  $N_{\text{rm}}$  lowest importance coefficients are then removed from the mechanism and a skeletal mechanism of size  $N_{\text{skel}}$  is hence created by removing from the detailed mechanism any reaction in which a removed species appears as reactant or as product. In the remaining part of this section,

the definition of the importance coefficients will be described.

**Direct Interaction Coefficients** Direct interaction coefficients are defined as the measure of the coupling between two species that are directly related through an elementary reaction, that is, two species that appear concurrently in the same reaction. In the DRG method [77, 78], the coupling coefficient between two directly related species  $A$  and  $B$ , is estimated as follows:

$$r_{AB}^{\text{DRG}} \equiv \frac{\sum_{i=1, n_R} |\nu_{i,A} \omega_i \delta_B^i|}{\sum_{i=1, n_R} |\nu_{i,A} \omega_i|}, \quad (2.10)$$

where

$$\omega_i = \omega_{f,i} - \omega_{b,i} = k_{f,i} \prod_{j=1}^{n_{E,i}} [S_j]^{\nu'_{i,j}} - k_{b,i} \prod_{j=1}^{n_{P,i}} [S_j]^{\nu''_{i,j}}. \quad (2.11)$$

Here,  $n_R$  is the total number of reversible reactions in the mechanism,  $\omega_{f,i}$ ,  $\omega_{b,i}$  and  $\omega_i$  are the forward, backward, and net reaction rates of the  $i^{\text{th}}$  reaction, respectively.  $\nu'_{i,j}$  and  $\nu''_{i,j}$  are the stoichiometric coefficients of species  $j$  in reaction  $i$  on the reactants and products sides, respectively, and  $\nu_{i,j} = \nu''_{i,j} - \nu'_{i,j}$  is the net stoichiometric coefficient of species  $j$  in reaction  $i$ .  $n_{E,i}$  and  $n_{P,i}$  are the number of educts and products in reaction  $i$ , respectively.  $k_{f,i}$  and  $k_{b,i}$  are the rate coefficients of the forward and backward parts of the  $i^{\text{th}}$  reaction.  $k_{b,i}$  is either computed from the equilibrium constant, which is given by thermodynamic properties, or expressed explicitly in Arrhenius form in the mechanism.  $\delta_B^i$  is defined as:

$$\delta_B^i = \begin{cases} 1 & \text{if the } i^{\text{th}} \text{ reaction involves species } B, \\ 0 & \text{otherwise.} \end{cases} \quad (2.12)$$

If  $A$  and  $B$  are directly related, then both  $r_{AB}$  and  $r_{BA}$  exist, are non-zero, and generally not equal. Whenever a graph is displayed in the following,  $r_{AB}$ , representing the influence of species  $B$  on species  $A$ , will be represented schematically as a directed arrow from  $A$  to  $B$ . The definition given in Eq. 2.10 is an estimate of the error made in the prediction of species  $A$  if species  $B$  is neglected. Production and consumption reactions are considered equally. However, removing a species that contributes exclusively to the consumption of the target

$A$  will not have the same effect as removing a species that contributes the same amount to the production and to the consumption of  $A$ . For the same value of the coefficient  $r_{AB}^{\text{DRG}}$ , the first species will introduce a larger error in the net production rate of  $A$  than the latter that might introduce virtually no error. The reason is that in the latter case, a part of the error from removing the production term is compensated by also removing the associated consumption term. This example stresses the fact that a more accurate quantity to consider is the net contribution of species  $B$  to species  $A$ , rather than production and consumption individually.

Other alternative definitions of the direct interaction coefficient were discussed by Lu and Law [79]. These definitions included normalizing the coefficient by the net production rate of species  $A$ , which becomes singular when  $A$  approaches steady state, or considering backward and forward reactions as distinct, which fails when the rate controlling reaction is dominated by a fast pseudo-equilibrium (PE) reaction.

Here, a new definition of the direct interaction coefficient is introduced, which is motivated by the shortcomings of earlier formulations, namely:

$$r_{AB} \equiv \frac{\left| \sum_{i=1, n_R} \nu_{i,A} \omega_i \delta_B^i \right|}{\max(P_A, C_A)}, \quad (2.13)$$

where

$$P_A = \sum_{i=1, n_R} \max(0, \nu_{i,A} \omega_i), \quad (2.14)$$

$$C_A = \sum_{i=1, n_R} \max(0, -\nu_{i,A} \omega_i). \quad (2.15)$$

This coefficient is well defined and bounded between 0 and 1, which can be easily demonstrated:

$$\begin{aligned} \left| \sum_{i=1, n_R} \nu_{i,A} \omega_i \delta_B^i \right| &= \left| \sum_{i=1, n_R} \max(0, \nu_{i,A} \omega_i \delta_B^i) - \sum_{i=1, n_R} \max(0, -\nu_{i,A} \omega_i \delta_B^i) \right| \\ &= |P_{AB} - C_{AB}|. \end{aligned} \quad (2.16)$$

The terms on the right hand side correspond to the production and consumption of species  $A$  from reactions including species  $B$ . Then, as  $0 \leq P_{AB} \leq P_A$  and  $0 \leq C_{AB} \leq C_A$ , it follows that  $-C_A \leq P_{AB} - C_{AB} \leq P_A$ , which is equivalent to  $|P_{AB} - C_{AB}| \leq \max(P_A, C_A)$ . This inequality simply means that the net contribution of a species  $B$  to a target species  $A$  cannot exceed the total production or consumption, whichever is larger, of species  $A$ .

As an example, let us consider the following extreme case. Suppose that species  $B$  is present in all consumption reactions for target  $A$ , but in none of its production reactions. If  $B$  is removed,  $A$  is produced, but not consumed anymore. The evolution of  $A$  will be significantly impacted only if the total consumption of  $A$  is at least comparable to its production. If  $C_A \geq P_A$ ,  $r_{AB} = 1$ . If  $C_A < P_A$ ,  $r_{AB}$  reduces to  $C_A/P_A$ , which compares directly production and consumption of  $A$ . If consumption is negligible compared with production, then  $B$  can be safely neglected. Figure 2.7 compares the coefficients computed with Eq. 2.10,  $r_{AB}^{\text{DRG}}$  and with Eq. 2.13,  $r_{AB}$ . For this case, both coefficients are similar when

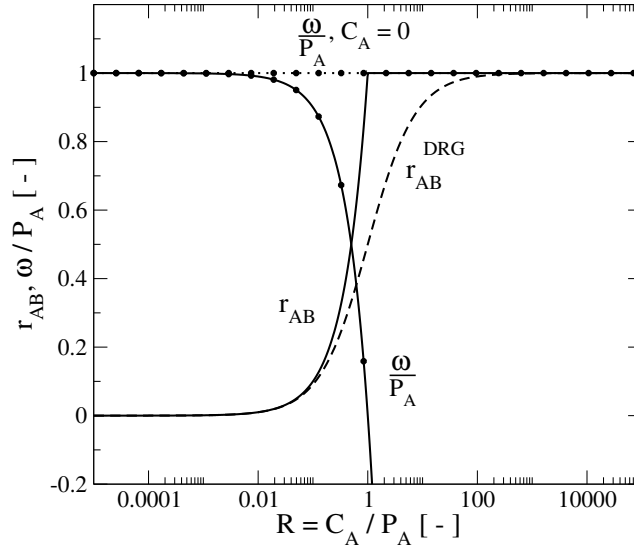


Figure 2.7: Comparison of the direct interaction coefficients computed using Eq. 2.13 ( $r_{AB}$ , solid line) and using Eq. 2.10, ( $r_{AB}^{\text{DRG}}$ , dashed line), in the case of a species  $A$  being consumed exclusively through reactions containing species  $B$ .  $B$  is not involved in any production reaction for  $A$ . Also shown is the normalized source term of the evolution equation for species  $A$ , including (dotted, solid line) and neglecting (dotted, dashed line) species  $B$ .

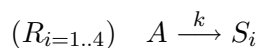
the production of  $A$  is dominant compared to its consumption. However, they start to differ

when  $C_A$  is comparable to  $P_A$ , as  $r_{AB}$  increases faster than  $r_{AB}^{\text{DRG}}$  to reach 1 instead of 1/2 when  $P_A = C_A$ . Also shown in Fig. 2.7 is the comparison between the initial source term normalized by the production rate of  $A$  and the modified source term if  $B$  is removed. When  $P_A = C_A$ , the source term exhibits an error of 100% if  $B$  is removed, as indicated by  $r_{AB} = 1$ . In this case, the conventional DRG coefficient underestimates the contribution of  $B$ .  $r_{AB}$  quantifies how much removing  $B$  disturbs the established balance between production and consumption in the source term of  $A$ .

An interesting feature of this definition is that for a given species  $A$ ,  $r_{AA}$  is not automatically unity. Keeping in mind that the coefficients are computed based on instantaneous reaction rate data, if  $A$  is in quasi-steady state, then the net production, i.e. the source term of the equation for the evolution of  $A$  is small. Setting it to 0 at that time would not introduce a significant error in the evolution of  $A$ . The coefficient  $r_{AA}$  is indeed small and goes to 0 as  $A$  approaches a quasi-steady state. On the other hand, if the consumption rate of  $A$  is small compared to its production rate,  $r_{AA}$  will approach unity.

**Group-Based Direct Interaction Coefficients** Equation 2.13 provides an estimate of the impact that removing one species has on the calculated concentration of the remaining species. However, the goal of the reduction procedure is to remove the largest possible set of species from the mechanism while keeping errors below a given tolerance. Considering one species independently of the group of removed species in which it will eventually belong, might lead to a very inaccurate estimate of the importance of each species. The following example illustrates such a case.

A reactant  $A$  is consumed through four parallel reactions to form the four products  $S_{i=1..4}$ . All the reactions have the same rate coefficient  $k$ :



If species  $S_1$ , for instance, is removed from this mechanism, that is, reaction  $R_1$  is removed,

the relative error introduced in the consumption rate of  $A$  will be:

$$\epsilon_{C_A} = \frac{4k[A] - 3k[A]}{4k[A]} = \frac{1}{4}. \quad (2.17)$$

This is in perfect agreement with the direct interaction coefficient between  $A$  and species  $S_1$  given by Eq.2.13:

$$r_{AS_1} = \frac{\omega_1}{\sum_{j=1}^4 \omega_j} = \frac{1}{4}. \quad (2.18)$$

Suppose that an additional species  $S_2$  is removed. The error on the rate of consumption of  $A$  is now  $\epsilon_{C_A} = 1/2$ . This is not well represented by the direct interaction coefficient  $r_{AS_2} = 1/4$ , because the definition from Eq. 2.13 does not take into account the contribution from the species  $S_1$ , previously removed.

This observation leads to the extension of Eq. 2.13 given a set of removed species:

$$r_{AB,\{S\}} \equiv \frac{\left| \sum_{i=1, n_R} \nu_{i,A} \omega_i \delta_{B,\{S\}}^i \right|}{\max(P_A, C_A)}, \quad (2.19)$$

where  $\{S\}$  is the set of species already removed.  $\delta_{B,\{S\}}^i$  is unity, if the  $i^{\text{th}}$  reaction involves  $B$  or any species in subset  $\{S\}$ , and 0 otherwise. Using this extended definition, the contribution for  $S_2$  is now:

$$r_{S_2} = \frac{\omega_1 + \omega_2}{\sum_{j=1}^4 \omega_j} = \frac{1}{2}, \quad (2.20)$$

which is a better estimate of the effect of removing the group of species  $\{S_1 + S_2\}$  from the mechanism.

**Error Propagation** For each species  $A$  present in a kinetic mechanism, a set of primary dependent species can be defined, consisting of the species that appear explicitly in elementary reactions involving  $A$ . The strength of the interaction between  $A$  and each species of this primary dependent set is defined by the interaction coefficient  $r_{AB}$  defined in Eq. 2.13. If a species  $B$  is not in the primary dependent set of  $A$ , then  $r_{AB} = 0$ .

Before discussing the error propagation method that has been developed in this work, it

is interesting to look in more detail at the selection procedure used in the DRG methodology proposed by Lu and Law [77, 78]. In the DRG method, a directed relation graph between species can be constructed, the strength of each edge from one species  $A$  to another species  $B$  being equal to the coefficient  $r_{AB}$ . Given a parameter  $\epsilon$  representing the desired degree of reduction of the skeletal mechanism, any species reachable from a given set of targets through edges with strength greater than  $\epsilon$  is included in the skeletal set of species. A more convenient way to formulate this DRG selection procedure is to assign directly to each species the value of  $\epsilon$  above which the species is excluded automatically from the skeletal set. This value will be called  $R_{AB}^{\text{DRG}}$ . To do that, a path-dependent coefficient on a certain path  $p$  that links two species  $A$  and  $B$ , that are not necessarily directly related, can be defined as:

$$r_{AB,p}^{\text{DRG}} = \min_{i=1}^{n-1} r_{S_i S_{i+1}}, \quad (2.21)$$

with  $S_1 = A$ ,  $S_n = B$ . For each path that leads from  $A$  to  $B$ , the weakest link is identified so that above this threshold, the connection is severed and species  $B$  cannot be selected through this path. The definition of  $R_{AB}^{\text{DRG}}$  follows quite straightforwardly:

$$R_{AB}^{\text{DRG}} \equiv \max_{\text{all paths } p} r_{AB,p}^{\text{DRG}}. \quad (2.22)$$

Equations 2.21 and 2.22 highlight the fact that in the DRG species selection process, a path between  $A$  and  $B$  is fully characterized by its weakest contribution, regardless of its length. Intuitively however, the farther away from the target a species is, the smaller the effect of changing or removing this species should be. A simple example is depicted in Fig. 2.8. Suppose species  $A$  is the target,  $B$  and  $D$  are directly linked to  $A$  with coefficients 5% and 4% respectively. Another species  $C$  is directly linked to  $B$  with coefficient 5%. The weakest link being  $r_{AD}$ , species  $D$  would be the first species removed from the skeletal set in the DRG methodology, which introduces an estimated 4% error in the production rate of the target  $A$ . Still, removing species  $C$  would cause approximately a 5% error in species  $B$  that has to propagate through the graph to reach  $A$ . Doing so, this error is damped due to the weak contribution of  $B$  to the source term of target  $A$ . First removing  $C$  instead of

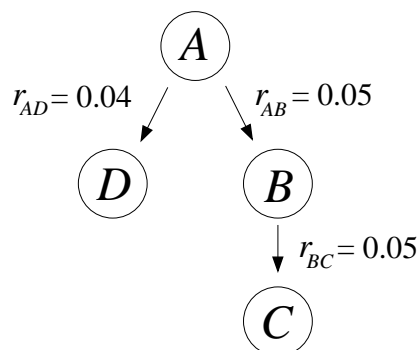


Figure 2.8: Part of a directed relation graph involving four species. Although the link between species  $B$  and  $C$  is not the weakest in the graph, removing  $C$  should introduce the smallest error in the prediction of the target  $A$ .

$D$  presumably introduces a smaller error in  $A$ , as  $C$  is not directly linked to the target. To take into account this error propagation process, a geometric damping has been introduced in the selection procedure. Equation 2.21 becomes:

$$r_{AB,p} = \prod_{i=1}^{n-1} r_{S_i S_{i+1}}, \quad (2.23)$$

while Eq. 2.22 is left unchanged:

$$R_{AB} \equiv \max_{\text{all paths } p} r_{AB,p}. \quad (2.24)$$

If some error is introduced in the prediction of a species  $B$ , the longer the way this error has to propagate to reach the target  $A$ , the smaller its effect will be typically. This technique is target-oriented and is expected to provide a finer selection of the chemical paths necessary for the accurate prediction of the set of targets by keeping species associated with large  $R$  coefficients, and discarding species with small  $R$  coefficients. The validity of this error propagation assumption will be demonstrated in a subsequent section.

### 2.2.3 Species Reduction Algorithm

As mentioned above, a skeletal mechanism is generated for a given set of targets over a given domain of applicability. Once these inputs are well-defined, the mechanism goes through several distinct reduction phases. The first phase is the selection of a subset of important species using the importance coefficient  $R$  presented above. This step, which is the most important one, as it reduces the number of differential equations that have to be solved, is described next.

**Sampling Process** Guidelines to adequately sample the parameter space, for which to perform the reduction process, and for which to test the validity of the reduction, have been described earlier. The numerical solutions are computed for all sample points and the solutions are stored for further analysis. For this, it is important that a sufficient numerical accuracy is ensured, especially for premixed flames and unsteady ignition configurations. The DRGEP analysis can then be performed using the chemical production rates for each discrete point in time or space for a given sample point. However, since numerical accuracy is typically defined for a solution, even if a solution is smooth, the production rates for this solution might still exhibit numerical noise, such as oscillations, especially if non-dissipative numerical schemes are used. Because of this, and to improve the computational time for the reduction algorithm, the production rates used in the reduction procedure are smoothed using a filter kernel that is substantially larger than the grid or time spacing, but much smaller than the total integration time or space. Here we typically use approximately 20 grid points or time intervals of the solution and perform a top-hat filter. More elaborate filter kernels could be employed, but it is important to keep in mind that the filter width is defined not by a given length in time or space, but the number of intervals, since most numerical chemistry solvers use adaptive methods in space and time. In the examples considered below, the filtering has consistently provided similar results as computing the coefficients at each point, but it decreases the computational time significantly.

**Scaling** The DRGEP coefficients  $R_{AB}$  are relative quantities by construction. As a result, they do not differentiate between a solution point where the target has been consumed entirely and a solution point where target production or consumption is at its maximum. In the first case, the coefficients are meaningless, in the latter case, they can be crucial to get an accurate skeletal mechanism. To prevent ill-defined coefficients to override meaningful ones, a scaling factor  $\alpha_T$  is defined that quantifies the contribution at a time  $t$  of each target  $T$  to the overall activity of the system. For this, we write the element balance resulting from chemical reactions as the difference of the contributions from reactions that consume species containing a certain element and reactions that produce species with this element. These pseudo-production and consumption rates can be written as:

$$P_a = \sum_{\text{all species } S} N_{a,S} \max(0, P_S - C_S) \quad (2.25)$$

and

$$C_a = \sum_{\text{all species } S} N_{a,S} \max(0, C_S - P_S) . \quad (2.26)$$

In these equations,  $a$  refers to different elements present in the system (C, H, O and N for conventional hydrocarbon combustion),  $N_{a,S}$  is the number of atoms  $a$  in species  $S$ , and  $P_S$  and  $C_S$  are the production and consumption rates respectively of any species  $S$ . At each time,  $P_a - C_a = 0$ . The scaling coefficient associated with a specific atom  $a$  and target  $T$  is defined as:

$$\alpha_{a,T}(t) = \frac{N_{a,T} |P_T - C_T|}{P_a}, \quad (2.27)$$

and the global normalized scaling coefficient is:

$$\alpha_T(t) = \max_{\text{all atoms } a} \frac{\alpha_{a,T}(t)}{\max_t \alpha_{a,T}(t)}. \quad (2.28)$$

This scaling coefficient that evaluates the relative contribution of a target to the global atom fluxes, is unity when the target contributes to its maximum to the exchange of atoms between species, and zero when, for instance, the species mass fraction is constant, at

chemical equilibrium, or when the target has been consumed entirely. To give an example, let us consider the rich homogeneous ignition of CO in air: as sole provider of carbon atoms, the fuel will have a scaling coefficient equal to unity, as long as it is consumed actively. When oxygen has disappeared, the fuel reaches a plateau, and its scaling coefficient rapidly decreases to zero. Such a scaling naturally overcomes problems of loss of significant digits, which happens at chemical equilibrium, as pointed by Lu and Law [79], and smoothes out the artificially large coefficients often encountered at early times, when some species are marginally produced through negligible paths.

Finally, the importance of a species  $S$  given a set of targets  $\{\mathcal{T}\}$  and a set of sample points  $\{\mathcal{D}\}$  is quantified by a single parameter defined as:

$$\bar{R}_S = \max_{\substack{T \in \{\mathcal{T}\} \\ k \in \{\mathcal{D}\}}} (\alpha_{T,k} R_{TS,k}). \quad (2.29)$$

The maximum norm has been selected for its universality over different physical conditions and targets. Species associated with the smallest coefficients  $\bar{R}_S$  are removed first and these coefficients are periodically re-evaluated during the reduction procedure to take advantage of the group-based direct interaction coefficients.

**Integrity Check** Every intermediate species in a skeletal mechanism must have at least one production and one consumption paths. During the DRGEP reduction process, some species might fail this requirement, especially for high reduction ratios in the context of complex, highly non-linear kinetic schemes. Two basic observations can be made. In a closed system, any intermediate species that is not produced anymore remains at its initial zero concentration and can be removed from the mechanism. On the other hand, if a species is produced, but not consumed anymore, it creates a sink of mass that may impact greatly the final concentration of the products. This complex non-linear behavior cannot be detected by a method based solely on the analysis of the detailed production rates. That is why a simple algorithm has been designed to prevent these situations from occurring. A list of species, sorted by order of importance for the targets, is first obtained by computing

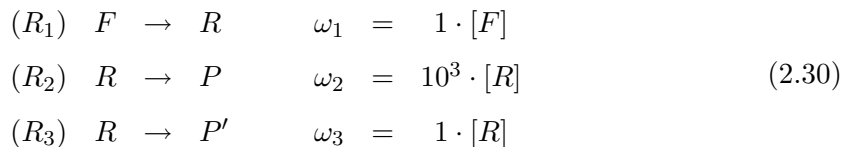
the DRGEP coefficients using Eq. 2.13. Then, this list is slightly modified so that, for any value of the cutoff parameter, the group of species kept in the skeletal mechanism forms a consistent chemical scheme with no truncated paths. The re-ordering proceeds as follows:

Species are moved to the set of removed species one after the other, starting from the less important ones. For each candidate species  $A$  to be removed, the integrated production and consumption rates of the species  $S_i$  directly linked to  $A$  are re-evaluated using the detailed data, by setting the contribution from species  $A$  to zero. If the integrated production rate of  $S_i$  is less than a percent of its detailed value, that is,  $S_i$  is virtually not produced anymore,  $S_i$  is linked to species  $A$ , and the two-species group is assigned the DRGEP coefficient of species  $A$ . If any one of the species in the group is removed, the rest of the group is removed as well. A similar grouping procedure is adopted when  $S_i$  is not consumed anymore, except that the  $\{S_i, A\}$  group is assigned the larger DRGEP coefficient  $R_{S_i}$ , that is, the group is moved up in the ordered list.

During the re-ordering sweep, DRGEP coefficients are recomputed regularly using the group-based definition given in Eq. 2.19. All the computations during this stage are based solely on the detailed data, no reduced solution is computed. The list of individual and indivisible groups of species obtained at the end of the integrity check is used to evaluate skeletal mechanisms of various sizes to get the shortest mechanism satisfying the accuracy requirements.

**Theoretical Examples** The applicability of the directed relation graph method has been extensively reviewed by Lu and Law [79]. A number of generic cases including quasi-steady state, partial equilibrium, and dormant mode problems were analyzed in details using DRG. The present error propagation method leads to similar, equally good conclusions for these cases, which can be demonstrated very easily. This will be shown here in two examples. The first one considers an artificial reaction mechanism, in which an intermediate species

is in quasi-steady state:



The rates of the reactions were evaluated in [79] as  $\omega_2 \approx \omega_1$  and  $\omega_3 = \omega_2/10^3$ . The direct interaction coefficients defined by Eq. 2.13 are:

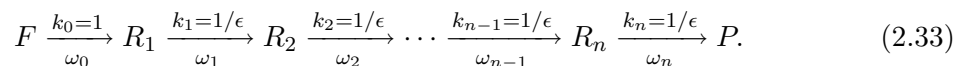
$$\begin{aligned}
 r_{FR} &= \frac{\omega_1}{\max(P_F, C_F)} = \frac{\omega_1}{\omega_1} = 1, & r_{RF} &= \frac{\omega_1}{\max(P_R, C_R)} = \frac{\omega_1}{\omega_1} = 1 \\
 r_{RP} &= \frac{\omega_2}{\max(P_R, C_R)} = \frac{\omega_2}{\omega_1} = 1, & r_{PR} &= \frac{\omega_2}{\max(P_P, C_P)} = \frac{\omega_2}{\omega_2} = 1 \\
 r_{RP'} &= \frac{\omega_3}{\max(P_R, C_R)} = \frac{\omega_3}{\omega_1} \approx 10^{-3}, & r_{P'R} &= \frac{\omega_3}{\max(P_{P'}, C_{P'})} = \frac{\omega_3}{\omega_3} = 1
 \end{aligned} \tag{2.31}$$

If species  $F$  is the target, the corresponding DRGEP coefficients are obtained straightforwardly:

$$\begin{aligned}
 R_{FR} &= r_{FR} = 1, \\
 R_{FP} &= r_{FR} \cdot r_{RP} = 1, \\
 R_{FP'} &= r_{FR} \cdot r_{RP'} \approx 10^{-3}.
 \end{aligned} \tag{2.32}$$

The right conclusion can be derived from these coefficients, that is, species  $P'$  can be safely removed, it will not introduce a large error in the prediction of  $F$ . But both  $R$  and  $P$  should be kept in the mechanism.

Another case of interest is the rapid conversion of a reactant into a product through a succession of quasi-steady state intermediates. This case was handled correctly by the DRG method, but not by the error propagation method presented in [103]. Let us consider a path from a fuel  $F$  to a product  $P$  that goes through several intermediate species  $R_1$  to  $R_n$ , as depicted in the following mechanism:



The rate-limiting step is the first reaction, and the remaining reactions are fast, so that all species  $R_{i,i=1,n}$  can be considered in quasi-steady state. Then, the rates of all reactions appearing in the mechanism 2.33 are approximatively equal:

$$\omega_0 \approx \omega_1 \approx \dots \approx \omega_n \approx \omega. \quad (2.34)$$

As a species  $R_i$  is produced only by  $R_{i-1}$ , and is consumed to produce one single species  $R_{i+1}$ ,  $\max(\omega_i, \omega_{i-1}) = \omega$ , and all direct interaction coefficients  $r_{R_i R_{i\pm 1}}$  are unity. Figure 2.9 shows the corresponding relation graph. From this figure, the effect of the fuel  $F$  on the

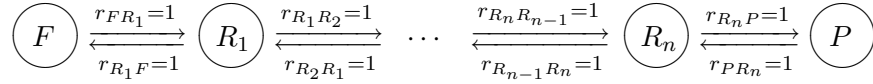


Figure 2.9: Direct interaction coefficients between species involved in Mechanism 2.33.

product  $P$  described by the DRGEP coefficient  $R_{PF}$  is

$$R_{PF} = r_{PR_n} \cdot r_{R_nR_{n-1}} \cdot \dots \cdot r_{R_2R_1} \cdot r_{R_1F} \approx 1. \quad (2.35)$$

The importance of  $F$  to  $P$ , as the only source of production for  $P$  is recovered thanks to the more appropriate definition of the direct interaction coefficients. Thus, in this example, if  $P$  is the target, no species can be removed, as removing the fuel or any intermediate species would introduce 100% error in the prediction of the product  $P$ .

## 2.2.4 Reaction Reduction Algorithm

Removing species decreases the number of differential equations that have to be solved, and, since the computational time scales as the square of the number of species, this is the most efficient way to speed up numerical simulations. However, the computational time also depends on the number of reactions, which can be significant. In addition, as mentioned before, the elimination of elementary reactions renders further reduction more efficient. The first step of reduction provides the set of species that have to be kept in the

system to achieve the desired accuracy. Then, the resulting mechanism is made up of all reactions among those species. However, not all reactions are necessary for an accurate representation of the original dynamic system. Specifically, the importance of a reaction depends on the contribution to the involved species, and the importance of those species for the targets. This information is used to identify reactions that have minimal impact on the targets, and thus can be removed safely. For this stage, backward and forward reactions are considered as being independent from one another.

A strategy similar to the one used for species selection is adopted here. The direct interaction coefficient between a species  $A$  and a reaction  $r_i$  is written as:

$$r_{Ar_i} \equiv \frac{|\nu_{i,A}\omega_i|}{\max(P_A, C_A)}. \quad (2.36)$$

Then, the impact of removing reaction  $r_i$  on a given target  $T$  is evaluated through error propagation using the DRGEP coefficients for the species, as follows:

$$R_{Tr_i} \equiv \max_{S \in \{\mathcal{S}\}} (R_{TS} r_{Sr_i}), \quad (2.37)$$

where  $\{\mathcal{S}\}$  refers here to the set of species present in the mechanism. The reactions are sorted by increasing order of importance using the single parameter:

$$\bar{R}_{r_i} = \max_{\substack{T \in \{\mathcal{T}\} \\ k \in \{\mathcal{D}\}}} (\alpha_{T,k} R_{Tr_i,k}). \quad (2.38)$$

Equations 2.36 and 2.37 are extended easily to take into account the set of already discarded reactions, as is done for species in Eq. 2.19. The coefficients  $\bar{R}_{r_i}$  are recomputed regularly to take advantage of these group-based coefficients. An integrity check is performed during the reaction reduction to ensure that every species remaining in the mechanism retains at least one major production and one major consumption path for the physical conditions considered in the reduction. The species are represented more or less accurately depending on their own global importance for the targets. An additional limited number of species

might be removed during the reaction reduction when high reduction ratios are reached.

### 2.2.5 Practical Examples

**Validation of the Error Propagation Assumption** Before applying the above reduction methodology, it is necessary to appraise the validity of the error propagation assumption in the DRGEP method. This assumption states that the effect on a target introduced by the removal of a species can be approximated through geometric damping along the directed relation graph, from the target to the removed species. This can be written as:

$$E_T \propto R_{TS} \quad (2.39)$$

where  $E_T$  is the error between the prediction of the target using the detailed and skeletal mechanisms, and  $R_{TS}$  measures the importance of a species  $S$  with respect to the target, as defined by Eqs. 2.13 and 2.24. This proportionality can be verified *a posteriori* using a practical case. The coefficients  $R_{TS}$  were computed for the adiabatic, isochoric auto-ignition of a stoichiometric mixture of iso-octane and air at 13 bar and 1000 K, with iso-octane as the only target. The mechanism used for the simulation was the iso-octane oxidation scheme by Curran et al. [26]. The error introduced in the prediction of iso-octane by removing each species individually was computed using the integrated error measure introduced in section 2.1.2. The progress variable  $Y_C$  for this case is the sum of CO, CO<sub>2</sub>, and H<sub>2</sub>O mass fractions.

Figure 2.10 shows the correlation between this error and the computed coefficients obtained using error propagation. For comparison, the correlation between the error and the coefficients obtained without error propagation is also shown in the same figure. These coefficients are obtained using the definition for  $r_{AB}$  from Eq. 2.13 and the DRG selection method used by Lu and Law (Eq. 2.22). The solid line represents the optimal case, that is, a hypothetical parameter whose value would be exactly equal to the error introduced if the species is removed. Several comments can be made at that point. First, a very small error of the order of  $10^{-7}$  is introduced systematically due to numerics and grid resolution.

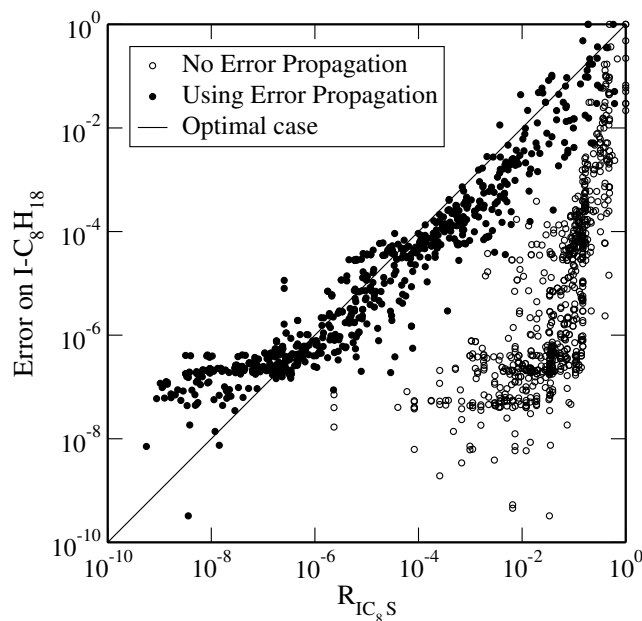
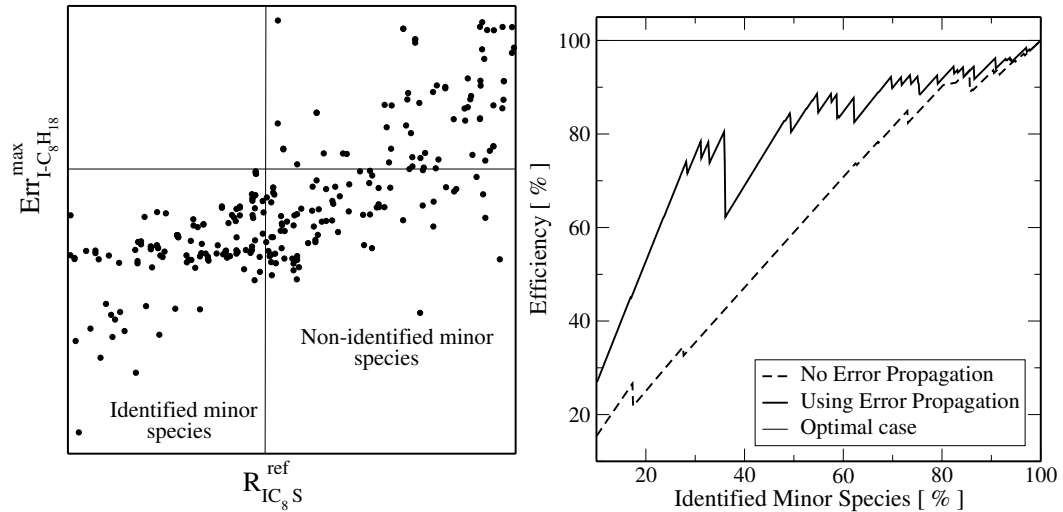


Figure 2.10: Correlation between the error introduced in the fuel prediction and the species coefficients  $R_{IC_8S}$  obtained with or without error propagation during the isochor, adiabatic auto-ignition of a stoichiometric mixture of iso-octane and air at 13 bar and 1000 K.

This accounts for the asymptote observed in Fig. 2.10 for relatively small  $R$  coefficients. The coefficients obtained using error propagation are smaller than those obtained without propagation, as a geometric damping is used to evaluate them. The errors introduced by removing individual species correlate extremely well with the error propagation coefficients, with a small scatter in the data, whereas the correlation is not as obvious when using the DRG selection procedure. Figure 2.10 also shows that the error propagation method leads to an order unity coefficient in Eq. 2.39, while the original DRG method does not. This means that the importance coefficients evaluated by DRGEP are a direct measure for the error in the resulting mechanism. However, a more detailed analysis is needed here to appraise the performances of both methods.

For a given value  $R_{IC_8S}^{\text{ref}}$  of the selection parameter, the species can be divided into three groups, which will be defined using the example shown in Fig 2.11. The first group contains the species whose coefficients are smaller than  $R_{IC_8S}^{\text{ref}}$ . These species are labeled “identified minor” species.  $\text{Err}_{I-C_8H_{18}}^{\text{max}}$  is defined as the maximum error introduced by one of the

identified minor species. It is important to note that  $\text{Err}_{\text{I-C}_8\text{H}_{18}}^{\max}$  is different from the error obtained when removing the whole minor species group, as the system is highly non-linear. This issue is dealt with using the group-based coefficient technique that will be validated in the next section. The remaining species, for which  $R > R_{\text{IC}_8\text{S}}^{\text{ref}}$ , are divided into two further groups: the species that introduce an error larger than  $\text{Err}_{\text{I-C}_8\text{H}_{18}}^{\max}$ , and those introducing a smaller error. The latter species are labeled “non-identified minor” species, as they could have been included in the minor species set without increasing the maximum individual error  $\text{Err}_{\text{I-C}_8\text{H}_{18}}^{\max}$ . These subdivisions are detailed in Fig. 2.11(a), that is a close-up view of Fig. 2.10. A good selection parameter limits the number of non-identified minor species as



(a) Close-up view of Fig. 2.10.

(b) Selection of minor species. Comparison between DRG selection and error propagation selection.

Figure 2.11: Validation of the error propagation assumption.

much as possible, to ensure that for a given value of the cut-off parameter, the maximum number of species is selected introducing the smallest possible error. This efficiency can be quantified by the ratio between the number of identified minor species and the number of species that should have been identified as minor, that is, the total number of identified and non-identified minor species. Using Fig. 2.11(a) as an example, this means comparing the number of species contained in the lower left quadrant to the number of species in the

lower half of the graph, for an increasing value of the cut-off parameter  $R_{IC_8 S}$ , that is, for an increasing number of species identified as minor.

The results are shown in Fig. 2.11(b). The optimal case corresponds to a constant value of 100%, as all the species that can be classified as minor are identified. Also, an error propagation based selection parameter clearly is more efficient than the standard DRG selection. This result can be interpreted in two ways. The first one is that for a given number of species selected as minor, the maximum individual error over those species is larger when using DRG compared to the error propagation method. Or conversely, for a given maximum error, more species introducing an error smaller than this maximum are identified using error propagation than using DRG.

This analysis shows that the error propagation assumption can be considered as valid and appropriate, and represents a significant improvement over the species selection presented in earlier work [78, 79].

**Efficiency of Group-Based Coefficients and Integrity Check** The efficiency of the group-based coefficients and the integrity check is illustrated next. The detailed mechanism for iso-octane oxidation from Curran et al. [26] is reduced for a single initial physical condition, the homogeneous, adiabatic auto-ignition at constant volume of a stoichiometric mixture of iso-octane and air at an initial pressure of 13 bar and an initial temperature of 625 K. The targets are fuel, CO, CO<sub>2</sub>, and temperature. Figure 2.12 shows the evolution of the error in ignition delay time and in the final mass fraction of carbon monoxide as function of the number of species kept in the skeletal mechanism. When the definition of Eq. 2.13 is used, the error in the final mass fraction of CO in the system quickly reaches a few percents and keeps increasing. This is due to truncated chemical paths appearing as species are removed. Carbon mass accumulates in large quantities in intermediate species, which shifts considerably the chemical equilibrium of the system. When group-based coefficients and integrity check are included in the reduction process (the coefficients are recomputed once every 50 species removed), the error in the final mass fraction of CO remains extremely small and the error in ignition delay time is improved considerably.

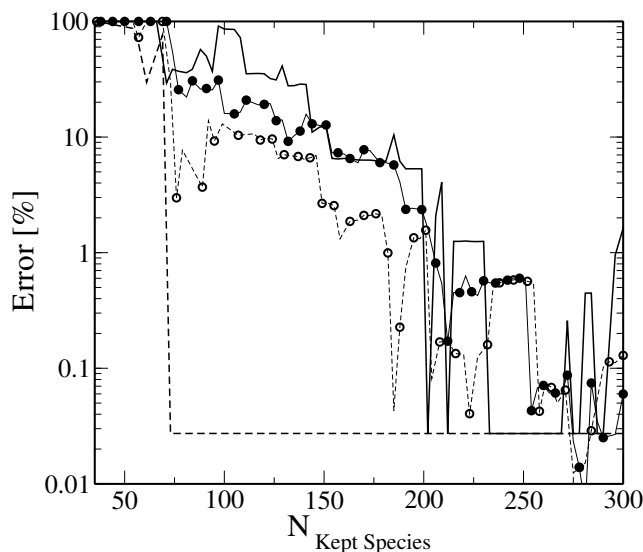


Figure 2.12: Iso-octane auto-ignition at low temperature. Evolution of the error in ignition delay time (lines with symbols) and final mass fraction of CO (plain lines) when the group-based coefficients and the integrity check algorithm are used (open symbols, dashed lines) or not (filled symbols, solid lines).

**Iso-octane Auto-ignition** To demonstrate the full capabilities of the DRGEP method, the same very large mechanism for iso-octane oxidation [26] is reduced for adiabatic auto-ignition at constant volume in a large range of initial conditions relevant for engine-related applications (ignition delay times less than one second). The initial conditions include equivalence ratios between 0.5 and 2, pressures between 1 bar and 40 bar, and temperatures between 600 K and 1500 K. The detailed mechanism comprises 850 species and 7212 reactions. Targets for the reduction are fuel  $i\text{-C}_8\text{H}_{18}$ , major products CO and  $\text{CO}_2$ , and temperature. The DRGEP coefficients for temperature are evaluated using heat release data. The error in ignition delay time, first-stage ignition delay time, and the maximum error in the final value of the major products appearing in the definition of the progress variable  $Y_C$  are shown as function of the number of species kept in the skeletal mechanism in Figure 2.13. The progress variable is case-dependent and includes the major products of the simulation, so that it contains at least 90% of the carbon, oxygen and hydrogen mass present in the system. Usually,  $\text{CO}_2$  and  $\text{H}_2\text{O}$  are used, with CO and  $\text{H}_2$  added when

needed.

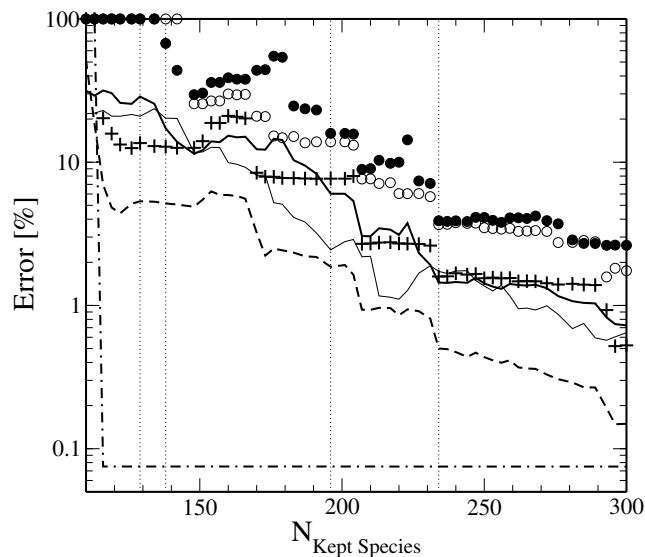


Figure 2.13: Iso-octane auto-ignition. Evolution of the maximum (symbols) and average (lines) errors on ignition delay time (bold line, filled circles), first stage ignition delay time (thin line, open circles) and fuel profile (dashed line, plus signs) as function of the number of species during the reduction of the iso-octane mechanism. The dash-dotted line represents the error of the final value of the progress variable  $Y_C$ . Dotted vertical bars indicate the sizes of the skeletal mechanisms used in the comparison shown in Fig. 2.14

Overall, errors are increasing monotonically as the number of species is reduced. Error on the progress variables is everywhere small enough to neglect any effect on the change of coordinates for the detailed and skeletal mechanisms. Figure 2.14 shows a comparison of the ignition delay time over a wide range of temperature and pressure for stoichiometric mixtures for several sizes of the skeletal mechanism, namely 234, 196, 138, and 129 species. For clarity, vertical bars have been added at the corresponding abscissas in Fig. 6. The 234 and 196 species mechanisms correspond to the smallest mechanisms with a maximum error of less than 5% and 15% respectively, the 138 species mechanism is the smallest mechanism with an average error of less than 15%, and the 129 species mechanism is the smallest mechanism for which ignition occurs at all, even if not accurate, for all cases in the mechanism. It can be seen that the high and low temperature regions are reproduced very well, even for very small mechanisms. However, the negative temperature coefficient

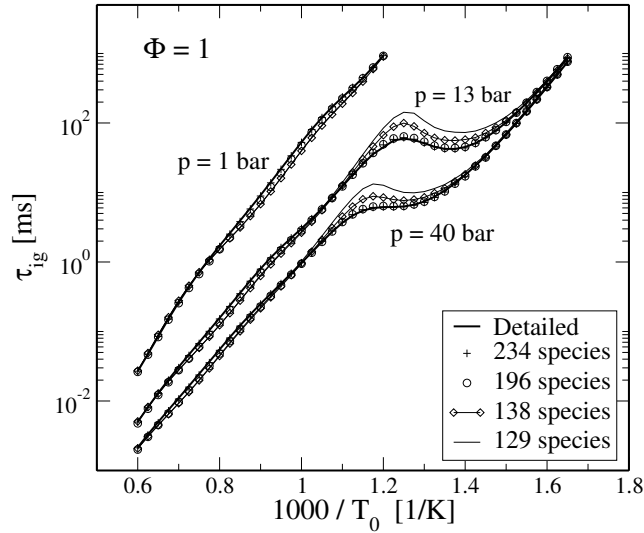


Figure 2.14: Comparison of ignition times obtained with the detailed iso-octane mechanism and skeletal mechanisms of various sizes.

region, which is the most sensitive to perturbations, concentrates the largest errors.

The total number of species kept for the first stage of reduction is chosen so that the maximum error over all targets is about 15%, which correspond to 196 remaining species and 1762 remaining reactions, forward and backward counted separately. Following this first step of reduction and with the same accuracy requirement, additional non-necessary reactions are removed, and the resulting skeletal mechanism comprises 195 species and 802 reactions, that is a reduction by a factor of 4.35 of the number of species, and a reduction by a factor of 9 of the number of reactions. Table 2.1 provides an estimation of the error introduced in ignition delay times over the entire reduction domain by this first stage of reduction.

$N_{\text{Species}}$	$N_{\text{Reactions}}$	Maximum Error [%]	Average Error [%]
196	1762	15.89	6.02
195	802	14.96	5.55

Table 2.1: Maximum and average errors introduced by the elimination stage of reduction, for initial conditions with pressures between 1 and 40 bar, equivalence ratios between 0.5 and 2, and temperatures between 600 K and 1500 K.

## 2.3 Compacting Stage: A Chemical Lumping Approach

The present section complements a second important aspect of kinetic reduction that aims to describe the system in terms of a reduced number of variables, called lumped variables, through a linear or non-linear transformation. It describes a statistical approach to chemical lumping and illustrates it using hydrocarbon oxidation mechanisms [104].

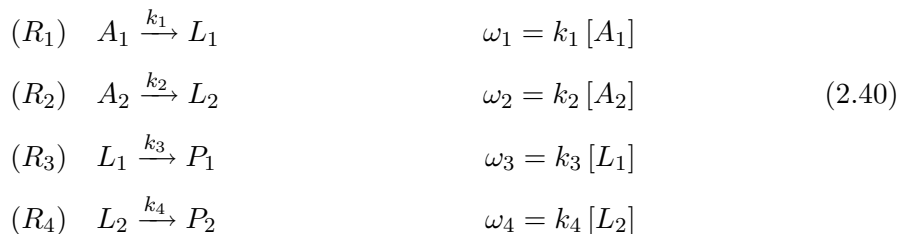
### 2.3.1 Background on Lumping Techniques

Depending on the applications, lumping can be either an essential modeling tool or a convenient reduction technique. For instance, the extremely large number of molecules in hydrocarbon feedstocks renders the task of developing a comprehensive model for fuel conversion very difficult. To model feedstock pyrolysis, Nigam and Klein [94] proposed to lump all the molecules into compound classes, e.g., normal and iso-paraffins, alkylbenzenes, alkylnaphthenes or alkylhydroaromatics, and the typical pyrolysis reactions into four families: bond homolysis, H atom abstraction,  $\beta$ -scission, and recombination reactions. Corresponding rate coefficients for this two-level lumping approach were obtained from available experimental data using Quantitative Structure-Reactivity Relationships (QSRR). To achieve a more detailed representation of the pyrolysis problem, Fake et al. [42] developed a mechanism-based lumping, in which all molecules in the mixture are described individually. However, the large number of radicals produced by these molecules were reduced to a mere 42-member lump subset representative of the current mixture. Reaction rates were expressed in terms of those lumped radicals using quasi-steady state and long chain [50] approximations, and the rate constants were estimated through QSRR. Systems involving infinite reaction sequences also require lumping as a numerical modeling tool. For example, Frenklach [48, 47] developed a lumping procedure for polymerization processes and applied it to polycyclic aromatic hydrocarbon growth in flames. The lumped solution of the chemical system was expressed in terms of moments of the species distribution function.

On the other hand, lumping can be a very efficient tool to reduce the computational burden of detailed models that can be formulated and solved. A significant effort was done

in an attempt to find a mathematical procedure that could be applied to any general reaction system to reduce the number of variables. Conditions for the exact and approximate linear [147, 67] or non-linear [70, 71] lumping of a system of ordinary differential equations (ODEs) have been established and subsequent studies show various successful applications and developments of the mathematical approach [72, 128]. However, although an optimal non-linear mathematical lumping would certainly provide the largest reduction potential for a given system of ODEs, no systematic procedure exists to find that optimal lumping transformation, and other more practical solutions have been sought, that exploit the specific features and topology of the system to lump.

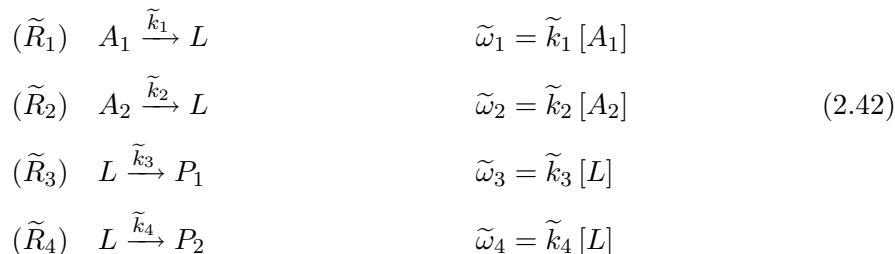
Significant simplification can be achieved by constraining the lumping procedure to linear transformations. This is easily demonstrated through the following simple reaction mechanism:



Suppose we want to lump  $L_1$  and  $L_2$  together. The representative species  $L$ , lump of species  $L_1$  and  $L_2$ , can be defined simply as:

$$[L] = [L_1] + [L_2] , \tag{2.41}$$

where  $[\cdot]$  represents a concentration. The lumped mechanism:



is equivalent to mechanism (2.40) provided that the rate coefficient of the reactions are modified adequately to account for the larger concentration of the lumped species  $L$  compared to the original species  $L_1$  and  $L_2$ . Production reactions are left unchanged, as their rates do not involve the lumped species concentration, i. e.  $\tilde{k}_1 = k_1$  and  $\tilde{k}_2 = k_2$ . The rate coefficients of the consumption reactions, however, must be decreased by a factor proportional to the respective contribution of each original species to the lumped species concentration:

$$\tilde{k}_3 = k_3 \frac{[L_1]}{[L]} \quad \text{and} \quad \tilde{k}_4 = k_4 \frac{[L_2]}{[L]}. \tag{2.43}$$

This result, easily extended to any lump group and reaction mechanism, shows that two different aspects have to be considered for linear lumping, that are not independent from one another. The first one is an appropriate definition of the lump groups, the second one is an accurate evaluation of the quantitative contribution of each species to its lump group. Withehouse et al. [149] and Huang et al. [57] showed that if the groups of species to lump are carefully chosen, the species distribution can be evaluated directly from the individual production rates of the species, which are available from the lumped scheme since the species production reactions are not modified by the lumping process. Withehouse et al. [149] lumped species with comparable time-scale and chemical behavior for the reduction of a mechanism describing atmospheric chemistry. Huang et al. [57] formalized the choice of the groups by introducing a numerical criterion based on local concentrations and formation rates obtained using the detailed mechanism. This criterion was applied successfully in the

context of isothermal conversion of methane. The lumping was done on the fly, with the rate-correcting factors evaluated at each time step. However, this approach prevents the lumping from being embedded directly into a stand-alone mechanism suitable for use in standard chemistry solvers. Moreover, the lump groups are chosen on numerical considerations, and thus, have little chemical meaning.

The oxidation chemistry of large hydrocarbon molecules suggests another natural way to define lump groups. Indeed, hydrocarbon oxidation involves a large number of functional isomer species, that is, species with similar composition and structure, but whose chemical functionalities such as radical sites or oxygenated groups are distributed differently on the molecule. Such species usually are formed through analogous chemical channels but may lead to different kinetic behavior depending on the chain branching, propagating or breaking nature of their decomposition pathways. Several approaches to the lumping of these isomers can be found in the literature that use different simplifying assumptions. In the case of high-temperature kinetics, Zeppieri et al. [155] and Chaos et al. [17] assume pseudo-equilibrium of the isomerization reactions to estimate the relative distribution of the isomers. While Zeppieri et al. [155] use empirical considerations to define appropriate rate constants for the lumped reactions, Chaos et al. [17] fit the temperature-dependent distributions to an Arrhenius-type law, so that the correcting factors can be directly incorporated into the reaction rate constants.

Isomer lumping is also widely used during the automatic generation of mechanisms for hydrocarbon oxidation, that proceeds hierarchically by adding the description of increasingly longer molecules to a basis mechanism. An efficient way to limit the size of the growing mechanism is to lump the isomer species appearing in the primary mechanism, that is, the part of the mechanism that converts the long fuel molecules into smaller ones already described in the basis scheme. In this context, the full detailed mechanism is not used in the solution. Instead, assumptions are made at the level of the primary mechanism to determine the correcting factors. Ahmed et al. [1] suppose an equi-repartition of the primary isomers and modify the pre-exponential factor of the lumped reactions accordingly. Bounaceur et al. [10] and Fournet et al. [45] express the reaction rates of the lumped mechanism in

terms of the radical species distributions, and evaluate those rates at a given temperature by applying quasi-steady state assumptions and long chain approximation to the primary mechanism. Also using QSSA, Ranzi et al. [116, 115, 114, 117] evaluate the rate constants of the lumped primary mechanism through least-square optimization of the primary product selectivity over a range of pressure and temperature. Additionally, parallel reactions with identical reactants are lumped together, the stoichiometry of the corresponding products being estimated at a given temperature using the detailed description of the reactions.

The lumping approaches mentioned above involve assumptions that may not be valid for all desired conditions. In this work, a general automatic lumping approach is derived, that directly uses simulation results obtained from the detailed mechanism to generate a lumped scheme valid over a user-specified range of conditions. The method, applied here to isomer lumping in hydrocarbon oxidation kinetic schemes, does not rely on equilibrium or quasi-steady state assumptions. In addition, the resulting lumped mechanisms are suitable for direct use in standard chemistry softwares. In the following, the proposed lumping procedure will be detailed, and compared to some of the techniques outlined above. The quality of the resulting lumped schemes will be assessed. Finally, the integration of the lumping procedure into a multi-stage reduction strategy will be discussed and illustrated.

### 2.3.2 Proposed Modeling Approach

**General Considerations** Suppose the original set of species  $\mathcal{S} = \{S_{i,i=1..N_S}\}$  is subdivided into  $\tilde{N}_S$  lumped groups  $\mathcal{L}_{I,I=1..\tilde{N}_S}^S$ . For each lumped group  $\mathcal{L}_I^S$ , a representative species is defined as a linear combination of the species of this group, such that:

$$\left[\tilde{S}_I\right] = \sum_{i \in \mathcal{L}_I^S} [S_i]. \quad (2.44)$$

We define the relative contribution of species  $S_i$  to its group as:

$$\alpha_i = \frac{[S_i]}{\left[\tilde{S}_I\right]}. \quad (2.45)$$

The reaction rate of a reaction  $j$  is defined as:

$$\omega_j = k_j \prod_{i=1}^{N_S} [S_i]^{\nu'_{i,j}}, \quad (2.46)$$

where  $\nu'_{i,j}$  is the stoichiometric coefficient of species  $S_i$  on the reactant side of reaction  $j$  and  $k_j$  is the rate coefficient of reaction  $j$ . Defining  $\tilde{\nu}'_{I,j} = \sum_{i \in \mathcal{L}_I^S} \nu'_{i,j}$  and using the fact that  $\mathcal{L}_{I,I=1..\tilde{N}_S}^S$  is a partition of  $\mathcal{S}$ , the reaction rate can be expressed using the lumped variables:

$$\begin{aligned} \omega_j &= k_j \prod_{i=1}^{N_S} \left( \alpha_i [\tilde{S}_I] \right)^{\nu'_{i,j}} \\ &= k_j \prod_{i=1}^{N_S} \alpha_i^{\nu'_{i,j}} \prod_{I=1}^{\tilde{N}_S} \prod_{i \in \mathcal{L}_I^S} [\tilde{S}_I]^{\nu'_{i,j}} \\ &= k_j \prod_{i=1}^{N_S} \alpha_i^{\nu'_{i,j}} \prod_{I=1}^{\tilde{N}_S} [\tilde{S}_I]^{\sum_{i \in \mathcal{L}_I^S} \nu'_{i,j}} \\ &= k_j \prod_{i=1}^{N_S} \alpha_i^{\nu'_{i,j}} \prod_{I=1}^{\tilde{N}_S} [\tilde{S}_I]^{\tilde{\nu}'_{I,j}}. \end{aligned} \quad (2.47)$$

At this stage, the reactions that have become identical after the lumping of species can also be lumped together. The set of reactions  $\mathcal{R} = \{R_{j,j=1..N_R}\}$  is sub-divided into  $\tilde{N}_R$  lumped groups  $\mathcal{L}_{J,J=1..\tilde{N}_R}^R$  that combine identical reactions. Most lumped reaction groups are trivial, that is, contain a single reaction. The reaction rate for each lumped reaction becomes, as  $\tilde{\nu}'_{I,j} = \tilde{\nu}'_{I,J}$  for each  $j \in \mathcal{L}_J^R$ :

$$\tilde{\omega}_J = \sum_{j \in \mathcal{L}_J^R} \omega_j = \tilde{k}_J \prod_{I=1}^{\tilde{N}_S} [\tilde{S}_I]^{\tilde{\nu}'_{I,J}}, \quad (2.48)$$

with

$$\tilde{k}_J = \sum_{j \in \mathcal{L}_J^R} \left( k_j \prod_{i=1}^{N_S} \alpha_i^{\nu'_{i,j}} \right). \quad (2.49)$$

This transformation corresponds to an exact linear lumping if  $\tilde{k}_{J,J=1..\tilde{N}_R}$ , and therefore,

the relative contributions  $\alpha_{i,i=1..N_S}$ , are known functions of time and space. Unfortunately, these functions usually are unknown and a closed form has to be assumed. In this work, rather than specifying the relative distributions as functions of physical space and time, models for these distributions will be formulated in terms of the state space:

$$\left\{ T, P, \left[ \tilde{S}_I \right]_{I=1..\tilde{N}_S} \right\} . \quad (2.50)$$

Suppose that a subset  $\Pi$  of the state space variables is chosen to parameterize a set of data  $\sigma$ . In our case,  $\sigma$  refers to the relative distributions  $\alpha_{i,i=1..N_S}$  or to the lumped rates  $\tilde{k}_{J,J=1..\tilde{N}_R}$ . In most cases, there is no explicit relationship between the data and the chosen state parameters. Therefore, a model  $f^\sigma(\Pi)$  has to be formulated, that will approximate the actual data by a function of the parameters included in  $\Pi$ . Both the choice of the set of parameters and the definition of the function  $f$  will impact the quality of the model. To assess the accuracy of the model function  $f$ , an error measure can be defined as the  $L^2$  norm of the difference between the data  $\sigma$  and the model  $f^\sigma(\Pi)$ :

$$\epsilon = \left\langle (\sigma - f^\sigma(\Pi))^2 \right\rangle , \quad (2.51)$$

where  $\langle \cdot \rangle$  denotes statistical averaging.

For a given set  $\Pi$ , the function  $f$  must be chosen so that it will minimize the error  $\epsilon$ . A procedure to construct such a function has been applied by Moreau et al. [90] in the context of sub-grid scale models for large eddy simulations. They demonstrated that if Eq. 2.51 is used to measure the error, the best possible representation of a set of data  $\sigma$  is given by the conditional mean with respect to the parameters used to describe  $\sigma$ , that is,

$$f_{\text{opt}}^\sigma(\Pi) = \Omega^\sigma(\Pi) = \langle \sigma | \Pi \rangle . \quad (2.52)$$

$\Omega^\sigma(\Pi)$  is called the optimal estimator of the data  $\sigma$  given the set of parameters  $\Pi$ . The error introduced by using the optimal estimator instead of the actual data  $\sigma$  corresponds to the minimal error a model based linearly on  $\Pi$  can possibly introduce, and thus, is called

the irreducible error.

The concept of optimal estimator provides a convenient tool to assess the relevance of the chosen set of parameters. Indeed, it is expected that the more parameters are used, the smaller the error will be. However, some parameters might be more relevant than others in describing a particular set of data. This is demonstrated here for a practical case. A skeletal mechanism for iso-octane oxidation was derived from the comprehensive mechanism by Curran et al. [26] using the Directed Relation Graph with Error Propagation (DRGEP) reduction procedure [103]. Using this mechanism, a large number of simulations of homogeneous reactors at various pressures, initial temperatures, and equivalence ratios have been run. For each simulation, the evolution of the ratios between the four iso-octyl radicals and the corresponding full state space have been recorded. This can be seen as a statistical database for the relative contributions  $\alpha_i$  of the iso-octyl isomers. Figure 2.15 shows the quadratic errors  $\epsilon$  obtained using the optimal estimator based on conditional averages for the four isomers, for different sets of variables  $\Pi$ . These errors correspond to the minimal

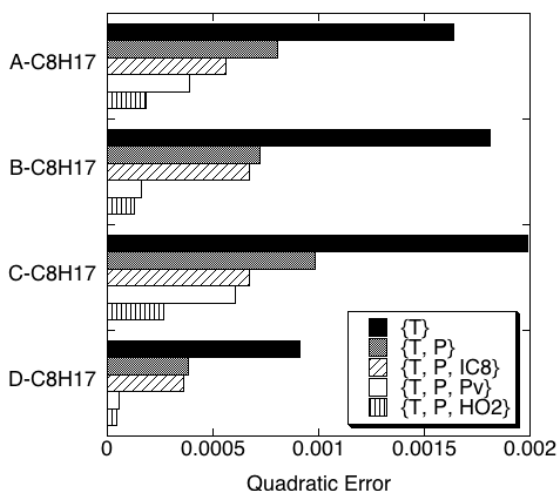


Figure 2.15: Quadratic error  $\epsilon_i = \langle (\alpha_i - \langle \alpha_i | \Pi \rangle)^2 \rangle$  in the representation of the relative contributions  $\alpha_i$  for iso-octyl radicals in homogeneous reactors for different sets of parameters  $\Pi$ .  $P_v$  is a progress variable defined as the sum of CO, CO<sub>2</sub>, H<sub>2</sub>O and H<sub>2</sub>.

error level introduced in the representation of the relative contributions by assuming that they can be expressed as functions of the given state space. As expected, the error decreases as the number of variables used increases, and the overall error level remains small, even when a single parameter is used. But the results also show that different sets of variables produce different levels of error. For example, representing  $\alpha_i$  using temperature, pressure, and  $\text{HO}_2$  is better than using the fuel or a progress variable as the third independent coordinate. A possible explanation is that the fuel is depleted when the intermediate iso-octyl species reach their peak concentrations, and the major products are produced only when the iso-octyl radicals are already present in large quantities. Thus, neither of these variables can provide a good representation of the evolution of the radicals over their entire production and consumption cycle. The evolution of  $\text{HO}_2$  concentration, on the other hand, roughly follows that of the iso-octyl radicals, which explains the small error obtained when using it as the third parameter.

**Evaluation of the Model Function** Now that we have seen that the optimal estimator provides a convenient procedure to choose the most adequate set of parameters  $\Pi$ , the next step is to find practical ways to evaluate the model function  $f^\sigma(\Pi)$ , so that it accurately represents the conditional expectation. A promising approach is to use non-linear data modeling tools such as artificial neural networks, which can be seen as parametric functions whose weights are adjusted by training the network to minimize errors [8]. This technique allows to retain the dependence of the data on a large number of state variables, thus introducing very little error in the model. However, the training process is not an easy and straightforward procedure, and the resulting mechanism would not easily be used in standard chemistry packages, such as the Chemkin libraries, as extra routines need to be provided to evaluate the lumped rate constants. Therefore, for practical reasons, the approach will be demonstrated and analyzed by considering only constant values or temperature dependent values of  $\alpha_i$ . To increase accuracy, the modeling procedure will be applied directly to the lumped rate coefficients  $\tilde{k}_J$ , instead of the relative contributions  $\alpha_i$ . Then, the lumped rate coefficients can be expressed in Arrhenius form and the lumped

reactions readily incorporated into the lumped mechanism that retains the same format as the detailed mechanism. Accordingly,  $\tilde{k}_J$  will be modeled using a basis function of the form:

$$f^{\tilde{k}_J}(T) = \beta T^\gamma e^{-\frac{\delta}{RT}}. \quad (2.53)$$

The determination of the unknown coefficients  $\beta$ ,  $\gamma$ , and  $\delta$  is done using the detailed simulation data. To illustrate the soundness of this simplifying assumption, the data for the iso-octyl isomers obtained in the example above are projected onto the temperature and shown in Fig. 2.16. An important observation is that the role played by these isomers in the overall dynamics of the system might be more or less important depending on the configurations. A global interaction coefficient was defined as part of the DRGEP methodology presented in [103], that quantifies the impact of a species on major parameters such as ignition delay time, laminar burning velocities, or fuel consumption. This DRGEP coefficient  $R$  is computed for all cases and used as a weighting factor to analyze the relative contribution of each iso-octyl isomer. In Fig. 2.16, darker colors mean larger coefficients  $R$ , that is, a higher importance of the radicals in the mechanism. These data demonstrate that keeping

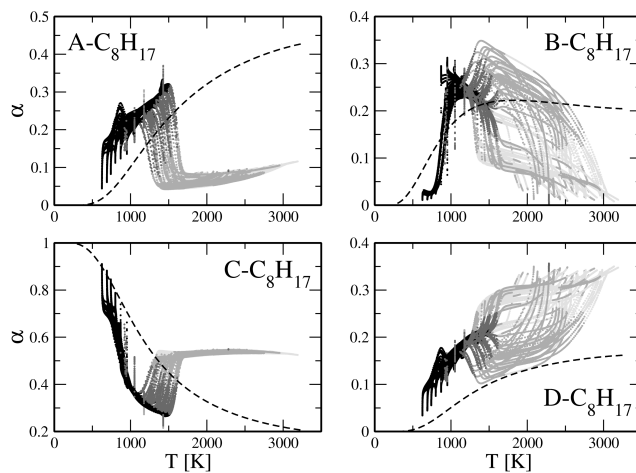


Figure 2.16: Iso-octyl radical distribution as function of the temperature for homogeneous and flame configurations. Darker colors mean higher DRGEP coefficients. Dashed lines correspond to thermodynamic equilibrium ratios.

only the temperature dependence of the distribution functions  $\alpha$  is a good approximation

at low temperatures, whereas some scatter is observed at higher temperatures. However, less accuracy in the isomers distribution will have little impact on the prediction of the targets, as indicated by smaller DRGEP coefficients. Also shown in Fig. 2.16 are the relative contributions computed using the equilibrium constants of the isomerization reactions. Although the trends are similar, using the pseudo-equilibrium assumption to evaluate  $\alpha$  might introduce large inaccuracies in the reaction rates. This will be demonstrated in more detail below.

### 2.3.3 Technical Description

**Choice of Groups of Isomers** The identification of the potential lump groups can be based on mathematical criteria such as the one developed by Huang et al. [57]. Two intermediate species were included in the same lump group if their concentration over formation rate ratios evolved similarly. Such criterion ensures that the lumping transformation gives accurate results. However, it was designed so that the relative contribution of each species inside a lump group could be computed explicitly at run time from the kinetic parameters of the original scheme, which can be an overly restrictive selection procedure. Moreover, especially in the case of hydrocarbon oxidation mechanisms, it is desirable to keep in the lump mechanism the overall organization of the detailed scheme, with representative elementary steps for each specific class of reactions. In that case, the reduced mechanism can still be used to get insight into the dynamic chemical processes occurring during combustion. A simple way to achieve that is to lump together chemical isomers, as these species have potentially similar formation and decomposition pathways. Ahmed et al. [1] further refined this approach by subdividing isomers depending on the type of intermediate chemical complex appearing during the formation of the species and the primary or secondary position of the radical site on the molecules. With this definition, the lump groups are more consistent in terms of energy levels and reactivity, which may lead to a more accurate lumping, at the expense of larger lumped mechanisms. In the present work, the lump groups consist of chemical isomer species. It was found in the mechanisms used as examples, that the distinction between primary and secondary radical sites was not important, but that for

some cases, taking into account the size of the ring in the transition states, as suggested by Ahmed et al. [1], improved results dramatically with a small loss in the degree of reduction.

**Procedure** The first step is to define the physical space, for which the lumping process will be performed and the validity of the reduction tested. Then, this domain is densely sampled so that if the lumped mechanism is a good approximation to the detailed mechanism at each sample point, it can be reasonably assumed that it will be valid also between sampled points. Solutions using the detailed mechanism are computed at each of the sample points. From these solutions, statistical data on the relative contribution of the isomers and the corresponding temperature are gathered, each data point being weighted by the corresponding DRGEP coefficient of the isomers. The definition of the lump groups determines the list of lump reactions  $\mathcal{L}_{J,J=1..\tilde{N}_R}^R$ , and the value of their rate coefficients  $\tilde{k}_J$  are evaluated at each sample point, forward and backward reactions being treated separately, using the previously obtained values for  $\alpha$ . Assuming an Arrhenius-like temperature dependence, a least-square regression algorithm is used to determine the optimal pre-exponential factor, temperature exponent and activation energy of each of the lumped reactions. The default representation uses a 3-parameter Arrhenius basis function. However, if the resulting curvature is too large, a 2-parameter model function is used to prevent numerical overflow. In this work, the exponent of the rate parameters are restricted to two digits only. Although this simplification might be detrimental to the accuracy, it applies only to a few percent of the lumped reactions and was found not to affect the quality of the results. The resulting kinetic mechanism will have less species and less reactions. A few comments can be made at this point. First, as the obtained rate coefficients are solutions of a fitting process, they are not chemically meaningful. Then, backward rates are not determined using thermodynamic data anymore, but must be explicitly specified in the lumped mechanism as output from the algorithm.

**Thermodynamic Data** The issue of thermodynamic data for the representative species in each lump group was not studied in detail in previous work. Two reasons can be found

for this. The first one is that some of the lumping methods detailed above were used in situations for which thermodynamic properties of the lumped species mattered very little, such as iso-thermal conditions with irreversible reactions, or lumped species that have identical thermodynamic properties. In other cases, the thermodynamic data were taken as the ones of the first species appearing in the lumped group. In the current approach, because the rate coefficients of the lumped backward reactions are specified explicitly, thermodynamic data for the lumped species appear only in the energy equation. To keep a more consistent approach to the overall lumping procedure, the same treatment was applied to the thermodynamic data as for the species themselves. However, to avoid any fitting problems, the relative contribution of each species in the lump was averaged over the range of temperature relevant to the domain of applicability of the lumped mechanism, and the thermodynamic coefficients were computed as the weighted average of the coefficients of each species. In the context of large hydrocarbon molecules oxidation mechanisms, this procedure was found to have very little consequence on the lumping accuracy.

### 2.3.4 Results and Validation

The skeletal mechanism for iso-octane oxidation obtained through species and reaction elimination [103] is used as starting mechanism to demonstrate the efficiency of the lumping approach. This mechanism contains 195 species and 802 reactions, backward and forward reactions counted separately. Among those species, 27 lump groups involving 88 chemical isomer species can be identified, leading to a reduction of the number of species from 195 to 135 if all groups of isomers are lumped, and a reduction of the number of reactions to 611.

**Evaluation of the Relative Contributions  $\alpha(\mathbf{T})$**  The accuracy of the lumping procedure depends on the quality of the model  $f^{\tilde{k}_J}(T)$  describing the lumped rate coefficients. In Eq. 2.49 defining  $\tilde{k}_J$ , all the terms are known analytically except the  $\alpha$  functions that need to be estimated. The current approach, in which the  $\alpha$  values are taken directly

from simulations using the detailed mechanism, can be compared to three other methods. The first one assumes a pseudo-equilibrium of the isomerization reactions to compute temperature-dependent values for  $\alpha$  based on thermodynamic data [17]. The second one supposes constant  $\alpha$  values, computed as the average over all sample points of the actual ratio of isomers. Finally, following the equi-repartition approach by Ahmed et al. [1],  $\alpha$  can be defined as the reciprocal of the number of isomers in the lump. For this comparison, the thermodynamic data of the representative species were chosen as those of the isomer present in largest concentration. Lumping was performed for isochoric homogeneous auto-ignition cases in engine-relevant conditions, that is, with pressures ranging from 1 to 40 bar, equivalence ratios varying from lean ( $\phi = 0.5$ ) to rich ( $\phi = 2$ ), and temperatures between 600 K and 1500 K. No simulation was included that led to ignition delay times larger than a couple of seconds. Results for ignition delay times of stoichiometric mixtures are shown in Fig. 2.17. As logarithmic plots are misleading in estimating the error level, Fig. 2.18

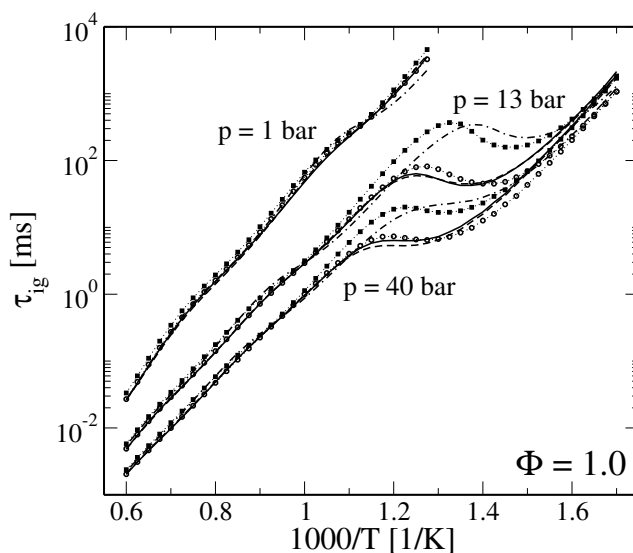


Figure 2.17: Ignition delay times obtained using different explicit methods. Comparison between the skeletal mechanism (solid lines), and lumped mechanisms obtained using fitted ratios (dashed lines), constant ratios (circles), thermodynamic equilibrium (filled squares) and equi-repartition (dash-dotted lines).

shows as an example the differences in percent between detailed and lumped schemes on a

linear scale for a pressure of 13 bar. From these two figures, it is apparent that all methods

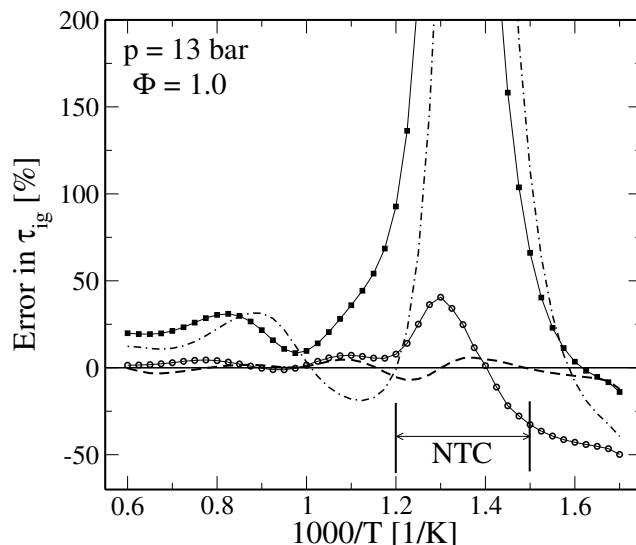


Figure 2.18: Error in ignition delay times. Comparison between the skeletal mechanism (solid lines), and lumped mechanisms obtained using fitted ratios (dashed lines), constant ratios (circles), thermodynamic equilibrium (filled squares) and equi-repartition (dash-dotted lines).

give an accurate representation of the high temperature chemistry, but perform very differently around the negative temperature coefficient (NTC) region and for low temperatures. The method proposed here is the most accurate, with only a small under-prediction of the ignition delay time at high pressure around the NTC region. At  $\phi = 1$  and  $p = 13$  bar, the maximum error between the skeletal mechanism and the lumped mechanism is always smaller than 8%. On the other hand, approximating the isomer distribution by constants is a correct approximation for high to medium temperatures, but the solutions diverge significantly in the low temperature regime, with errors up to 50%. The other two methods perform extremely poorly in the NTC region, both predicting the roll-over of the ignition delay time at too low temperatures. This proves that an accurate fitting of the ratio as a function of temperature is an essential step to correctly reproduce the temperature selectivity of the original mechanism.

**Impact on Chemical and Dynamic Characteristics of the Mechanism** In addition to the auto-ignition configurations used to generate Fig. 2.16, the lumped mechanism obtained above with the proposed method was used to simulate atmospheric plug flow reactors, modeled by isobaric homogeneous systems, and atmospheric one-dimensional laminar premixed flames. Table 2.2 provides the errors obtained over all conditions between skeletal and lumped schemes for ignition delay times and laminar burning velocities, which are two parameters describing the global behavior of the considered systems. Virtually no error on the final concentration of the products was observed. The small errors show that the

Error in $\tau_{ig}$ [%]	Max	16.19
	Avg	4.75
Error in $S_L$ [%]	Max	1.05
	Avg	0.67

Table 2.2: Comparison of global parameters between skeletal and lumped iso-octane mechanisms.

prediction of global parameters is quite accurate. More remarkable is the fact that even though the lumped rate coefficients were modeled using homogeneous reactor data only, the resulting scheme is applicable to different configurations such as flames. However, additional comparisons are required to ensure that the lumping does not affect fundamental aspects of the original mechanism, for example, mass fluxes between species and dynamic properties such as reaction classes sensitivities [1]. The adequate representation of a group of isomers can be assessed by comparing the sum of the concentration of isomers of the lump group to the actual concentration of the representative species. For an accurate lumping, these two quantities should be equal, as indicated by the fundamental definition of the representative species in Eq. 2.44. This is demonstrated for the iso-octane lumped mechanism, in a few representative configurations: in a PFR simulation at atmospheric pressure,  $\phi = 0.5$  and initial temperature of 945 K (case *a*), in a premixed stoichiometric flame, for which the discrepancy with the skeletal mechanism was the largest (case *b*), and for auto-ignition, by selecting the worst case (case *c*) and some initial conditions corresponding to the average

error over all cases included in the lumping process (case *d*). The concentration of the representative octyl radical is compared to the sum of the four octyl radicals lumped together. Results are shown in Fig. 2.19. Because of the unsteady character of the cases studied,

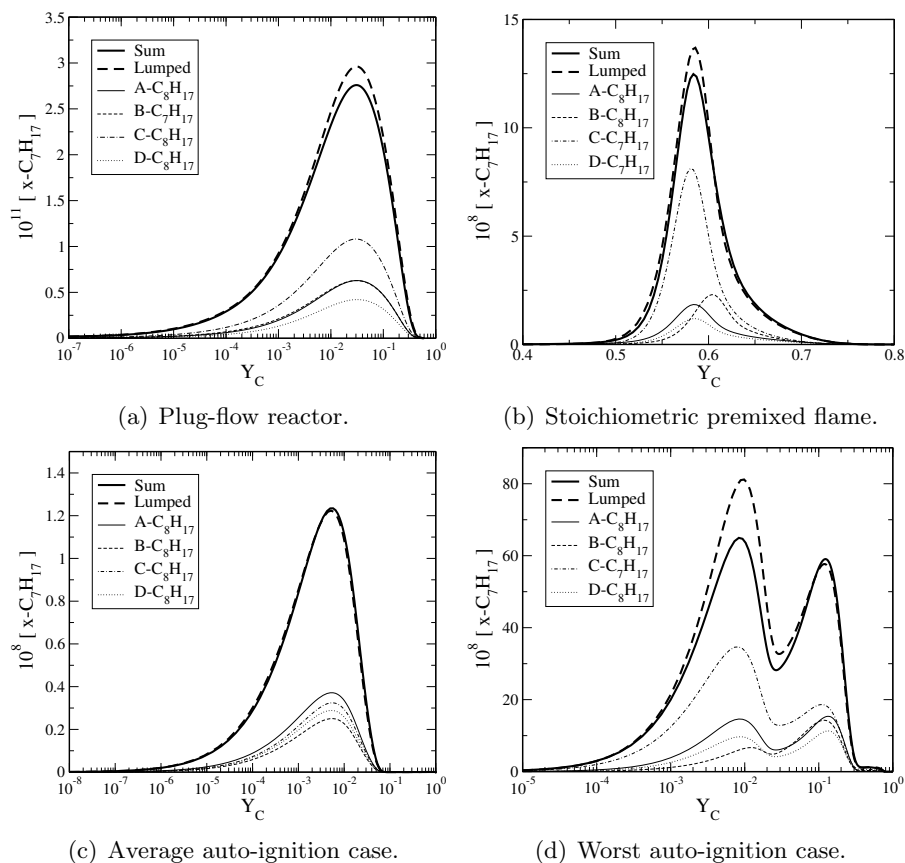


Figure 2.19: Comparison of iso-octyl isomers and lumped representative species concentrations in selected configurations.

instead of considering the concentrations in physical space (time or space coordinates), the comparison is done with respect to a progress variable [103]. This progress variable is composed of the main products, that is  $\text{H}_2\text{O}$  and  $\text{CO}_2$  for cases *a* and *b*,  $\text{H}_2\text{O}$ ,  $\text{CO}_2$ ,  $\text{H}_2$ , and  $\text{CO}$  in cases *c* and *d*. Good agreement is obtained for cases *a* and *b*, and excellent agreement is obtained for the representative average ignition configuration. In the worst possible case for ignition, there is an over-prediction of the total iso-octyl concentration around the first stage ignition, which leads to an under-prediction of the main ignition delay time. However,

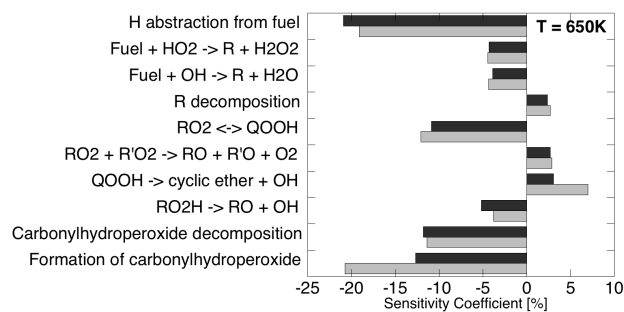
the iso-octyl concentration is very well reproduced at ignition.

The impact of lumping on the main dynamics of the reactive system can be quantified by the changes introduced by the lumping process on the original sensitivities of the system, as suggested by Ahmed et al. [1]. Kinetic mechanisms for alkane pyrolysis and oxidation, including the one used in this example, are usually built hierarchically by defining a number of reaction classes that are applied to each size of alkane molecules. For iso-octane, 25 reaction classes were defined in [26] to generate the comprehensive iso-octane mechanism, but only 20 of them are still present in the skeletal mechanism. The sensitivity of the system to each class of reactions can be evaluated by comparing the solution obtained with the original rates to the one obtained using a mechanism in which forward and backward rate coefficients of the reactions are multiplied by a factor of 2. Sensitivity of the most important classes of reactions on ignition delay time for auto-ignition of a stoichiometric mixture of iso-octane and air at 13 bar and various initial temperatures are shown in Fig. 2.20. The most sensitive classes of reactions change as the initial temperature increases, as expected. Unimolecular fuel decomposition, negligible at low temperatures, becomes more and more important as the temperature increases. H atom abstraction from the fuel is important in all cases, but with various intensity. Ignition delay time is very sensitive to low temperature-type chemical reactions, especially those producing small radicals or OH. Good agreement is observed between the lumped mechanism and the skeletal mechanism, proving that the lumping procedure did not affect too much the natural dynamics of the system.

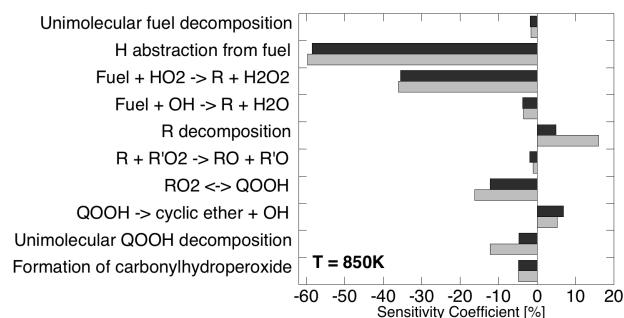
## 2.4 Introduction of Modeling Assumptions: The Quasi-Steady State Approximation

### 2.4.1 Selection of Suitable QSS Species

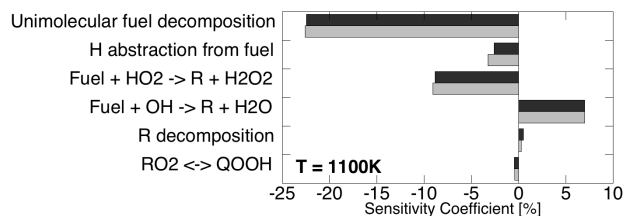
To additionally increase the speed up of the skeletal mechanism obtained through species and reaction elimination and chemical lumping, a straightforward strategy is the introduction of quasi-steady state assumptions that replace part of the differential equations by



(a) 650K



(b) 850K



(c) 1100K

Figure 2.20: Sensitivities of the most important classes of reactions. Comparison between the skeletal (dark bars) and the lumped (light grey bars) iso-octane mechanisms.

algebraic equations, which are much faster to evaluate. Several methods to systematically identify suitable QSS species can be found in the literature [132, 19, 88]. An interesting criterion defined by Lovas et al. [76, 75] is based on an estimation of the instantaneous error in the concentration of a species if set in steady state, i.e. the deviation between the exact solution and the quasi-steady state approximation. In this approach, called the Level of Importance (LOI) method, the instantaneous error is assumed to be proportional to the product of the lifetime of species  $i$  and its concentration  $c_i$ , and this proportionality

was demonstrated *a posteriori* using a kinetic mechanism for methane. The lifetime of the species,  $\tau_i$ , is related to the diagonal elements of the Jacobian of the system of governing equations:

$$\tau_i = -\frac{1}{J_{ii}} = -\left(\frac{\partial\omega_i}{\partial[S_i]}\right)^{-1}, \quad (2.54)$$

where  $\omega_i$  and  $[S_i]$  are the source term and concentration of species  $i$ , respectively. Additionally, in the LOI method, a sensitivity coefficient is introduced so that species with longer lifetime but small sensitivity to the overall system can be selected as suitable candidates:

$$LOI_i = S_{x,i}^S [S_i] \tau_i, \quad (2.55)$$

where  $\tau_i$  is defined by Eq. 2.54 above and  $S_{x,i}^S$  is the species sensitivity of a relevant parameter  $x$  on species  $i$ .

In the present work, a steady state parameter based on lifetime analysis has been chosen, that is very similar to the Level Of Importance (LOI) criterion. However, because of the number of cases and the typical size of the skeletal mechanisms obtained after the DRGEP and lumping reductions, sensitivity coefficients are still very expensive to compute. On the other hand, scaled, time-dependent DRGEP coefficients are readily available and are used in place of sensitivity coefficients. The steady state parameter  $Q$  can be expressed as:

$$Q_S(t) = \alpha_T R_{TS}[S] \tau_S, \quad (2.56)$$

where  $[S]$  is the concentration of species  $S$  and the lifetime of this species can be expressed in terms of its production and consumption rates

$$\tau_S = -\left[\frac{\partial(P_S - C_S)}{\partial[S]}\right]^{-1}. \quad (2.57)$$

As suggested in [76, 75], the species with small  $Q$  values for all cases can be set in steady state. For simplicity, only linear coupling between steady state species is allowed, so that explicit expressions can be written automatically for a direct use in a combustion code. Still,

the application of steady-state assumptions for non-linearly coupled species can often lead to very good results, especially since recent work has focused on the optimization of the extra cost associated with the evaluation of the non-linear quasi-steady state equations [2, 20].

To assess the validity of the method, the values for the steady state parameter  $Q$  given by Eq. 2.56 were computed using the 195 species iso-octane mechanism obtained after the elimination stage, for all cases and targets used in the validation of this mechanism. Additionally, the actual error in ignition delay time obtained when setting species in steady state one after the other was computed for each configuration. This error is correlated with the corresponding value of  $Q$  for the species. Results are presented in Fig. 2.21. A very

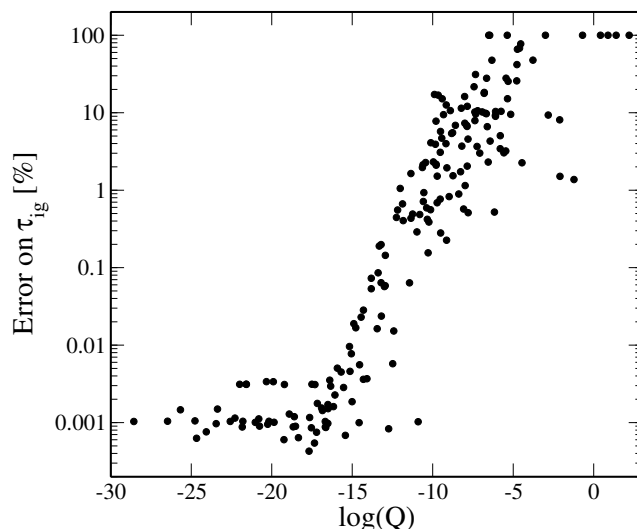


Figure 2.21: Maximum error in ignition delay time against the steady state parameter  $Q$  of each species when set in steady state over the specified range of initial conditions used for the reduction of the iso-octane mechanism.

small error of the order of  $10^{-5}$  is introduced systematically, that is due to numerics and grid resolution. A clear trend is observed, with species having small  $Q$  values introducing comparatively smaller error than species with large  $Q$  values. For example, a cut-off value of  $Q = 10^{-12.25}$  identifies correctly 80 out of 83, that is, 96 % of the species introducing less than 0.2% error on ignition delay time when set in steady state.

The procedure to select QSS species is as follows. The parameter  $Q$  is computed for each

species, at each sample point of the domain of applicability. Species with small maximum  $Q$  values are added to the list of potential QSS candidates. A species is added to the list only if it does not introduce quadratic coupling, that is, the system of algebraic equations giving the concentrations of QSS species remains linear. The algorithm stops when the  $Q$  parameter of the next species to be set in QSS is larger than a pre-defined cut-off value (in this work,  $10^{-7}$  was usually used) or when no more species can be included without introducing quadratic coupling.

### 2.4.2 Decoupling QSS Algebraic Equations

For each species  $S_q$  included in the set of quasi-steady state species, the QSS approximation can be written as

$$\sum_{i=1}^{N_R} \nu_i^q k_i \prod_{j=1}^{N_S} [S_j]^{\nu'_{i,j}} = 0, \quad (2.58)$$

where  $N_R$  is the total number of reactions, backward and forward treated separately. Because no quadratic coupling is allowed, this set of algebraic equations can be put in the form

$$\mathbf{A} S_Q = \text{RHS}, \quad (2.59)$$

where  $S_Q$  is a vector containing the concentration of each QSS species. The matrix  $\mathbf{A}$  and the right-hand side involve the concentrations of non-QSS species, thus, the linear system must be evaluated and inverted a large number of times during the building of the Jacobian. To speed-up the evaluation of the QSS species concentrations, it is desirable to formally invert the system beforehand, and provide decoupled, explicit expressions for each QSS species. This can be done using exact Gauss pivoting. However, the matrix  $\mathbf{A}$  is usually sparse and the number of operations needed to evaluate the explicit expressions can be decreased drastically by reordering the vector  $S_Q$  so that  $\mathbf{A}$  becomes block-triangular. The procedure followed is illustrated through a simplified example.

Suppose a kinetic mechanism in which species  $S_{i,i=1..8}$  are suitable for QSS approximation. The concentrations of these QSS species depend on the concentration of both other

QSS species and non-QSS ones. Species  $S_i$  will be coupled to another QSS species  $S_j$  if  $S_j$  appears as reactant in a reaction that produces  $S_i$ . For example, in the reaction



$S_1$  is coupled to  $S_8$ , but  $S_8$  is not coupled to  $S_1$ , as the evaluation of the concentration of  $S_8$  does not involve that of  $S_1$ . Through a thorough examination of the production rates of each of the QSS species, a QSS graph can be drawn that identifies the various couplings, as is illustrated in Fig. 2.22. The form of the linear system corresponding to this QSS graph

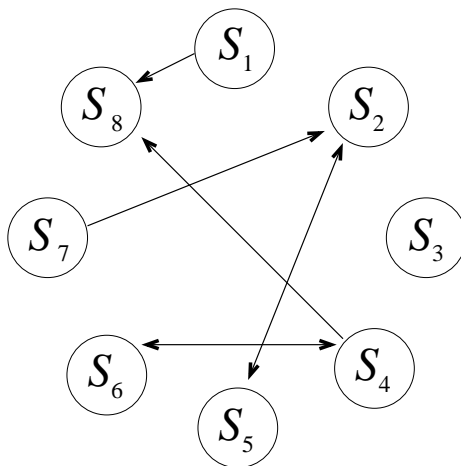


Figure 2.22: Example of QSS graph and coupling between species.

is given in Fig. 2.23. The diagonal terms are always non-zero. An off-diagonal term  $A_{i,j}$  will be non-zero only if species  $i$  is coupled to species  $j$ . Among the QSS species, some are independent from the others, such as  $S_8$ , and some are inter-dependent and cannot be evaluated independently from each other, for example, the group of species  $S_2$  and  $S_5$ .

A search algorithm identifies groups of inter-dependent species (that might contain more than two species), and re-orders the QSS species or inter-dependent groups of species such that the resulting matrix is block-triangular, meaning that during the inversion of the system, a species will only require species concentrations that have been already evaluated. The re-ordered QSS vector and the corresponding matrix operator for our simple example is shown in Fig. 2.24. Explicit expressions for each species is found automatically by formally

$$\begin{pmatrix} \blacksquare & & & & & & & & \blacksquare \\ & \blacksquare & & & & & & & \\ & & \blacksquare & & & & & & \\ & & & \blacksquare & & & & & \\ & & & & \blacksquare & & & & \\ \blacksquare & & & & & \blacksquare & & & \\ & \blacksquare & & & & & & & \\ & & \blacksquare & & & & & & \\ & & & \blacksquare & & & & & \\ \blacksquare & & & & & & & & \\ & & & & & \blacksquare & & & \\ & & & & & & \blacksquare & & \\ & & & & & & & \blacksquare & \\ & & & & & & & & \blacksquare \end{pmatrix} \begin{pmatrix} S_1 \\ S_2 \\ S_3 \\ S_4 \\ S_5 \\ S_6 \\ S_7 \\ S_8 \end{pmatrix} = \text{RHS}$$

Figure 2.23: Linear system of equations corresponding to the coupled system shown in Fig. 2.22. Black squares represents a non-zero entry in the matrix.

$$\begin{pmatrix} \blacksquare & & & & & & & & \\ & \blacksquare & & & & & & & \\ & & \blacksquare & & & & & & \\ & & & \blacksquare & & & & & \\ & & & & \blacksquare & & & & \\ & & & & & \blacksquare & & & \\ \blacksquare & & & & & & & & \\ & \blacksquare & & & & & & & \\ & & \blacksquare & & & & & & \\ & & & \blacksquare & & & & & \\ \blacksquare & & & & & & & & \\ & & & & & \blacksquare & & & \\ & & & & & & \blacksquare & & \\ & & & & & & & \blacksquare & \\ & & & & & & & & \blacksquare \end{pmatrix} \begin{pmatrix} S_3 \\ S_8 \\ S_2 \\ S_5 \\ S_7 \\ S_1 \\ S_4 \\ S_6 \end{pmatrix} = \text{RHS}$$

Figure 2.24: Re-ordered linear system of equations corresponding to the coupled system shown in Fig. 2.22. The system is now block-triangular and will require fewer operations to be explicitly inverted.

applying Gauss pivoting to the re-ordered linear system. A similar approach was presented by Lu and Law [80] for non-linear systems of algebraic equations.

## 2.5 Integration into a Multi-Stage Reduction Strategy

### 2.5.1 Influence of the Ordering of the Reduction Techniques

All techniques described above achieve high reduction ratios when applied individually. The next step is to push further the reduction by integrating the various methods into a more comprehensive, multi-stage reduction strategy that includes explicit removal of species and elementary reactions using the DRGEP method, chemical lumping and introduction

of quasi-steady state assumptions. At that point, it is necessary to determine if the order in which the various reduction techniques are applied has an impact on the final degree of reduction and error levels achieved. To answer this question, the detailed Lawrence Livermore National Laboratories mechanism for *n*-heptane oxidation by Curran et al. [25] has been reduced for auto-ignition configurations in two different ways: first DRGEP, then the chemical lumping, and the reverse, first chemical lumping, then DRGEP. The sample state space is similar to the one used for the lumping of the iso-octane mechanism. In the first case, the comprehensive mechanism is reduced until the maximum error on ignition delay time over all initial conditions is around 15 %. Then, all possible isomer groups are lumped together. For this example, the Ahmed et al. [1] criterion to select groups of isomers had to be applied for the two groups of heptyl oxygenated radicals  $\dot{Q}OOH$  and  $\dot{O}_2QOOH$ . Instead of lumping all isomers into a single group, distinction between isomers is made depending on the size of the transition state ring involved in the isomerization reaction. An example of isomerization involving a 6-membered transition state ring is depicted in Fig. 2.25, and the four lump groups obtained by applying this criterion for the  $\dot{Q}OOH$  radical in Curran et al. [25] mechanism are shown in Fig. 2.26. The molecule names are taken from the Curran et al. [25] nomenclature.

In the second case, the isomer groups are lumped first, then DRGEP is used to remove species and reactions, so that the final reduced mechanisms obtained from both combinations have similar sizes: 127 species and about 600 reactions. The intermediate mechanisms contain 177 and 252 species in the first and second cases, respectively. Comparisons of ignition delay times obtained from the reduced mechanisms are shown in Fig. 2.27, while error levels are displayed in Table 2.3. Each reduction technique introduces roughly the same amount of error, regardless of their order in the reduction procedure. Lumping isomers first decreases slightly the accuracy of the final mechanism, but the difference is not significant, which suggests that both approaches are valid. Moreover, the chemical pathways retained in both reduced mechanisms are very similar. However, removing first from the mechanism

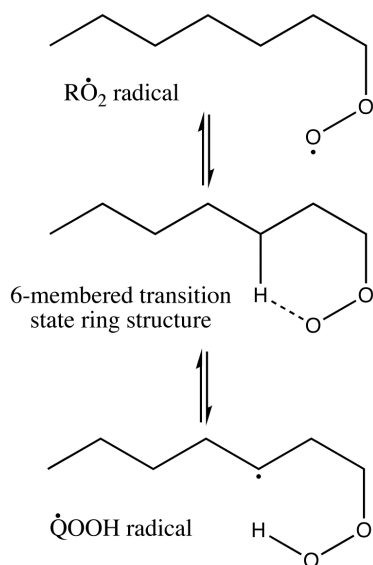


Figure 2.25: Example of  $\text{RO}_2$  isomerization reaction.

Size of transition state ring	
5	6
$\text{C}_7\text{H}_{14}\text{OOH1-2}$	$\text{C}_7\text{H}_{14}\text{OOH1-3}$
$\text{C}_7\text{H}_{14}\text{OOH2-1}$	$\text{C}_7\text{H}_{14}\text{OOH3-1}$
$\text{C}_7\text{H}_{14}\text{OOH2-3}$	$\text{C}_7\text{H}_{14}\text{OOH2-4}$
$\text{C}_7\text{H}_{14}\text{OOH3-2}$	$\text{C}_7\text{H}_{14}\text{OOH4-2}$
$\text{C}_7\text{H}_{14}\text{OOH3-4}$	$\text{C}_7\text{H}_{14}\text{OOH3-5}$
$\text{C}_7\text{H}_{14}\text{OOH4-3}$	
7	8
$\text{C}_7\text{H}_{14}\text{OOH1-4}$	$\text{C}_7\text{H}_{14}\text{OOH1-5}$
$\text{C}_7\text{H}_{14}\text{OOH4-1}$	$\text{C}_7\text{H}_{14}\text{OOH2-6}$
$\text{C}_7\text{H}_{14}\text{OOH2-5}$	$\text{C}_7\text{H}_{14}\text{OOH3-7}$
$\text{C}_7\text{H}_{14}\text{OOH3-6}$	

Figure 2.26: Lumped group of QOOH isomers. In  $\text{C}_7\text{H}_{14}\text{OOHX-Y}$ , X denotes the site of  $\text{O}_2$  addition, Y denotes the radical site.

Reduction Stage	Reference Mechanism	Type of Error	DRGEP $\rightarrow$ Lumping	Lumping $\rightarrow$ DRGEP
Stage I	Detailed	Max	15.17 %	9.45 %
		Avg	6.19 %	3.14 %
Stage II	Stage I	Max	10.81 %	13.32 %
		Avg	2.64 %	4.52 %
	Detailed	Max	16.70 %	18.83 %
		Avg	5.66 %	6.42 %

Table 2.3: Ignition delay times of *n*-heptane. Comparison between two different reduction strategies that differ in the order in which the individual reduction techniques are applied. The “Reference Mechanism” column defines the mechanism against which the reduced schemes are compared.

the isomers that have negligible contributions might, in general, prevent more important regression error in the lumping stage. In the next example, the DRGEP technique will be applied first.

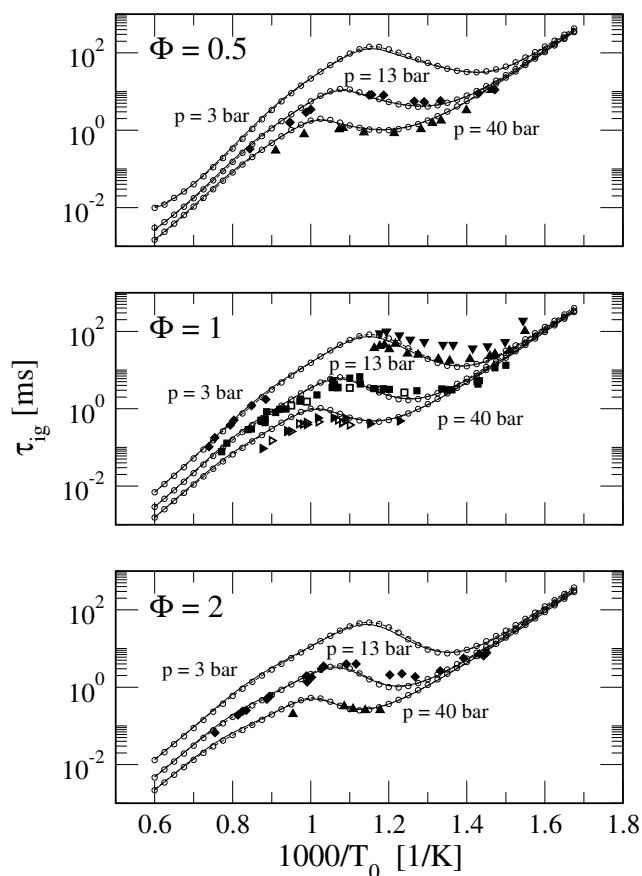


Figure 2.27: Ignition delay times for *n*-heptane. Comparison between experiments [21, 86, 49] (symbols), detailed mechanism (solid lines), mechanism lumped at the detailed level (dashed lines), and at the skeletal level (dotted lines with circles).

### 2.5.2 Full Reduction of an Iso-Octane Detailed Mechanism

As a final example, the three reduction techniques are applied successively to reduce the LLNL comprehensive iso-octane oxidation mechanism by Curran et al. [26]. The sample state space includes auto-ignition, plug-flow reactors, and premixed flames. The order of the reduction techniques is as follows. First, DRGEP removes negligible species and reactions until some error tolerance of about 15% for the chosen targets is reached. Removing more species at this stage would bring the error up considerably, as parts of some important parallel pathways would be removed. Although each channel individually does not contribute much to the global fluxes, discarding too many of them ends up introducing a lot of

error. These pathways are lumped together in the next stage of reduction using the isomer lumping method presented above. Then, an additional stage of DRGEP can be applied to bring the number of species further down. Finally, QSSA are introduced to speed-up the computational process. A final reduced mechanism is obtained, that consists of 109 species and 504 reactions, among which 52 can be set in steady-state. Comparison of the results at various stages of reduction are shown in Figs. 2.29 to 2.30.

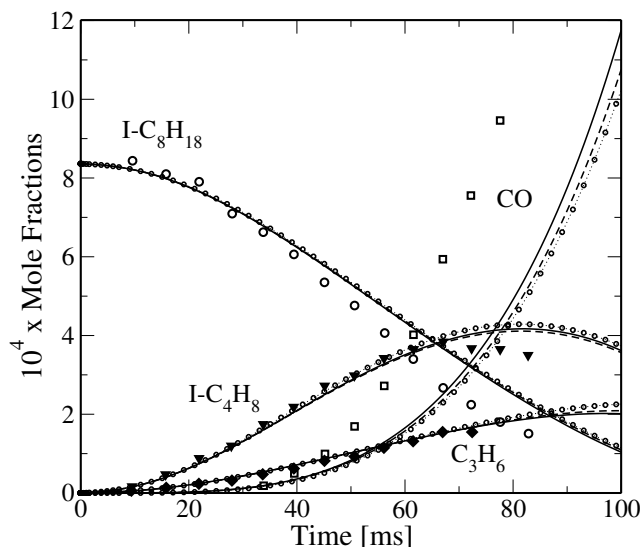


Figure 2.28: Very lean iso-octane oxidation in an atmospheric plug-flow reactor at 945 K. Comparison between experiments [18] (symbols), detailed (solid lines), 195 species skeletal (dashed lines), and 57 species reduced mechanism (dotted line with circles).

Overall, the reduced mechanism reproduces correctly the detailed results for ignition timing, very lean oxidation in PFR and flame propagation. The errors introduced by the reduction are small considering the high reduction ratio, and everywhere negligible compared to the discrepancies with experimental data. For example, laminar burning velocities near stoichiometry or the CO profile in PFR are not correctly modeled by the detailed kinetic scheme. Therefore, it would be more interesting to improve the detailed predictions rather than setting stricter error tolerances in the reduction procedure.

To appraise the benefits of the mechanism reduction, average computational costs are recorded for each skeletal or reduced mechanism, and compared to the cost of using the

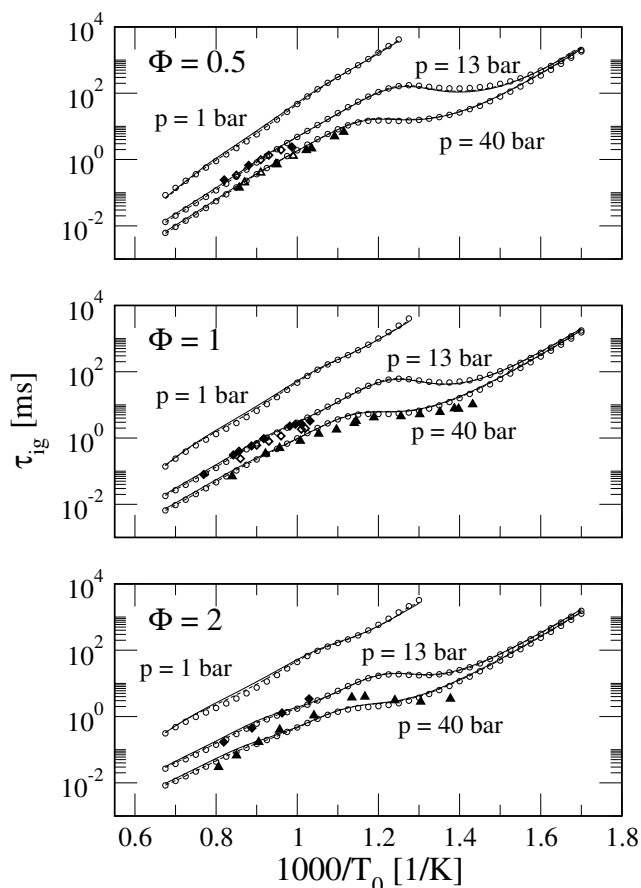


Figure 2.29: Ignition delay times for iso-octane. Comparison between experiments [31, 44, 16] (filled symbols), detailed (solid lines), 195 species skeletal (dashed lines), and 57 species reduced (open circles) mechanisms. Maximum error in ignition delay time is 34.94 %, average error is 10.86 %. Errors in the final concentration of the major products  $\text{H}_2\text{O}$  and  $\text{CO}_2$  do not exceed 0.5 %.

full detailed model. Results are shown in Table 2.4 for homogeneous cases and in Table 2.5 for 1D laminar propagating flames. Moreover, the relative computational costs are plotted versus the relative number of species in Fig. 2.31. Clearly, for both homogeneous and one-dimensional configurations, the observed computational gain scales roughly like the square of the number of variables kept in the system, with a small additional benefit probably linked to the elimination of non-important reactions.

It is interesting to compare the effect of the reduction procedure on the major chemical

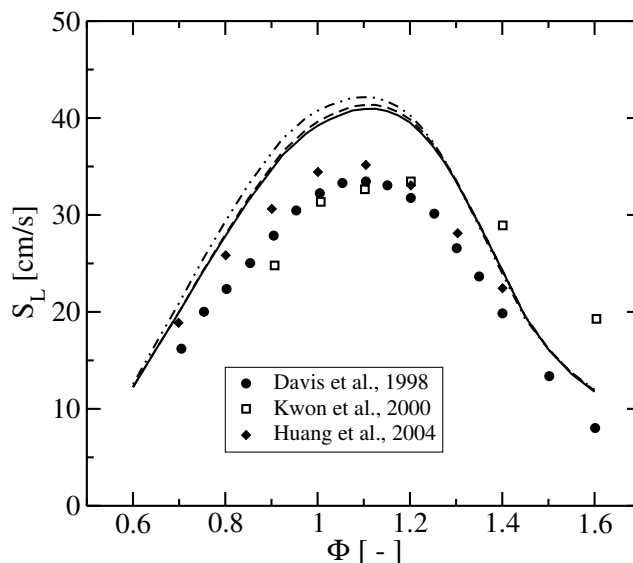


Figure 2.30: Atmospheric laminar burning velocity for iso-octane and air mixtures at 298 K. Comparison between experiments [32, 68, 58] (symbols), 195 species skeletal mechanism (solid line), 134 species lumped (dashed line), and 57 species reduced mechanisms (dash-dotted line). Maximum error with respect to the skeletal mechanism is 5.45 %, average error is 2.81 %.

	Number of species kept		Relative cost
Full mechanism	850	100 %	100
DRGEP (species elimination)	196	23.06 %	4.37
DRGEP (reaction elimination)	195	22.94 %	2.82
Lumping	134	15.76 %	2.16
DRGEP (extra)	109	12.82 %	1.65
QSS	57	6.70 %	0.98

Table 2.4: Relative computational cost for homogeneous simulations of the intermediate skeletal and final reduced mechanisms produced during the integrated multi-stage reduction of a detailed mechanism for iso-octane.

pathways responsible for hydrocarbon auto-ignition over a wide range of temperatures. Curran et al. [25, 26] suggested a few key reaction pathways responsible for the non-monotonic reactivity of alkane/air mixtures with temperature. The first one concerns the fate of the alkyl radical  $\dot{R}$ , that can either decompose through  $\beta$ -scission, or react with molecular oxygen to form  $\dot{R}O_2$  and the subsequent low temperature species. A second one is the

	Number of species kept		Relative cost
DRGEP (species elimination)	196	100 %	100
DRGEP (reaction elimination)	195	99.49 %	94.35
Lumping	134	68.37 %	34.77
DRGEP (extra)	109	55.61 %	21.38
QSS	57	29.08 %	6.03

Table 2.5: Relative computational cost for propagating flame simulations of the intermediate skeletal and final reduced mechanisms produced during the integrated multi-stage reduction of a detailed mechanism for iso-octane.

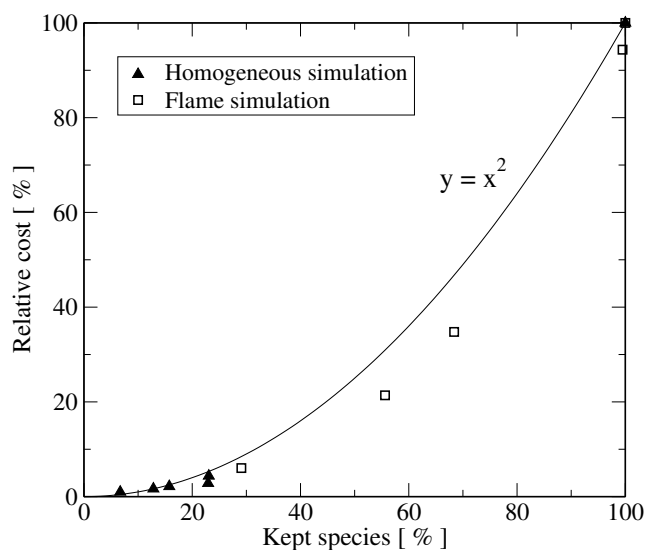


Figure 2.31: Relative computational cost versus the number of variables kept in the kinetic system, for both homogeneous and propagating flame simulations using the intermediate skeletal and final reduced mechanisms produced during the integrated multi-stage reduction of a detailed mechanism for iso-octane.

consumption of the alkylperoxy radical  $\dot{Q}OOH$ , that can either follow a chain-propagating path toward epoxides, olefins and  $\beta$ -scission products, or a chain-branching one through a second  $O_2$  addition. Figure 2.32 shows the relative contribution of the main consumption paths of the alkyl and the alkylperoxy radicals as function of the temperature for both the detailed and the 57 species reduced mechanism. At high temperature, the addition of oxygen to the alkyl radical is negligible in both detailed and reduced mechanisms. However, the  $\beta$ -scission pathway accounts for only 80 to 90% of the consumption of  $\dot{R}$  in the detailed

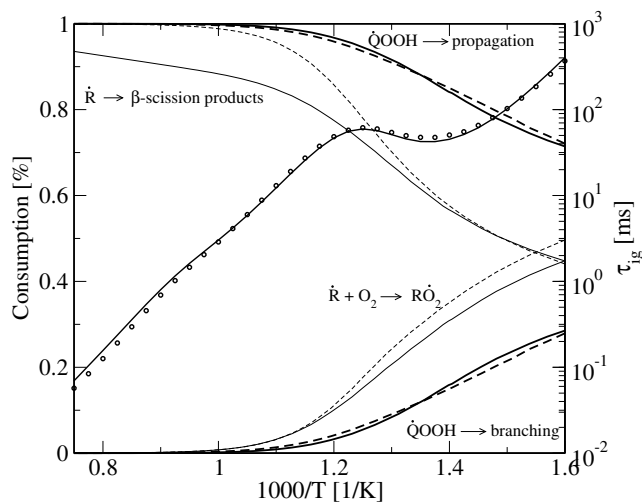


Figure 2.32: Effect of reduction on key consumption pathways of the alkyl radical  $\dot{R}$  and alkyperoxy radical  $\dot{Q}OOH$  as function of the temperature in auto-ignition of iso-octane: Comparison between detailed mechanism (solid lines) and reduced mechanism (dashed line). Corresponding ignition delay times are added for reference.

mechanism, whereas it appears as the only pathway retained in the reduced mechanism. The elimination of the additional consumption channels might explain the somewhat larger error introduced in ignition delay time at such high temperatures. Also, reaction paths accounting for about 5% of  $\dot{R}$  consumption at low temperature have been discarded during the reduction procedure. On the other hand, the branching ratio between chain-propagating and chain-branching  $\dot{Q}OOH$  consumption paths is accurately reproduced by the reduced mechanism.

## 2.6 Summary

An error propagation method has been proposed and evaluated for the systematic and fully automatic reduction of large kinetic mechanisms. Coupled with a directed relation graph method, the technique leads to a finer selection of the chemical paths important for a set of targets. Adequate scaling and consistency checks have been introduced that greatly enhance the efficiency of the reduction procedure. Also, a lumping method has been devised, that leverages information from the detailed mechanism to accurately derive kinetic rate

coefficients for the lumped scheme. It was applied in the reduction of large hydrocarbon oxidation mechanisms, by replacing chemical isomers by one single representative lump. The rate optimization procedure was shown to be more accurate than other existing methods, especially in the very sensitive NTC region typical of low temperature ignition of large alkane molecules. Mass fluxes through the isomers and dynamic properties of the system were conserved satisfactorily. An additional module that identifies suitable quasi-steady state species and that automatically produces efficient QSS equation evaluation code has been added. The different reduction techniques were incorporated into a more general multi-stage reduction strategy. The quality of the results was fairly insensitive to the order in which the reduction techniques were applied. Whereas one single technique is not powerful enough to reduce comprehensive mechanisms to a practical size, the combination of several methods has been shown to achieve such reduction levels. As an example, an 850 species mechanism was reduced to a 57 species scheme that still has excellent predictive capabilities.

## Chapter 3

# A Modular Approach to Model Transportation Fuel Chemistry

### 3.1 From Real Fuels to Surrogate Fuels

As a very large portion of primary energy production in the world comes from burning fossil fuels, it is not surprising that fuels currently used for transportation purposes are derived quite exclusively from petroleum, although a major effort is on-going to diversify the energy sources. A simple way to consider the different types of petroleum-based fuels is to associate each of them to a specific engine technology: gasoline with internal combustion, spark-ignition engines, diesel fuel with internal combustion, compression-ignition engines and jet fuel, or kerosene, with gas turbine engines. This partition results from both technical and historical factors that influenced the evolution of transportation means over the last century.

The best performance is obtained when the characteristics of the engines match those of the fuel used to run the engine. Therefore, a brief description of the different types of engines and the required properties of the corresponding fuels is provided here. In an internal combustion, spark-ignition engine, a premixed fuel/air mixture is introduced in a combustion chamber, or cylinder, compressed, and ignited by a spark plug. A flame front develops from the spark and propagates through the chamber to burn the entire mixture.

The engine most often runs on a four-stroke cycle, with an intake stroke, during which the fuel/air mixture is introduced in the cylinder, a compression stroke, a power stroke where the hot gases produced by combustion expand and an exhaust stroke, that gets rid of the burned gases. One of the physical phenomena most detrimental to a gasoline engine's efficiency is engine knock. As the flame front propagates through the cylinder, local composition or temperature inhomogeneities may cause the mixture to auto-ignite locally, resulting in a sharp rise of pressure inside the chamber. This very undesirable behavior may engender a loss of power and some local over-heating, and at term, damage the engine. Knocking can be avoided if the fuel used is resistant to auto-ignition, which can be measured through the octane rating of the fuel. The higher the octane number is, the less susceptible the fuel will be to knocking.

The situation for diesel compression-ignition engines is quite different. Indeed, in this type of engine, the fuel is injected only after air has been compressed in the cylinder. The air temperature has been increased by the compression stroke, causing the injected fuel to evaporate quickly and ignite, without the use of a spark plug. Therefore, combustion relies on the capability of the fuel to auto-ignite, which is measured using a different scale called the cetane rating. A high cetane number fuel will auto-ignite more readily than one of low-cetane number. Definition of octane and cetane ratings will be given later. Compression-ignition engines, running on diesel fuel, have comparatively a higher efficiency than gasoline engines, mostly because the fuel-air ratio can be varied depending on the desired power output. This mode of combustion, however, that may produce fuel-rich pockets and higher burning temperatures, leads to increased pollutant formation, that recently restricted the use of diesel engine to heavy-duty or stationary engines. Present technical progress in engine designs and after-treatment of exhaust gases, however, will probably change this trend in the future.

An hybrid technique between gasoline spark ignition and diesel compression ignition has gained much interest lately. This technique, called homogeneous charge compression ignition (HCCI), uses premixed fuel and air mixtures, as in conventional spark ignition, but relies on the compression stroke to auto-ignite the fuel. As ignition is kinetically controlled,

an accurate modeling of the chemistry, specifically the auto-ignition characteristics of the fuel, is especially important to study and develop this new technology. Both gasoline and diesel fuels are being considered for use in HCCI-type engines.

Jet engines, on the other hand, are not based on pistons and intermittent fuel injection. Instead, the fuel is injected continuously, mixes with surrounding air and burns through a stabilized flame. Therefore, combustion timing is less critical in jet engines than in internal combustion engines. However, other factors such as aromatic content or thermal stability are of crucial importance to those engines, due to the specific, in-flight conditions of operation.

Gasoline, jet and diesel fuels are all produced through crude oil refining processes. These processes can be classified into three distinct categories [38, 40, 39]:

- **Separation processes** The most common is distillation, and this process is also the defining process for transportation fuels, as these are mostly defined by their boiling range, shown in Figure 3.1. The feed is heated at the bottom of a distillation

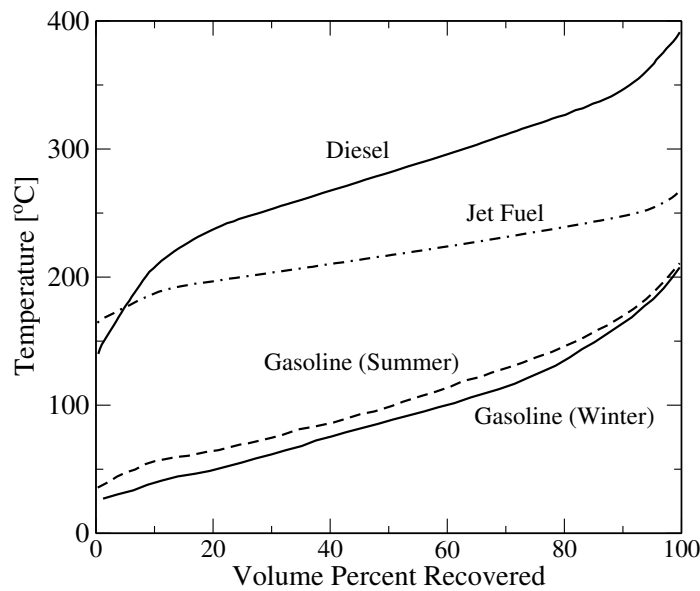


Figure 3.1: Typical boiling curves of the three main transportation fuels.

column, and distillates are removed at different levels of the column depending on their boiling characteristics. The most volatile compounds, such as propane and butane rise to the top of the column. Then, feeds of gasoline, the lightest, kerosene and diesel fuel, the heaviest are extracted from the side, at successively lower points of the column. The remaining part of the feed, too heavy to vaporize, remains at the bottom. The products of the distillation process are called straight-run fuels. However, relying only on this separation process to produce the various fuels is not sufficient. First, distillation yields too much heavy products, not directly usable in conventional engines. Then, the lightest products are often of poor quality and need additional treatment to meet the engine requirements.

- **Conversion processes** These processes change the molecular composition of the feed. Cracking is used to break the heavy molecules left at the end of the distillation process into lighter molecules that can be incorporated in the various fuels. Other conversion processes are used to improve the quality of straight-run fuels. For example, straight-run gasoline has a low octane rating that renders it unsuitable for direct use. Its octane number is increased through reforming, alkylation or isomerization processes, that transform low octane number paraffinic molecules into high octane number ones, such as aromatics or olefins.
- **Upgrading processes** Those are chemical processes that do not change the bulk properties of the fuel, but remove trace species that would otherwise degrade its performances. For example, crude oil and straight-run feeds contain sulfur compounds that are very corrosive, even in trace amounts, and are responsible for sulfur dioxide emissions, a major precursor to acid rains.

The various refinery processes are applied until the obtained fuels meet the requirements of the American Society for Testing and Materials (ASTM). This organization provides a list of the necessary fuel specifications and standard tests to measure the corresponding properties. This list includes for example ignition characteristics (cetane or octane numbers), vapor pressure, distillation profile, sulphur content, flash and freezing points, oxidation and

thermal stability, aromatic content, emission levels and many more. Because the specifications are fairly broad, transportation fuel compositions may vary widely, and at best, only average properties are available. Some of these properties, relevant for the rest of this work, are listed in table 3.1. In this table, HV refers to the heating value, or energy content of the fuel, and MW to its approximate molecular weight. To complicate further the picture,

	Gasoline (regular)	Gasoline (premium)	Jet Fuel	Diesel Fuel
Lower Net HV [MJ/kg]	43.4	42.95	43.3	42.7
Avg. Carbon number	6.9	7.1	11	16
Carbon number Range	4 – 12	4 – 12	8 – 16	9 – 23
Approx. Formula	$C_{6.9}H_{13.5}$	$C_{7.1}H_{13}$	$C_{11}H_{21}$	$C_{16}H_{28}$
MW [g/mol]	$\approx 96.3$	$\approx 98.2$	$\approx 153$	$\approx 220$
Liq. density [kg/m <sup>3</sup> ]	735	755	775 – 840	850

Table 3.1: Average properties of petroleum-based transportation fuels (data have been compiled from several sources [38, 40, 39, 36]).

the predicted scarcity of crude oil pushes towards alternative hydrocarbon fuels, such as synthetic fuels obtained through the Fischer-Tropsch process, or bio-derived fuels that often contain oxygenated moieties. These alternatives fuels do not have a fixed composition either, but are undefined mixtures of numerous compounds, and may be used blended with conventional petroleum-based fuels. Already, blended gasoline containing as much as 10% ethanol for example, is widely available.

Most engine experiments are done using fully blended fuels. However, there is no universal, long term fuel bank that could provide an average or reference fuel that could ensure that every experiment is reproducible. Moreover, improving engine efficiency and evaluating the impact of newly formulated fuels from synthesis or heavy tar requires to understand the underlying fundamental processes. To this end, reducing the chemical and physical complexity of the fuel is highly desirable. Moreover, from a numerical point of view, modeling

accurately all the details of fully blended fuels, for which an exact composition cannot be given, is close to impossible. To overcome these problems, the concept of surrogate fuel, that is, a well-defined mixture of a few components that matches some chemical or physical feature of a practical fuel, was introduced a couple of decades ago. An early example of the use of surrogate fuels can be found in the work of Wood et al. [150], who formulated a 14-species surrogate to simulate the distillation and compositional characteristics of a wide-cut jet fuel. The importance of surrogate fuels in both experimental and modeling work has been emphasized recently through the launching of a broad research effort [129, 110, 43, 22]. From this effort resulted some consensus on how to formulate appropriate surrogates for the three major transportation fuels.

It may be useful to report here the rationale behind the use of surrogates instead of real fuels, what results can be expected and how to validate the surrogate approach in the specific context in which we are interested, that is, fuel combustion in engines. The physical phenomena that have to be considered include injection of liquid fuel, atomization, evaporation, mixing, ignition, and combustion. For all of these, the surrogate simplification assumption is essential to enable the coupling between experimental and numerical work. Simple, well-controlled configurations, that involve a limited number of physical processes, provide a framework in which to test pure components, surrogate mixtures, and the practical fuels themselves. At this level, numerical models such as kinetic mechanisms can be constructed and validated. It has been acknowledged that the “one surrogate fits all” approach is not a realistic approach, and that instead, one should focus on developing an adequate surrogate for each application or physical phenomenon at hand. Then, the surrogate formulation can be assessed in these simple configurations, since a surrogate that exhibits the same trends and behavior as the real fuel in simple context will be more likely suitable for application in realistic devices.

On the other hand, for more complicated configurations such as a whole engine, a surrogate should not be expected to give the same results as the conventional fuels. Indeed, several complex physical and chemical processes may interact with each other, for example,

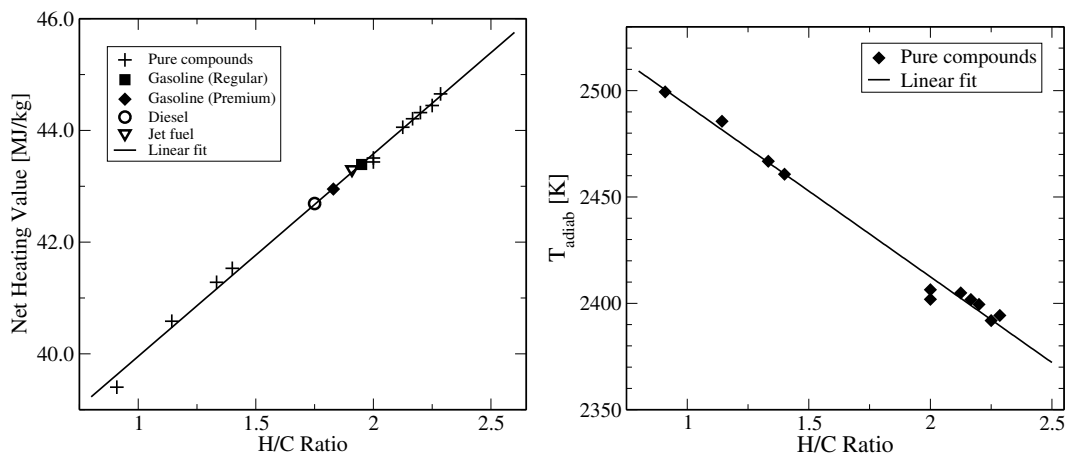
liquid fuel evaporation and gas phase combustion. In such cases, large modeling uncertainties clearly render any comparison meaningless. However, experimental data obtained with the surrogate are still necessary to validate the surrogate approach, enabling parametric studies that were prevented by the complexity and variability of the fully-blended fuels. As the surrogate has been validated in simple configurations to provide the same trends and behavior as the real fuel, we might expect that this holds true also for more complex geometries, and that varying some parameters, such as the amount of aromatics or oxygenated molecules in the surrogate will provide reasonable trends for the emission profiles, for example, enabling a much more focused access to extremely valuable information to design more efficient or greener engines and blended fuels.

Now remains the question of the formulation of the surrogate itself. Although this formulation can be refined further as more experiments and numerical modeling is done, a reasonable guess for the initial surrogate components and composition for various types of applications is needed. To obtain such an initial guess, we need first to identify the important parameters relevant to the physical process studied, relate these parameters to a set of rules or guidelines to choose adequate components and composition, and ideally, optimize these choices given the various constraints rising from safety, availability, or practical considerations.

## 3.2 Selection of Surrogate Components and Composition

As discussed by the surrogate fuels working groups mentioned above, the goal is to identify a limited number of hydrocarbon molecules that can be blended into useful experimental fuels and modeled computationally [110]. Numerical considerations imply that kinetic, thermodynamic, and physical data of adequate quality are available for each of the molecules included in the set. Then, careful analysis of the type of application for which the surrogate is needed must be done, as it will determine the set of relevant targets the surrogate will have to match. A non-exhaustive list of potential targets, their applicability and how they can be evaluated for a fuel mixture, is given next.

**Heating Value, or Energy Content of the Fuel.** This is one of the most important targets, applicable to each type of transportation fuel for combustion applications. It corresponds to the heat released when a known quantity of fuel is burned. The gross heating value of a fuel is obtained when the water produced during combustion is condensed to a liquid. As the water in the exhaust of an engine is in vapor state, a more relevant quantity is the lower net heating values, that considers the combustion products as gas. Heating value can be correlated to a quantity easy to evaluate, which is the hydrogen-to-carbon ratio of the fuel, as shown in Fig. 3.2(a) for a variety of pure hydrocarbon compounds, and average reported lower net heating value for regular and premium gasoline, diesel and jet fuel. Figure 3.2(b) shows that the H/C ratio correlates well with adiabatic temperature for pure compounds, proving that matching the H/C ratio ensures the right energy content and combustion temperature.



(a) Correlation between lower net heating values and hydrogen-to-carbon ratio.

(b) Correlation between adiabatic flame temperature and hydrogen-to-carbon ratio.

Figure 3.2: Correlation between parameters describing the energy content of a fuel and its hydrogen-to-carbon ratio for petroleum-based transportation fuels and a few relevant components present in Fig. 3.3.

**Average Carbon Number.** If both real fuel and surrogate fuel have the same average carbon number (listed in table 3.1), equivalence ratios will be comparable and the air flow will not need too much adjustment to maintain a constant mass flux.

**Physical Properties of Liquids.** These properties include liquid density  $\rho_{\text{liq}}$ , specific heat, viscosity, and thermal conductivity. Dodecane, for example, has physical properties similar to JP-8/Jet A over the 100 – 650°C temperature range and is therefore an adequate surrogate to estimate heat transfer inside fuel systems [36]. Physical properties may be important also in applications that consider the fuel injection system. Those properties usually are bulk properties, that are determined by the composition of the fuel as a whole. Therefore, properties of a surrogate mixtures are easily estimated through linear combination of the properties of the individual components.

**Boiling Characteristics.** As the fuel is inherently in liquid form, evaporation plays an important role in all combustion engines, especially in diesel and gas turbine engines. Atomization and spray combustion is still not fully understood, and these phenomena lack reliable models. To satisfactorily match a distillation curve such as those presented in Fig. 3.1, a surrogate needs to include a large number of components with different boiling points and molecular weights. Several surrogates have been formulated including this constraint, resulting in five- to twelve-component mixtures [35, 150]. However, given the lack of validation data and multi-component evaporation models, the uncertainties in the precise role of evaporation in the subsequent combustion process and the added complexity to the surrogate model, this target may be set aside until more information become available, at least from a modeling point of view. Also, in simulations, these can be independently specified.

**Reactivity.** Both gasoline and diesel engines require an accurate control of the reactivity of the fuel for optimal performance. For spark-ignition engine, the fuel should have a low tendency to auto-ignite, whereas compression-ignition engines rely on fuel auto-ignition to operate. Therefore, two distinct ratings have been developed to quantify the fuel reactivity,

the octane number for gasoline-type fuels, and the cetane number for diesel-type fuels. These numbers are evaluated by comparing the reactivity of a fuel to a reference mixture of two components that have been arbitrarily assigned the values 0 and 100, for different engine configurations. For octane rating, the reference fuels are heptane (fast ignition, value of 0) and iso-octane (slow ignition, value of 100). For cetane rating, these are hexadecane, also called cetane (fast ignition, value of 100) and 2,2,4,4,6,8,8-heptamethylnonane, which is also known as iso-cetane (slow ignition, value of 0). Again, the octane and cetane number of a mixture can be evaluated from those of the individual components [92]:

$$\text{ON}_{\text{mix}} = \sum_{i=1}^{N_S} V_i \text{ON}_i \quad (3.1)$$

$$\text{CN}_{\text{mix}} = \sum_{i=1}^{N_S} V_i \text{CN}_i \quad (3.2)$$

where  $N_S$  is the number of components in the surrogate,  $\text{ON}_i$ ,  $\text{CN}_i$  and  $V_i$  are the cetane number, the octane number and the liquid volume fraction of the individual component  $i$  in the mixture, respectively. Those numbers are not widely used or specified for jet fuels, as combustion in jet engines in normal conditions occurs through hydrodynamically stabilized flames for which reactivity is not important. However, they may have to be considered for more complicated conditions, such as altitude re-light.

**Pollutant Emissions.** It is challenging to estimate *a priori* the tendency of a fuel to form pollutants during engine combustion, as it is a strong function of the burning conditions. For example, nitrogen oxides are formed in higher quantity in rather fuel-lean, high temperature conditions, whereas soot forms primarily in fuel-rich, slightly lower temperature conditions. However, composition of the fuel definitely plays a role, as aromatic and branched hydrocarbons have consistently shown a higher propensity to form soot compared to other classes of compounds [53].

A convenient measure of the sooting propensity of a fuel is the smoke point (SP), which is the largest flame height without smoke emission under laminar diffusion combustion.

Indeed, its inverse, called the threshold sooting index (TSI), was found to correlate very well with actual particulate matter emissions [153]. TSI numbers were introduced by Calcote et al. [15] and are linear functions of the reciprocal of the smoke point involving the molecular weight of the molecule:

$$\text{TSI} = a \left( \frac{\text{MW}}{\text{SP}} \right) + b. \quad (3.3)$$

The  $a$  and  $b$  constants are fitted using two reference compounds so that the TSI can be used universally, independent of the apparatus used. The values  $a = 3.32$  and  $b = -1.47$  proposed by Gill et al. [52] are used to convert the smoke point measurements into TSI. The introduction of the molecular weight offsets the minor flame height increase caused by the increased fuel molecular weight, which requires a larger air/fuel volume ratio for stoichiometric combustion. TSI is usually preferred over smoke point because of its simple mixing rule [52]:

$$\text{TSI}_{\text{mix}} = \sum_k X_k \text{TSI}_k. \quad (3.4)$$

In this equation,  $\text{TSI}_{\text{mix}}$  is the TSI of the mixture,  $X_k$  and  $\text{TSI}_k$  are the mole fraction and the TSI of the pure component  $k$ , respectively. A fuel with a high sooting tendency will have a small smoke point, and conversely, a large TSI.

Smoke point, and therefore TSI, are part of the specification properties of jet fuels. The smoke point should not be lower than 20 mm, which corresponds to an approximate TSI high limit of 40. For the other fuels, threshold sooting indices are not widely used. Instead, specifying the maximum volume fraction of single-ring and multi-ring aromatics is a more common limitation.

**Class Composition.** Finally, it might be interesting to match the compound classes in fuel, namely the fractions of aromatics, naphthenes, paraffins, and olefins. Assuming that each class of hydrocarbon molecules have specific properties, conserving the relative quantity of each class in the surrogate might contribute to recover similar product distribution, reactivity, and emission profiles.

As mentioned above, appropriate hydrocarbon candidates to be included in surrogate fuels should have been studied both experimentally and kinetically, so that validated models of sufficient accuracy are available. A review of available detailed chemical kinetic models for the oxidation of hydrocarbon molecules has been done by Simmie [121]. The surrogate fuel working groups [110, 43, 22] have identified a certain number of such molecules, and their potential relevance to the three major transportation fuels. They are listed in Fig. 3.3. In this work, we have used a certain number of these compounds, namely *n*-heptane, *n*-dodecane for the linear paraffin group, iso-octane and methyl-cyclohexane as branched paraffins, and benzene and toluene as representing the aromatic group.

A constrained optimization algorithm has been developed to facilitate the formulation of surrogate composition. The procedure relies on the fact that most properties described above are bulk properties, and thus, easily expressed as combinations of the properties of the individual components. For properties such as threshold sooting indices, for which data may not be available for all components, a group contribution approach has been adopted, that estimates the properties of the mixture as function of the structural groups of the molecules included in the mixture. The procedure follows that described by Yan et al. [152], based on the initial work of Benson et al. [6]. Given a set of potential components, the algorithm returns the optimal composition that matches best the user-specified set of constraints. An example for a three-component surrogate including *n*-decane, methyl-cyclohexane, and xylene is given in table 3.2 for jet fuel.

Clearly, the components chosen are not heavy enough to provide a good representation of the average molecule of jet fuel. However, validated kinetic data for large molecules are very scarce and this constitutes a hard limitation to the choice of appropriate components. Other properties such as the important hydrogen-to-carbon ratio or the TSI of the fuel are easily reproduced. At that point, we have a reasonable surrogate composition that can be used in experimental and numerical studies in order to identify its strengths and weaknesses and further refine the composition.

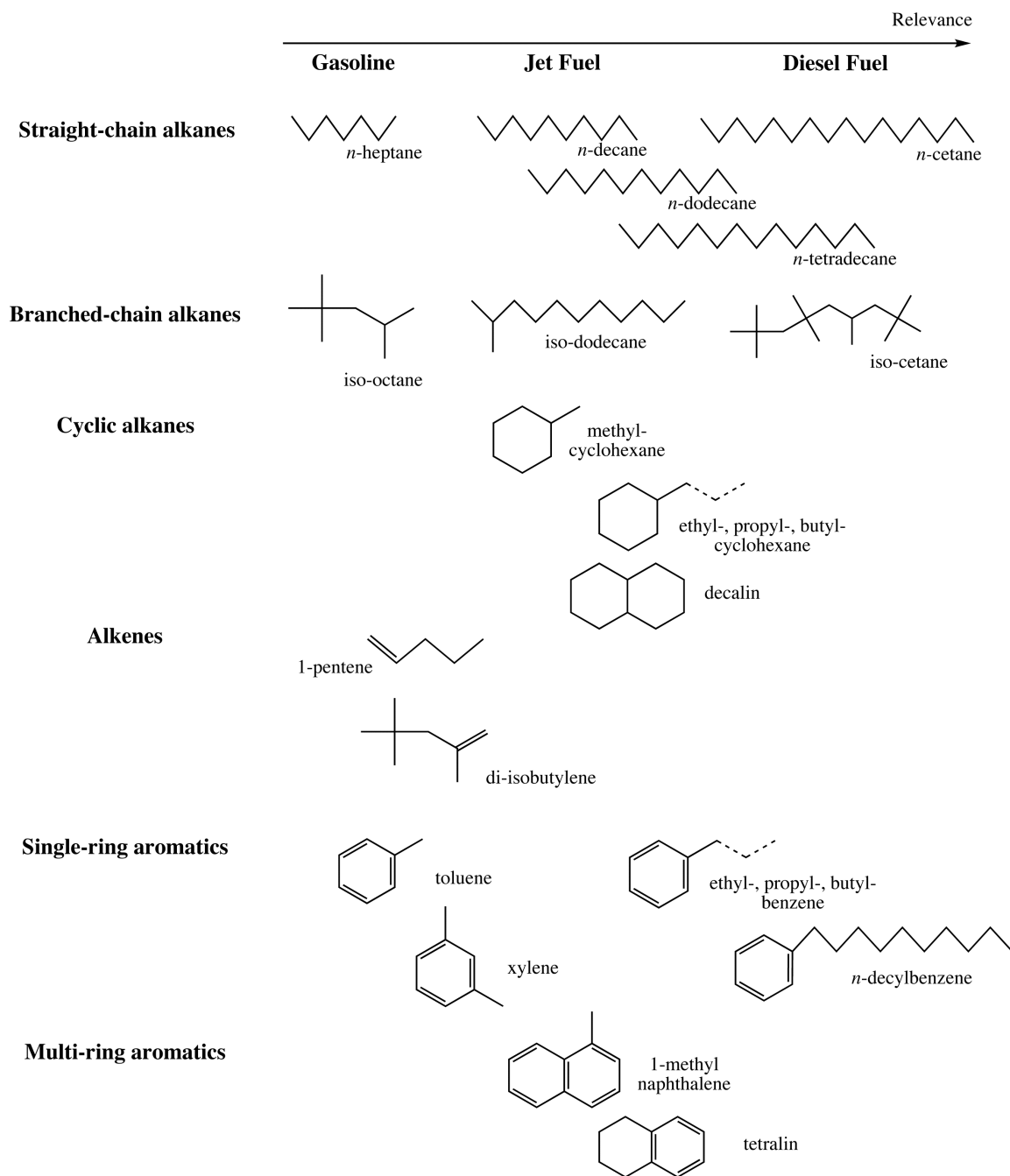


Figure 3.3: Potential components and their relevance to gasoline, diesel and jet fuels as determined by the surrogate fuels working groups [110, 22, 43]

Composition	Jet Fuel Properties <sup>a,b</sup>		Surrogate Example	
	paraffin	60 vol%	<i>n</i> -decane	50 vol%
	cycloparaffin	20 vol%	methylcyclohexane	30 vol%
	aromatics	≤ 20 vol%	xylene	20 vol%
HC ratio	1.91 ± 0.05		1.912	
Carbon number	11		8.4	
MW [g/mol]	153		117.2	
Liq. density [kg/L]	0.810		0.769	
TSI	15 (≤ 40)		15.3	

<sup>a</sup> [153]

<sup>b</sup> <http://www.desc.dla.mil/DCM/Files/2005PQISreport.pdf>

Table 3.2: Example of a three component jet fuel surrogate.

### 3.3 Component Library Approach

#### 3.3.1 Motivation and General Description

It can be inferred from above that developing a chemical model for a transportation fuel surrogate will not be done only once, but it will be rather a dynamic process. CFD simulations require models as short as possible. This requirement definitely sets aside the “one surrogate fits all” approach and favors surrogates tightly tailored to the considered application. But even then, the composition provided by the optimization approach that relies on global characteristics may not be fully adequate for the problem at hand and further experimental data may suggest some different composition or additional components. For example, the surrogate proposed by the jet fuel surrogate work group [22], composed of 50% *n*-decane, 25% *n*-butylbenzene, and 25% *n*-butylcyclohexane, was tested in a pressurized flow reactor and in a single cylinder research engine and its characteristics in terms of flame ignition and extinction in counterflow flames were compared to an average jet fuel. Although the surrogate matched the hydrogen-to-carbon ratio, it was consistently much more reactive than the fully-blended fuel, and therefore, was not an acceptable surrogate. They suggested the use of multi-substituted aromatics or iso-alkanes to reduce the reactivity of the mixture.

On the other hand, detailed chemical mechanisms undergo constant modifications, as the knowledge and understanding of the underlying kinetic processes increase, and these

modifications must be incorporated into the reduced schemes for surrogate fuels as well. An additional challenge lies in the sizes of detailed models. If the detailed kinetic description of a single component involves up to a thousand species and several thousands reactions, combining several of these to form the model for a surrogate is clearly not a trivial task, and the chance of introducing incoherences, such as truncated paths or involuntarily duplicated reaction pathways are very high. Moreover, mechanisms of these sizes are unpractical to use even in the simplest configurations, numerical problems may arise and most importantly, no accurate and detailed analysis and validation of the mechanism can be carried out, rendering any reduction algorithm inefficient or at best, extremely slow.

We propose here a methodology to construct reduced kinetic models for surrogate fuels that is based on two principles:

- **Simplification:** Each type of mechanism manipulation has to be done at its simplest level. For example, reduction should be done on single component mechanisms, as it reduces both the size of the initial scheme and the extent of the validation domain. Also, combining kinetic data of single components to form mechanisms that can handle mixtures should be done with the smallest possible starting mechanisms, ideally skeletal ones.
- **Flexibility:** The addition of another component in the definition of the surrogate mixture should not require the entire process to be repeated. Instead, only the parts relevant to this extra molecule should be added. In the same way, if some additional feature, such as the ability to predict nitrogen oxides, is desired, it should be possible to add it without changing the core of the remaining mechanism.

The layout of the approach followed in this work is provided in Fig. 3.4. It is a modular approach that relies on a library of skeletal mechanisms, or component library, to efficiently build kinetic schemes for mixtures. Given the type of fuel and the application, a surrogate composition can be devised through the optimization process presented above. On the chemistry side, existing detailed mechanisms for individual components are validated against experimental data, then reduced for various conditions to the skeletal level using

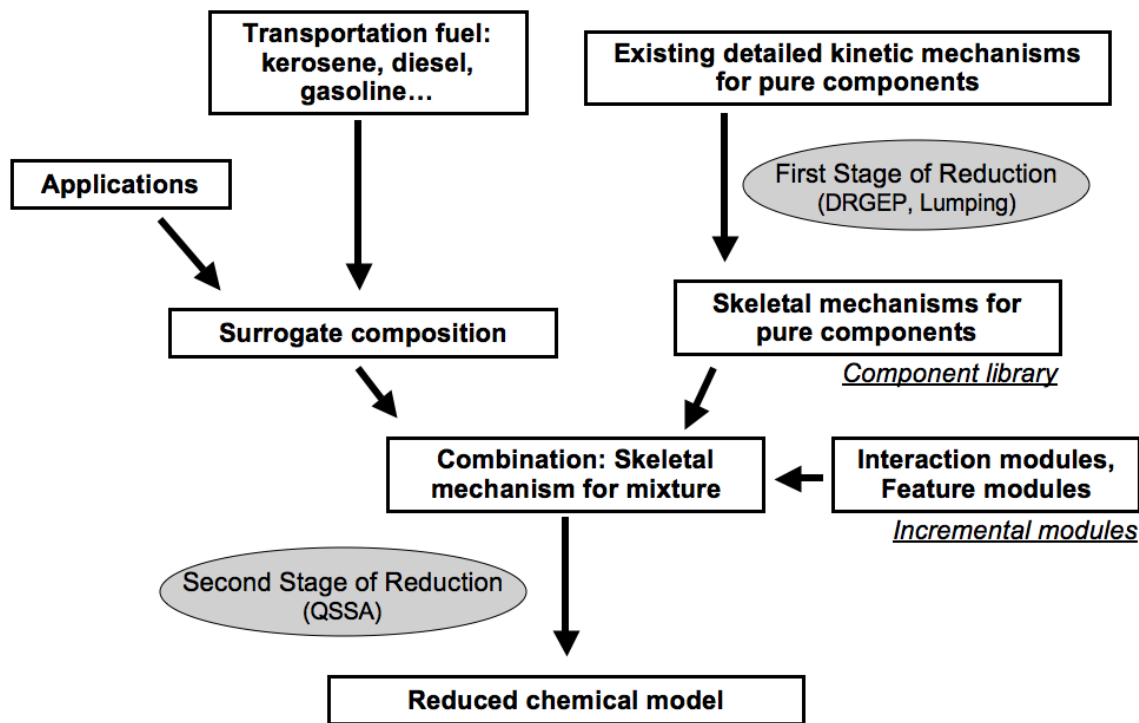


Figure 3.4: Layout and features of the component library approach.

two reduction techniques: the DRGEP method, and a chemical lumping technique. The collection of skeletal mechanisms forms the so called component library, to which several specific modules can be added, such as a description of soot formation or  $\text{NO}_x$  chemistry. The surrogate composition and its future use dictates the choice of modules that have to be included in the combined skeletal mechanism, so that only the necessary kinetics are taken into account. Then, a second stage of reduction is applied, that includes for example the introduction of quasi-steady state assumptions. The obtained reduced model can be validated using available experimental data. The results of this last step will provide additional constraints that have to be included in the surrogate definition phase, and the whole process can be repeated until an optimal surrogate is obtained. The major reduction steps, that is DRGEP and lumping, are done only once, which minimizes the turn-over time to produce the surrogate mechanism.

### 3.3.2 Assumptions and Challenges

The component library approach as described above and its efficiency are based on two major assumptions. The first one is that two different large hydrocarbon molecules will interact during combustion only at the level of small radicals and decomposition products that are present already in both detailed mechanisms. Cross-reactions between fuel-specific molecules are neglected. The main argument to justify this assumption involves steric factors: unless the pressure is very high, the reactive sites of large molecules or radicals are much less accessible by another large species than a small radical such as OH. The validity of this assumption was shown experimentally by Klotz et al [64] and numerically by Zhao et al [157] for toluene/alkane mixtures. In case the cross-reactions between two compounds are shown to be important, incremental sets containing the relevant reactions could be added in the library.

The second assumption is that not all reaction pathways are important for all configurations. This assumption allows the creation of modules through the reduction of the detailed mechanisms on complementary sub-domains of the parameter space. Then smaller multi-component mixtures are obtained by combining only the modules relevant to the application. The best example of this segregated approach is the temperature dependence of the hydrocarbon oxidation chemistry. As will be shown in the first section of chapter 4, the chemistry can be separated into a high temperature base chemistry and a low temperature module that can be superimposed on this base chemistry to represent the characteristic low temperature phenomena.

The chemistry reduction methods and how to determine an initial surrogate mixture composition have been described earlier. It remains to detail here how the various modules from the component library and incremental sets may be assembled together to form a multi-component mechanism. It must be emphasized first that this step is considerably simplified by the fact that the detailed mechanisms have been reduced already to a skeletal level. However, even with this simplification, combining kinetic data from potentially very different sources is a non-trivial task. Species, thermodynamic and transport data, and

elementary reactions need to be merged. To do that most efficiently, an interactive set-up has been designed, that automatically identifies identical species and reactions from the modules and records every multiple choice and incompatibility between the kinetic data sets, for example, species with the same formula, but different names, that could be identical molecules or different isomers of the same species, or identical reactions with significantly different rate coefficients. These discrepancies cannot be resolved automatically, therefore, they are subjected to the user's expertise, who decides which option is the best available.

The problems and incompatibilities usually arise for mechanisms with very different C<sub>0</sub>-C<sub>3</sub> base chemistry. For example, the 177-species skeletal mechanism for auto-ignition of *n*-heptane developed in section 2.5.1 is combined with the GRI3.0 mechanism, optimized for methane oxidation [123]. The GRI3.0 mechanism serves as reference, meaning that when a reaction is present in both mechanisms, but with slightly different rates, the rates from GRI3.0 are retained. Figure 3.5 shows ignition delay times as function of the temperature obtained with the initial skeletal *n*-heptane mechanism and those obtained with the combined GRI3.0/*n*-heptane mechanism obtained without modifying any rate coefficient. Clearly, the direct superposition of the two mechanisms introduces large discrepancies in the prediction of *n*-heptane ignition delay times. The few reactions responsible for the differences in auto-ignition behavior can be quickly identified as the branching ratio between



and



in the NTC region, and the reaction of the vinyl radical with oxygen at high temperature



In this case, it was possible to find an average rate between both kinetic sources that improved considerably *n*-heptane auto-ignition while degrading methane auto-ignition as little

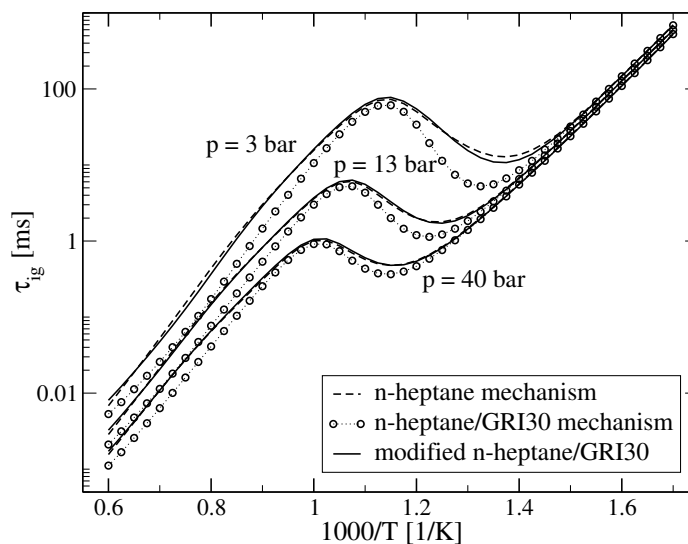


Figure 3.5: Combination of a skeletal mechanism for *n*-heptane and the GRI3.0 mechanism for methane oxidation: some reactions in the basis chemistry of both mechanisms are not directly compatible.

as possible. Ignition delay times obtained using the modified combined mechanism are also shown in Fig. 3.5. This kind of situation is expected to happen quite often, depending on which  $C_0$ - $C_3$  chemistry the mechanisms that are combined are based on. This approach might not always work. However, for the examples described in this work, the conflicts occurring during the combination could all be resolved with minimal user input. Additionally, recently developed detailed kinetic mechanism often rely on the the well-validated GRI3.0 mechanism, which simplifies greatly the combination procedure.

## Chapter 4

# Applications

Two main applications will be described next. The first one is the development of a reduced mechanism for the primary reference fuels *n*-heptane and iso-octane and their mixtures, especially designed to reproduce new measurements of laminar burning velocities at high pressures obtained by Jerzembeck et al. [60]. Therefore, the surrogate composition was fixed by the experimental setup, as a mixture of 87% iso-octane and 13% *n*-heptane. The second application is the development of a reduced mechanism for a jet fuel surrogate. Several components were included in the mixture, involving kinetic data from different sources. This case was chosen so that it gives a detailed illustration of all the steps involved in the derivation of the surrogate fuel mechanism, providing a thorough assessment of the potentials and shortcomings of the component library approach.

### 4.1 Gasoline Surrogate

Two different combustion technologies can be identified for gasoline internal combustion engines. The first one is the conventional Spark Ignition (SI) engine, in which a mixture of fuel and air is ignited by a spark and combustion proceeds by flame propagation through the cylinder. A thorough understanding of the transition from laminar to turbulent flame kernel and to turbulent flame propagation is essential for designing more efficient engines, and it has been shown that the laminar burning velocity is a key parameter for these

phenomena [106, 41, 4]. Auto-ignition of the mixture in an SI engine, relevant for engine knock, is a highly undesirable event that restricts the maximum operating compression ratio, and ultimately, the thermodynamic efficiency of the engine. The second technology is the relatively new homogeneous-charge compression ignition (HCCI) concept, in which premixed fuel and air is compressed until it ignites spontaneously. HCCI engines are of particular interest because of their potential to reduce  $\text{NO}_x$  and soot emissions and because of their higher thermal efficiency compared to SI engines. The performance of an HCCI engine relies on an accurate control of the auto-ignition timing of the mixture. Recent work has shown that charge stratification may be such that both auto-ignition and flame propagation can coexist during the combustion process [23]. Simulating HCCI combustion chemistry therefore requires the ability to accurately predict the auto-ignition behavior of the fuel at high pressures and low temperatures, along with the accurate prediction of flame propagation. Thus, a precise description of the chemical phenomena occurring in both homogeneous combustion and flame configurations is essential in the simulation of an internal combustion engine, either SI or HCCI.

Here, the primary reference fuels, *n*-heptane and iso-octane, will be used as gasoline surrogate components. Many studies, both experimental and numerical, have been conducted to characterize the auto-ignition and flame propagation characteristics of both *n*-heptane and iso-octane. Auto-ignition of *n*-heptane has been studied in shock tube [21, 49] and rapid compression machine [86] experiments, while auto-ignition characteristics of iso-octane and PRF mixtures at elevated pressures have been determined in [44, 16, 31]. Ignition delay times for gasoline have been measured mostly at elevated pressures in [31]. Laminar burning velocities of *n*-heptane, iso-octane, and various PRF mixtures have been measured at atmospheric pressure [32, 58, 65]. Bradley et al. [11] reported laminar burning velocities for iso-octane/air and *n*-heptane/iso-octane/air mixtures up to 10 atm. A few other studies have considered high pressure flame propagation of iso-octane, such as the work of Metghalchi et al. [85], in which data at high pressure were extrapolated from low pressure measurements, or the prior work of Gülder [54]. However, published data of high pressure laminar burning velocities remain scarce and are not always consistent with one another.

On the modeling side, comprehensive chemical mechanisms have been developed for *n*-heptane [25], iso-octane [26], and mixtures of both [27]. These detailed mechanisms have been validated over a wide range of pressures, temperatures, and equivalence ratios in homogeneous configurations. However, their extremely large sizes prevent them from being validated for flame propagation. Recently, Chaos et al. [17] developed a short chemical mechanism to describe the high temperature oxidation and pyrolysis of *n*-heptane, iso-octane, and their mixtures. This mechanism was validated against experimental data for *n*-heptane and iso-octane shock tube ignition delay times, laminar burning velocities at atmospheric pressure, and flow and jet-stirred reactors. Only temperatures above 950 K were considered. To model HCCI combustion, however, low temperature auto-ignition and the negative temperature coefficient (NTC) behavior are essential. As explained in the second chapter of this work, the low temperature chemistry largely differs from what takes place at high temperature and involves a large number of additional oxygenated species.

Using the chemistry reduction and combination techniques presented before, a short chemical kinetic mechanism has been developed, that can be used for gasoline engine simulations. Essential requirements for such a mechanism are the capability to simulate laminar burning velocities of the primary reference fuels and shorter alkanes such as methane, ethane, propane, butane, and iso-butane at low pressures, and an accurate prediction of auto-ignition of the primary reference fuels at all temperatures. Also, measurements of high pressure laminar burning velocities for primary reference fuels and standard commercial gasoline have been obtained to complement the experimental data available in the literature [60]. These new data are included in the validation set of the reduced mechanism as well. Due to the scarcity of experimental data, no mechanism for PRF mixtures have been validated for high pressure propagating flame configurations previously, and the reduced mechanism obtained in this work will be the first one to correctly take into account pressure dependences in flames for large hydrocarbons such as *n*-heptane and iso-octane.

The following sets of experimental data were used for the validation of the mechanism: shock tube ignition delay times for *n*-heptane [21, 86, 49] and iso-octane [31, 44]/air mixtures, with pressures ranging from 1 to 40 bar, equivalence ratios between 0.5 and 2,

and temperatures between 600 K and 1500 K, laminar burning velocities at atmospheric pressure for methane [141, 55, 133], ethane [37, 134, 61], propane [134, 61], butane and iso-butane [32], heptane, iso-octane, and PRF [32, 58, 65], laminar burning velocities at 5 atm for ethane and propane [61], and the new data for burning velocities at high pressure obtained in [60]. The comprehensive mechanisms for *n*-heptane [25] and iso-octane [26] auto-ignition from LLNL are used as starting schemes. This choice is motivated by the fact that these mechanisms are among the most comprehensive schemes existing in the literature.

Both starting mechanisms include hundreds of species and thousands of reactions. Such large sizes are unpractical for computing one-dimensional propagating flames and, therefore, smaller schemes have to be developed. The Directed Relation Graph with Error Propagation method has been used to automatically reduce the original mechanisms to a skeletal size. The reduction has been performed for auto-ignition over a chemical domain covering pressures from 1 to 40 atm, equivalence ratios from 0.5 to 2, and temperatures from 600 K to 1500 K. The temperature range ensures that both high and low temperature chemistry, which are extremely different in the case of large molecules such as *n*-heptane and iso-octane, are retained in the skeletal mechanism. Indeed, at high temperatures, oxidation proceeds through direct decomposition of the fuel radicals to smaller species, whereas at low temperatures, molecular oxygen addition on fuel radicals is favored, and the reaction pathway proceeds through oxygenated species such as ketohydroperoxides, leading to complex two-stage ignition and negative temperature coefficient behavior. The major assumptions made at this point are that the detailed mechanisms already include the correct chemical paths for propagating flames, and that this first reduction step does not remove any reactions significant for laminar flames. The latter assumption was verified for fuels up to butane by removing all species with more than four carbon atoms from the detailed LLNL mechanisms. These sub-mechanisms, including only about 200 species, were small enough to be used in 1D calculations. No significant differences, both in laminar burning velocity predictions and in the chemical structure of the flame, were found when comparing them to the skeletal mechanisms for auto-ignition, demonstrating that no major chemical paths

in flames were removed from the detailed mechanism.

Moreover, as will be confirmed below, low temperature chemistry plays a negligible role in propagating flames. For practical purposes, the skeletal mechanisms were further reduced for high temperature cases only, this time by including auto-ignition cases in the DRGEP process, with temperatures larger than 1000 K and a selection of 1D propagating flames for the various alkanes used for validation. The species and reactions discarded during this step constitute a low-temperature module that will be added to the kinetic scheme only when low-temperature auto-ignition characteristics are needed.

The reduction steps have been done for each mechanism, *n*-heptane and iso-octane, independently. As the goal is to derive a mechanism able to simulate PRF mixtures, the resulting skeletal mechanisms are combined. The original detailed mechanisms are very similar, as far as the base chemistry ( $C_1$  to  $C_4$  species) is concerned. For auto-ignition, the combined mechanism can be based on either base chemistry, the resulting differences in the numerical solutions were found to be negligible. However, one extremely sensitive reaction for methane burning velocity has a different rate in the detailed mechanisms, namely:



In the iso-octane mechanism, the third body efficiency of this reaction is set to unity for all species, whereas in the *n*-heptane mechanism, the third-body efficiency of water is set to 12. Figure 4.3(a) illustrates the effect of the definition of this reaction's third body on the burning velocity of methane. Using a large efficiency coefficient for water adds about 6 cm/s to the stoichiometric burning velocity, as compared to using a unity coefficient. In the combined mechanism, an intermediate third body has been chosen, in which water has an efficiency coefficient of 6. In the case where common reactions between the *n*-heptane and the iso-octane skeletal mechanisms have slightly different rates, the rates from the *n*-heptane mechanism are also retained. Aside from reaction 4.1, this choice does not affect the results.

The original detailed mechanisms from LLNL were not validated for propagating flames

due to their large size. When the skeletal high temperature mechanisms for *n*-heptane and iso-octane are compared to flame experiments, a consistent trend is observed for all data at low pressure and 298 K, in which the simulated burning velocities are much higher than the experimental values. On the other hand, data at higher pressures and temperatures are either predicted correctly or slightly under-predicted by the skeletal mechanism. The strategy chosen at that point for reaching a better agreement between simulated and experimental burning velocities  $S_u^0$  at all pressures was to assume that all necessary paths were already present in the mechanism, and to update those reaction rates most sensitive to flame propagation, but fairly insensitive to homogeneous cases. The objective here was to retain the same level of accuracy for homogeneous cases as for the detailed mechanisms.

The most sensitive reactions for all alkanes involve relatively small species (up to C<sub>4</sub> species). The rate for the reaction



was taken from the GRI 3.0 mechanism [123]. Reaction H147f



was taken from Dean et al. [33]. The H abstraction by the hydrogen radical is taken from the literature review by Tsang et al. [14] for propane and from the three-parameter fit of the NIST database [93] for butane. Large discrepancies are observed between experimental and simulated iso-octane burning velocities, with about 25% error overall. A limited number of reactions have been found to be sensitive for iso-octane flame propagation, but quasi-neutral in homogeneous configurations. These reactions mostly involve the iso-butenyl radical. Although new data are available for its decomposition into allene and methyl radical [158], this new rate was not sufficient to reach a reasonable agreement with experiments and the rate of this reaction was reduced further. Rates for O and OH additions on the iso-butenyl radical and H-abstraction from iso-butene were also modified in order to decrease

Mechanism	$N_S$	$N_{QSS}$	$N_R$
High Temp.	99	35	669
Low Temp. Module	104	65	403
Combined	203	100	1071

Table 4.1: Respective sizes of the mechanisms developed in this work.

the iso-octane burning velocities.

Using the modified rates above, an extra stage of reduction is performed, including chemical lumping and the introduction of quasi-steady state assumptions [105]. Two reduced sets of reactions are obtained at the end of the procedure. The first one contains the base chemistry and fuel decomposition reactions necessary to describe flame propagation and high temperature auto-ignition. In the following, we will refer to this set as the high temperature mechanism. The second set contains only the reactions that are important for low temperature ignition, such as molecular oxygen additions. This low temperature module is not a stand-alone mechanism, and must be added to the previous set to form a combined mechanism valid for both high and low temperature ranges. The sizes of the high temperature mechanism and low temperature module are specified in Table 4.1. In this table,  $N_S$  is the total number of species,  $N_{QSS}$  is the number of species that can be set in steady state without introducing errors in the simulations, and  $N_R$  is the total number of reactions, with forward and backward reactions counted separately. The relatively large size of the low temperature module indicates that it should be included in the mechanism only when low temperature phenomena are of interest, and discarded otherwise.

**Validation for High and Low Temperature Auto-ignition.** Figures 4.1(a) and 4.1(b) show a comparison between experimental data and *n*-heptane and iso-octane ignition delay times obtained using the high temperature mechanism, the combined high and low temperature mechanism, and the original detailed mechanisms from LLNL. The short high temperature mechanism reproduces the ignition behavior correctly up to 1000 K, but diverts from the detailed mechanism in the NTC region, as expected. A satisfactory agreement is obtained between detailed and reduced combined high and low temperature mechanism for

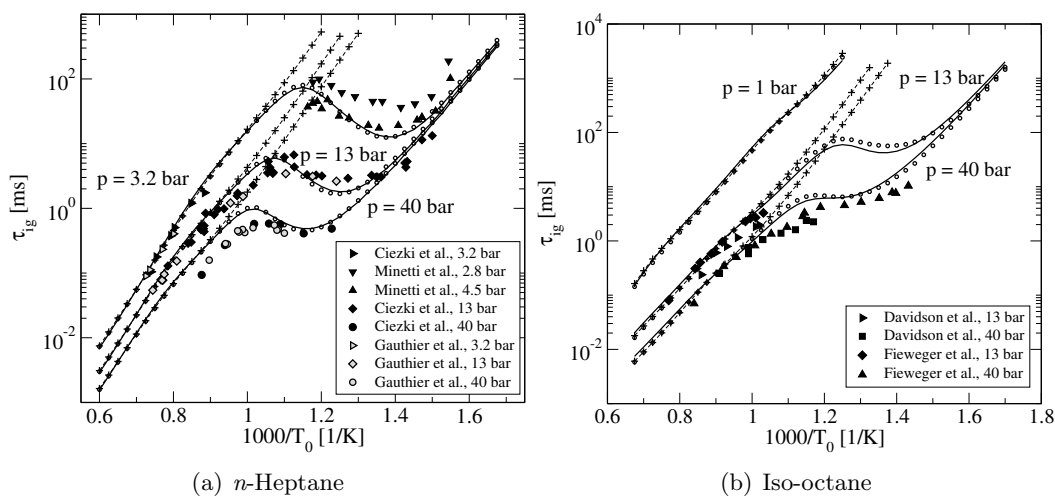


Figure 4.1: Ignition delay times for stoichiometric *n*-heptane/air and iso-octane/air mixtures. Comparison between experimental data (filled symbols) and numerical results obtained using the detailed LLNL mechanisms (solid lines), the reduced combined high and low temperature mechanism (open circles), and the reduced high temperature mechanism (plus symbols, dashed lines).

both *n*-heptane and iso-octane, the largest errors being obtained for iso-octane in the NTC region. Simulated ignition delay times for PRF 87 are compared with the experimental data for gasoline of Gauthier et al. [49] in Fig. 4.2. Although the detailed LLNL mechanism for PRF compares slightly better with experiments than the reduced scheme, the difference between the two mechanisms remains small. Both mechanisms predict longer ignition time than experiments, and the discrepancy can be attributed either to an inaccurate detailed chemical modeling, or an overly simplistic gasoline surrogate composition.

**Validation for Laminar Burning Velocities at Low Pressure.** Laminar burning velocities at low pressures are computed using the reduced high temperature mechanism and compared to experimental values for methane in Fig. 4.3(a), ethane in Fig. 4.3(b), propane in Fig. 4.3(c), butane and iso-butane in Fig. 4.3(d), *n*-heptane in Fig. 4.4(a), iso-octane in Fig. 4.4(b), and PRF 85 to 95 in Fig. 4.4(c).

The overall agreement is very good, especially if the scatter between the various sets of experimental data is considered. A few comments can be made about these results. First,

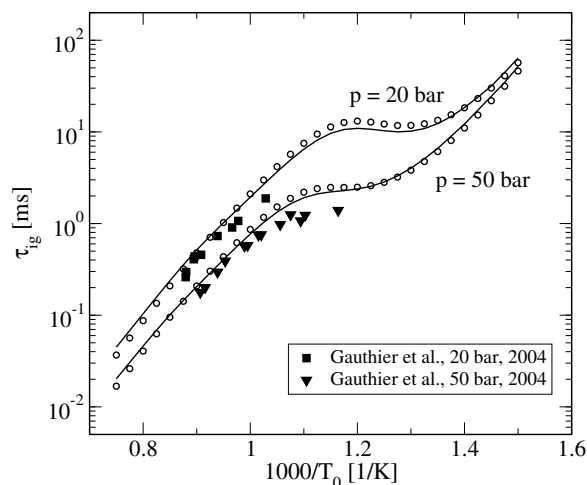


Figure 4.2: Ignition delay times for stoichiometric fuel/air mixtures. Comparison between experimental data for gasoline (symbols) and numerical results for PRF 87 obtained using the detailed LLNL mechanism for PRF [27] (solid lines) and the reduced combined high and low temperature mechanism (open circles).

large hydrocarbons burning velocities are under-predicted for rich configurations. Neither the detailed nor the reduced mechanisms contain an adequate description of the chemistry characteristic of rich oxidation, such as the formation of polycyclic aromatic hydrocarbons, which might explain the observed discrepancy. Also, it might appear that the laminar burning velocities of PRF mixtures are over-predicted when compared to the experimental data from Huang et al. [58]. However, the experimental data from the same group for *n*-heptane and iso-octane are lower than other reported datasets, for example by Davis et al. [32]. For reference, the laminar burning velocities for pure *n*-heptane and iso-octane from Davis et al. have been added in Fig. 4.4(c), and the simulated burning velocities for PRF are, as expected, between the lower values of pure iso-octane and the higher values of pure *n*-heptane. Finally, a comparison between the laminar burning velocities of *n*-heptane when using the high temperature mechanism or the combined high and low temperature mechanism is shown in Fig. 4.4(a). The negligible difference between the results confirms that low temperature chemical pathways play no role in propagating flames.

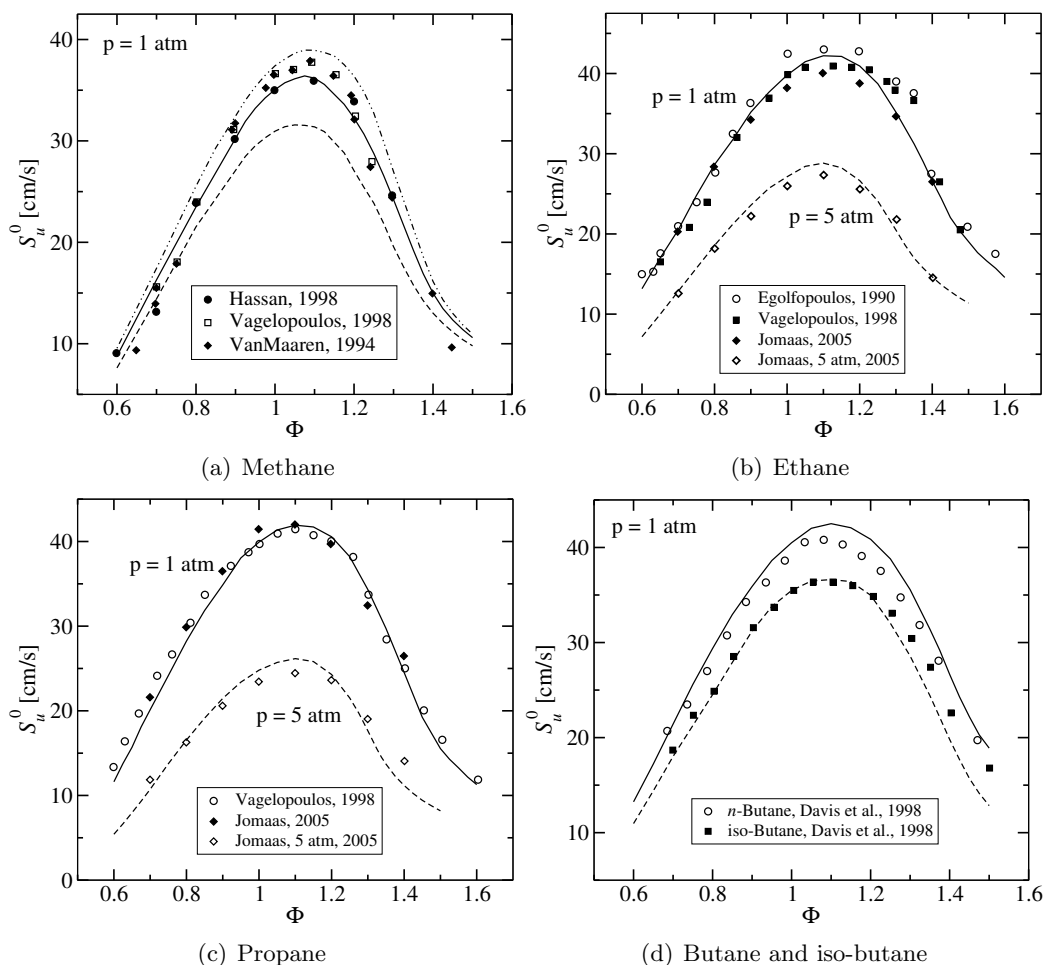


Figure 4.3: Small alkane laminar burning velocities for  $T_0 = 298$  K. Comparison between experimental data (symbols) and numerical results obtained using the reduced high temperature mechanism (lines). Figure 4.3(a) illustrates the sensitivity of  $S_u^0$  to  $\text{H}_2\text{O}$  third body efficiency in reaction H69f ( $= 1$ : dashed line,  $= 12$ : dash-dotted line,  $= 6$ : solid line).

**High Pressure Burning Velocities.** The results for the high pressure unstretched laminar flame velocities are summarized and discussed in the present section. Results are given in Fig. 4.5 for *n*-heptane/air mixtures, in Fig. 4.6 for iso-octane/air mixtures, and in Fig. 4.7 for PRF87 and standard gasoline/air mixtures. To widen the scope of the comparison, experimental data taken from related literature have been added, including the data from Bradley et al. [11] for iso-octane/air mixtures at  $p = 10$  bar and  $T_0 = 358$  K, as well as the extrapolated data by Metgalchi et al. [85], and data by Gülder [54] at  $T_0 = 373$  K.

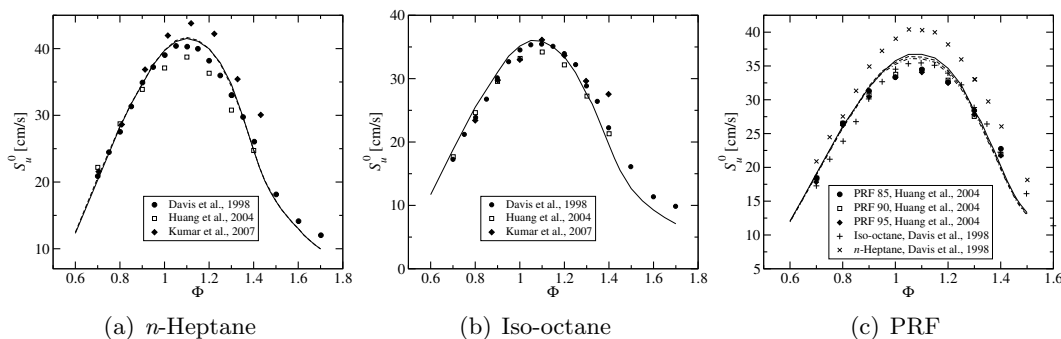


Figure 4.4: Large alkane laminar burning velocities at  $p = 1$  atm and  $T_0 = 298$  K. Comparison between experimental data (symbols) and numerical results obtained using the reduced high temperature mechanism (lines). The dashed line in Fig 4.4(a) is obtained using the combined high and low temperature mechanism, and illustrates the negligible role of the low temperature chemistry in flames.

Surprisingly, Gülders laminar burning velocities at high pressures differ to a great extent from the other sets of experiments and are even higher than data at atmospheric pressure. Therefore, their validity is questionable and these data should not be considered for the validation of the mechanism. Otherwise, the data of Metgalchi et al. [85], Bradley et al. [11] and Jerzembeck et al. [60] at an initial pressure of 10 bar are in excellent agreement with each other. In the following figures, experimental data are taken from Jerzembeck et al. [60], unless specified otherwise.

The predicted laminar burning velocities for *n*-heptane/air mixtures close to stoichiometry are lower than the experimental results for pressures up to 20 bar, whereas for lean conditions or at higher pressure, very good agreement between experimental and numerical results can be observed. In the case of pure iso-octane/air mixtures, simulated results show excellent agreement with experimental data for lean up to stoichiometric mixtures. However, for rich cases, the simulated values tend to have a stronger equivalence ratio dependence compared to experiments. As mentioned before, a possible explanation may be the inadequate representation of rich hydrocarbon oxidation.

PRF87, which consists of 87% iso-octane and 13% *n*-heptane by liquid volume at ambient condition, as well as standard gasoline (octane number 90) for automotive engines, were also investigated. Figure 4.7 shows experimental as well as numerical results for PRF87/air

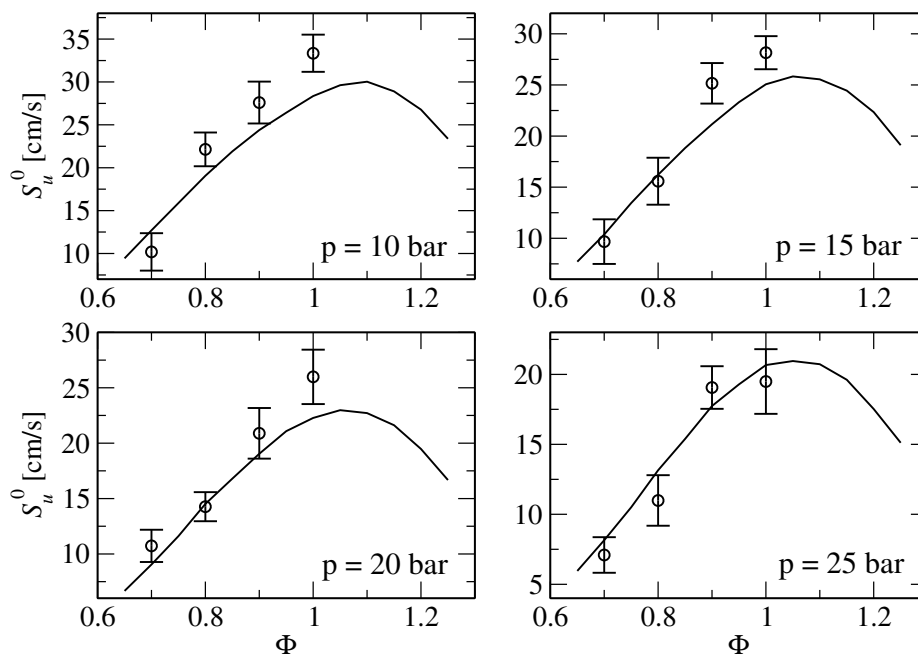


Figure 4.5: Laminar burning velocities of *n*-heptane/air ( $X_{O_2}^{\text{air}} = 0.205$ ) mixtures at high pressures and  $T_0 = 373$  K. Comparison between experimental data by Jerzembeck et al. [60] (symbols) and numerical results obtained using the reduced high temperature mechanism (solid lines)

and gasoline/air mixtures from 10 bar up to 25 bar at 373 K initial pressure. Laminar burning velocities for both PRF87/air mixtures and real gasoline/air mixtures are in good agreement for lean mixtures up to stoichiometric conditions, for which the computed values for the PRF87/air mixtures are approximately 10%-15% lower than the experimental data.

The comparison of the burning velocities of the different fuels shows that PRF87 appears to be a good surrogate for gasoline with similar properties at all pressures. For a better understanding of the pressure dependence with respect to the laminar burning velocity, a comparison is shown in Fig. 4.8. For the lean and stoichiometric mixtures,  $S_u^0$  is a monotonically decreasing function, well reproduced by the kinetic mechanism. As discussed earlier for the rich cases, the computed burning velocities are lower than those from the experiments, which reach an almost constant value for higher pressures.

As dilution of combustible mixtures is important for combustion in automotive engines,

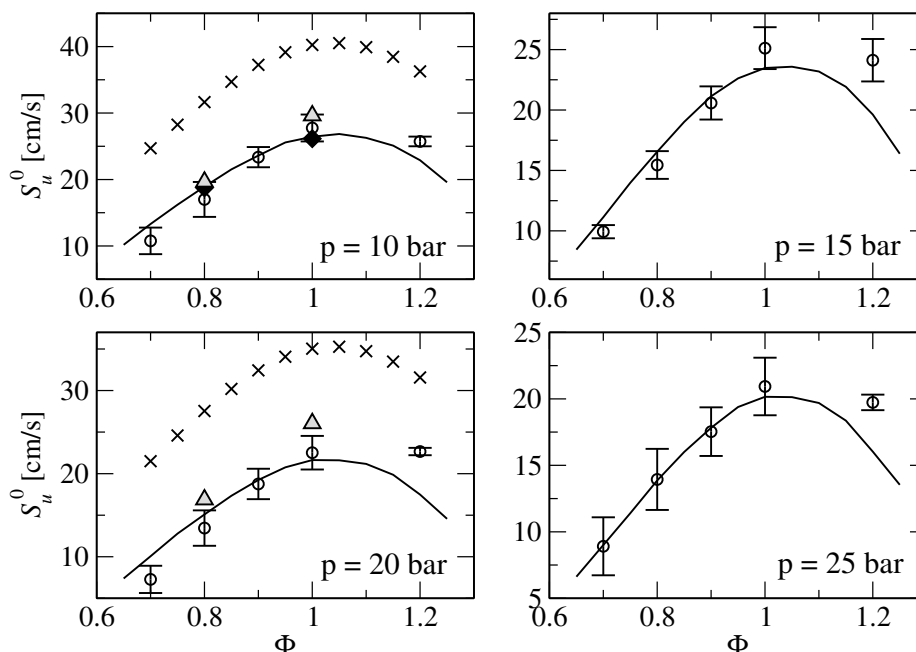


Figure 4.6: Laminar burning velocities of iso-octane/air ( $X_{O_2}^{\text{air}} = 0.205$ ) mixtures at high pressures. Comparison between experimental data at  $T_0 = 373$  K by Jerzembeck et al. [60] (circles), numerical results obtained using the reduced high temperature mechanism (solid lines), data from Bradley et al. [11] at  $T_0 = 358$  K (filled diamonds), data extrapolated at  $p = 10$  and 20 bar and  $T_0 = 373$  K from Metghalchi et al. [85] (triangles), and data by Gülder [54] at  $T_0 = 373$  K (crosses).

especially for EGR (Exhaust Gas Recirculation), laminar burning velocity measurements for diluted gasoline/air mixtures were also conducted in [60]. There are several reasons to dilute combustible mixtures for automotive engines, most importantly the reduction of burnt gas temperatures to reduce the emissions of oxides of nitrogen. Standard gasoline/air mixtures are diluted with pure nitrogen, which is used as a surrogate for engine exhaust gas. The data experimentally obtained for diluted gasoline/air mixtures are compared with computational results for the PRF87 surrogate. Results for two different diluted mixtures are presented in Fig. 4.9. The first mixture uses an oxidizer composed of 15% oxygen and 85% nitrogen, the second one uses an oxidizer composed of 17% oxygen and 83% nitrogen. Both experimental and numerical results show a strong dependence of the laminar burning velocities on the level of dilution of the mixtures. The numerical results agree reasonably

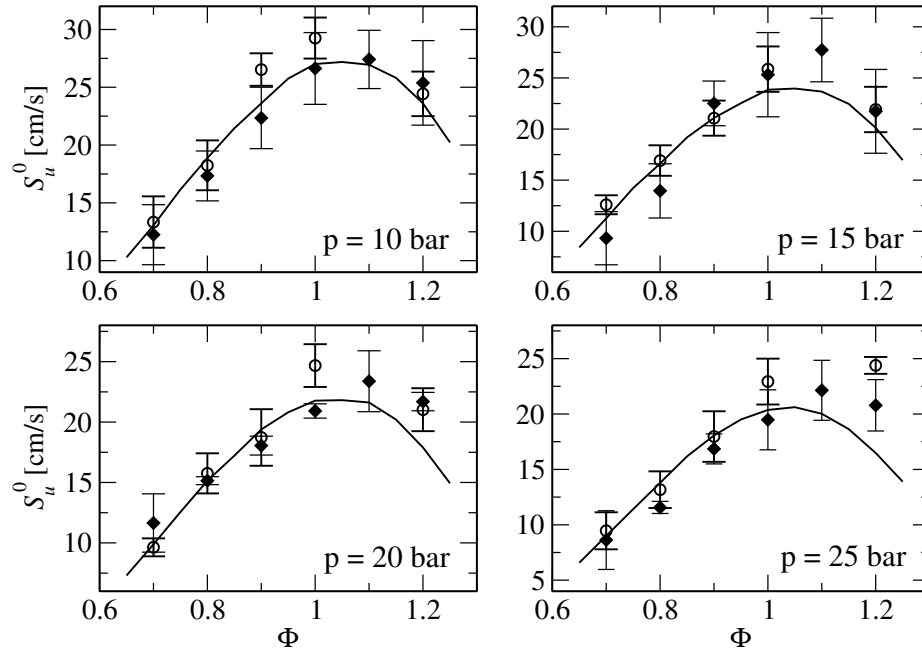


Figure 4.7: Laminar burning velocities of PRF/air ( $X_{O_2}^{\text{air}} = 0.205$ ) mixtures at high pressures and  $T_0 = 373$  K. Comparison between experimental data by Jerzembeck et al. [60] for PRF 87 (open circles) and gasoline (filled diamonds), and numerical results obtained using the reduced high temperature mechanism for PRF87 (solid lines).

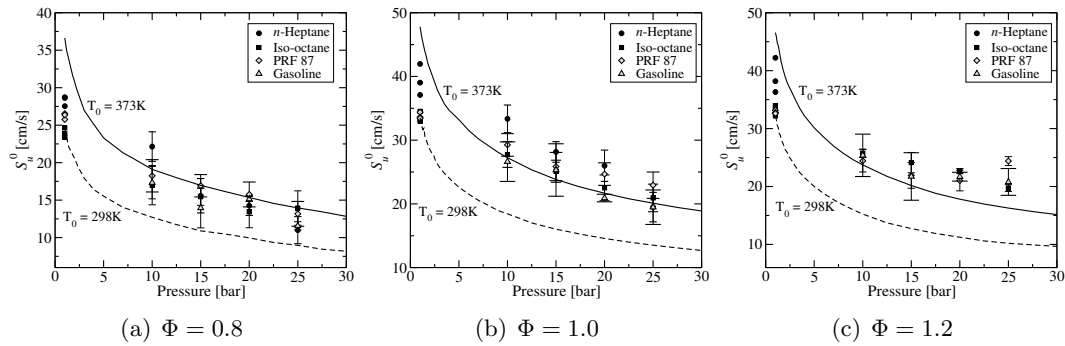


Figure 4.8: Pressure dependence of laminar burning velocities. Comparison between experimental data by Jerzembeck et al. [60] (symbols) and numerical results obtained using the reduced high temperature mechanism for PRF87 (lines). Data at 1 bar are obtained with  $T_0 = 298$  K (simulation: dashed line), data at higher pressures are obtained with  $T_0 = 373$  K (simulation: solid line)

well for the 17% oxygen case. For the 15% oxygen case, the predicted burning velocities are approximately 20%-25% higher than the experimental data for the 10 bar case. For higher

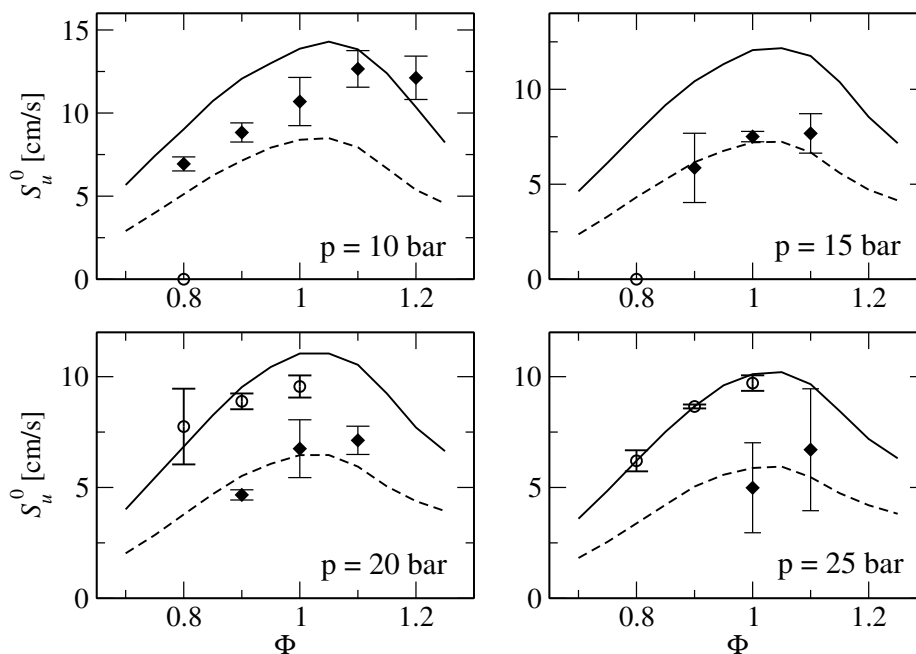


Figure 4.9: Laminar burning velocities of diluted fuel/air mixtures at high pressures and  $T_0 = 373$  K. Comparison between experimental data for gasoline by Jerzembeck et al. [60] ( $X_{O_2}^{\text{air}} = 0.17$ : open circles,  $X_{O_2}^{\text{air}} = 0.15$ : filled diamonds) and numerical results obtained using the reduced high temperature mechanism for PRF 87 ( $X_{O_2}^{\text{air}} = 0.17$ : solid lines,  $X_{O_2}^{\text{air}} = 0.15$ : dashed lines)

pressures, the agreement is quite good.

In summary for this part, a component library for iso-octane and *n*-heptane was created based on the detailed LLNL schemes that for both fuels consists of a skeletal basis module for high temperature auto-ignition and flame propagation, and an optional low temperature module that can be included when low-temperature behaviors such as NTC are necessary. It was demonstrated that the modules can be successfully combined and that the resulting mechanism is able to predict both ignition and burning velocity targets with a good accuracy. Because this mechanism was developed in conjunction with an experimental investigation of high pressure burning velocity characteristics of PRF and gasoline mixtures, a simple 2-component surrogate was used. Nevertheless, very good agreement was obtained between PRF87 and gasoline, both experimentally and numerically, suggesting that, at least for flame propagation, this simple approach is sufficient and the complexity introduced by

additional surrogate components is not needed.

## 4.2 Jet Fuel Surrogate

As a second application of the component library approach, the development of a skeletal model for a jet fuel surrogate has been chosen. Conventional jet fuels, called Jet-A for civil applications and JP-8 for military, have a relatively high average carbon number, and corresponding representative hydrocarbons are difficult to handle experimentally. As a consequence, little experimental data currently exist to assist in the development of detailed chemical mechanisms for large hydrocarbons. As new data become available, the kinetic models will be validated and refined over a wider range of conditions. Therefore, the present work does not attempt to produce a surrogate model that will match perfectly the few data available for jet fuel. Instead, it focuses on the method used to generate the reduced model, especially the successive validation steps. If rigorous validation is performed, discrepancies in the results can be attributed mostly to inaccuracies in the detailed mechanisms and inadequacy of the initial choice of components, which is currently very limited. The subsequent development of better surrogate models will simply follow from improved initial experimental and kinetic data.

### 4.2.1 Surrogate Formulation

Jet fuel is second only to gasoline in the amount of work done on the surrogate topic. Kerosene and its surrogates have been studied experimentally in jet-stirred reactors [30], shock tubes [142], and premixed [34] and counter-flow [24, 59] flame configurations. An exhaustive list of experimental data for kerosene, existing surrogate compositions, and their corresponding applications can be found in a review paper by Dagaut et al. [28].

The choice of the individual components for each hydrocarbon class was motivated mostly by the availability of a reasonably validated detailed chemical mechanism. They include *n*-heptane, iso-octane, and *n*-dodecane as alkanes, methyl-cyclohexane as naphthene,

and benzene and toluene as aromatic molecules. The base mechanism is taken from Blanquart et al. [9]. This mechanism was specifically developed to accurately represent soot formation and was extensively validated using experimental data for soot precursors, PAHs and soot volume fractions. Mechanisms for *n*-heptane, iso-octane, and methyl-cyclohexane are taken from Lawrence Livermore National Laboratories [25, 26, 111], and *n*-dodecane is modeled by a semi-detailed mechanism developed by Wang et al. [151]. The respective sizes of each detailed mechanism are indicated in table 4.2.

Mechanisms		$N_S$	$N_R$
Components	Basis Chemistry	151	1658
	Dodecane	174	2625
	Methyl-cyclohexane	996	8820
	<i>n</i> -Heptane	558	5078
	Iso-octane	850	7212
Multi-component Surrogate		181	1197

Table 4.2: Sizes of the various detailed mechanisms used in the component library approach for the development of a jet fuel surrogate kinetic model.

Three surrogate compositions will be considered. The first one is neat *n*-dodecane. The second surrogate was developed by Violi et al. [145, 35] based on a number of criteria, including sooting tendency and distillation characteristics. The third one is obtained through the optimization procedure described in section 3.2, by prescribing the hydrogen-to-carbon ratio, the average carbon number, the average composition in terms of hydrocarbon classes, the cetane number and the sooting tendency of the fuel. Only three different components were included in the optimization, namely *n*-dodecane, methyl-cyclohexane, and toluene. The resulting composition and a comparison of the properties of the three surrogates are shown in table 4.3.

The domain of applicability of the reduced surrogate models was chosen to represent the most probable operation conditions found in gas-turbine engines, namely high temperature, atmospheric to high pressures, and lean-to-rich conditions. Auto-ignition and pre-mixed conditions are included in the reduction procedure, as newly designed engines tend

		Average Jet Fuel	Neat Dodecane	Surrog. 1	Surrog. 2
Composition [% mol]	Dodecane	N/A	100	73.5	45
	Iso-octane		0	5.5	0
	MCH		0	10	26.1
	Toluene		0	10	28.9
	Benzene		0	1	0
H/C ratio		1.91	2.17	2.09	1.09
Formula		$C_{11}H_{21}$	$C_{12}H_{26}$	$C_{10.7}H_{22.3}$	$C_{9.3}H_{17.7}$
Hydrocarbon composition [% vol]	Paraffins	~60	100	88	62
	Naphthenes	~20	0	6.4	20
	Aromatics	~18	0	5.6	18
Cetane number		~42.7	80	73.4	58
Threshold sooting index		~15	5.2	9.3	16.3

Table 4.3: Compositions for jet fuel surrogate used in comparison with experimental measurements.

to run partially premixed, which inevitably leads to the necessity to control auto-ignition at operating conditions [22]. The detailed mechanisms for the individual components are reduced independently to a skeletal level using DRGEP and chemical lumping. Then, the resulting modules are combined together, with the base mechanism of Blanquart et al. [9] retained as reference. Validation is performed at each stage, and includes:

- Comparison of the detailed mechanism with experimental data
- Comparison of simulations obtained using the single component skeletal mechanism and the detailed mechanism from which it is extracted
- Comparison of simulations obtained for each individual component using the combined skeletal mechanism and the corresponding single component detailed mechanism
- Assessment of the performance of the combined surrogate mechanism by comparing simulation results with experimental data for jet fuels.

These comparisons are carried out in the following sections.

## 4.2.2 Validation of Individual Components

**Benzene and toluene.** Benzene and toluene are part of the base mechanism developed specifically for soot formation simulations. Therefore, the experimental validation set corresponds to the one used by Blanquart et al. [9] for the validation of the detailed mechanism itself. This validation set includes ignition delay time measurements at pressures close to atmospheric, high temperature and lean to rich equivalence ratios, and atmospheric laminar burning velocities. Results are shown in Fig. 4.10 for benzene and Fig. 4.11 for toluene.

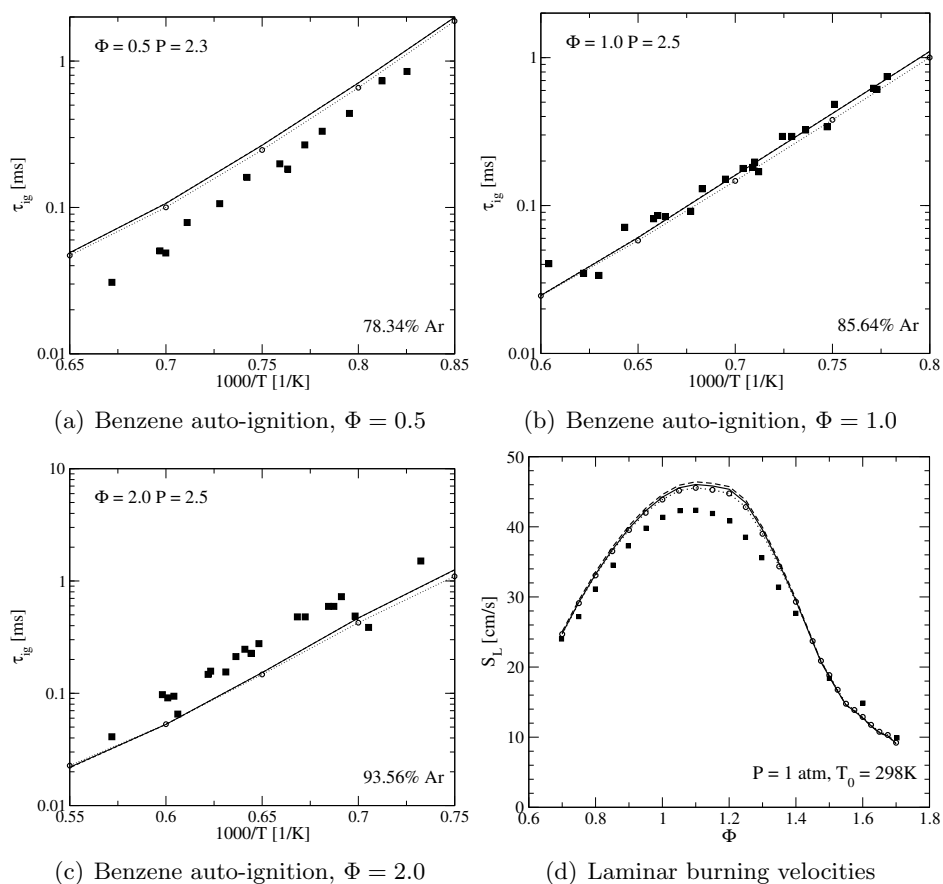


Figure 4.10: Validation of benzene component for auto-ignition (Figs. 4.10(a), 4.10(b) and 4.10(c)) and laminar burning velocity (Fig. 4.10(d)). Comparison between experimental data (filled squares, [13, 32]), detailed mechanism (solid line, [9]), single component skeletal mechanism (dashed line) and surrogate skeletal mechanism (dotted line with circles).

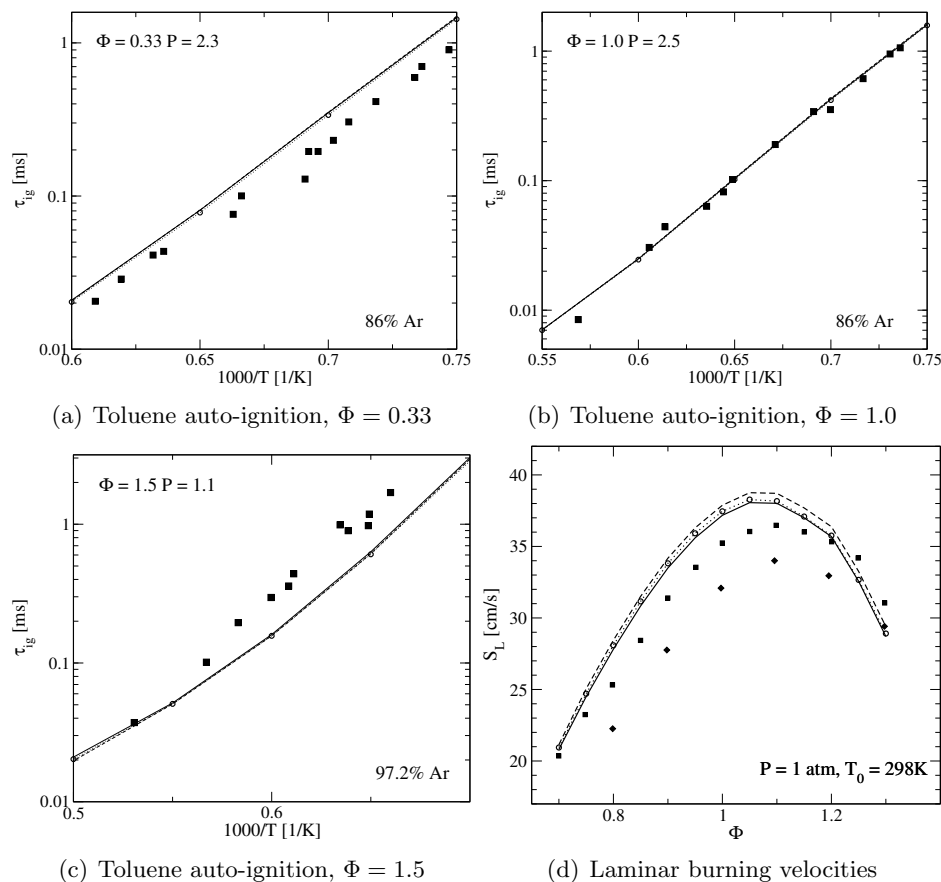


Figure 4.11: Validation of toluene component for auto-ignition (Figs. 4.11(a), 4.11(b) and 4.11(c)) and laminar burning velocity (Fig. 4.11(d)). Comparison between experimental data (filled squares, [13, 102, 32]), detailed mechanism (solid line, [9]), single component skeletal mechanism (dashed line) and surrogate skeletal mechanism (dotted line with circles).

The reduction and combination procedures have little impact on the prediction of ignition delay times and laminar burning velocities of both aromatic species. This was expected, as the reduction procedure is done with an error control, and because the mechanism developed for those two components was taken as reference in the combination procedure, meaning that the reactions involving  $C_0$  to  $C_4$  species used to validate the benzene and toluene chemistry were not affected by the combination process.

**Acetylene.** Although not a potential surrogate component,  $C_2H_2$  has been included in the validation procedure, because this molecule is a well-known soot precursor and plays a crucial role in soot formation. Validation includes ignition delay time measurements and a counter-flow flame with a partially premixed fuel/air mixture injected on the right side, and a fuel/ $N_2$  mixture injected on the left side. Temperature was not imposed from experimental measurements, but directly computed in the simulation. Comparisons between experimental data and the various kinetic mechanisms are shown in Fig. 4.12 for the auto-ignition cases and in Fig. 4.13 for the counter-flow configuration.

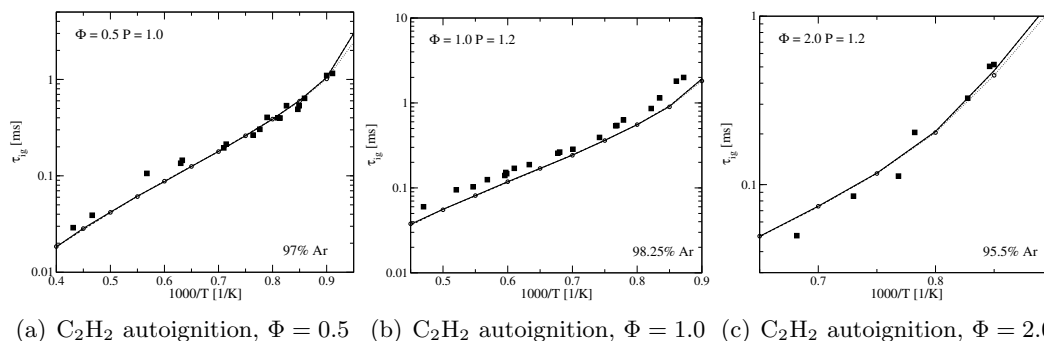


Figure 4.12: Validation of acetylene component for auto-ignition (Figs. 4.12(a), 4.12(b) and 4.12(c)). Comparison between experimental data (filled squares, [56, 118]), detailed mechanism (solid line, [9]), single component skeletal mechanism (dashed line) and surrogate skeletal mechanism (dotted line with circles).

Again, ignition delay times obtained with the skeletal and combined mechanisms agree very well with the original detailed mechanism. The major species profiles in the counter-flow flame are also in very good agreement, except for benzene, whose maximum concentration has been reduced to about half of the original value following the reduction procedure. This may be explained by the fact that benzene was not a target in the acetylene counter-flow flame. Therefore, some chemical pathways relevant to benzene production and consumption have been removed, which impact benzene concentration in the flame, but not global parameters such as benzene ignition delay time or laminar burning velocities. The combination step does not modify the predictions.

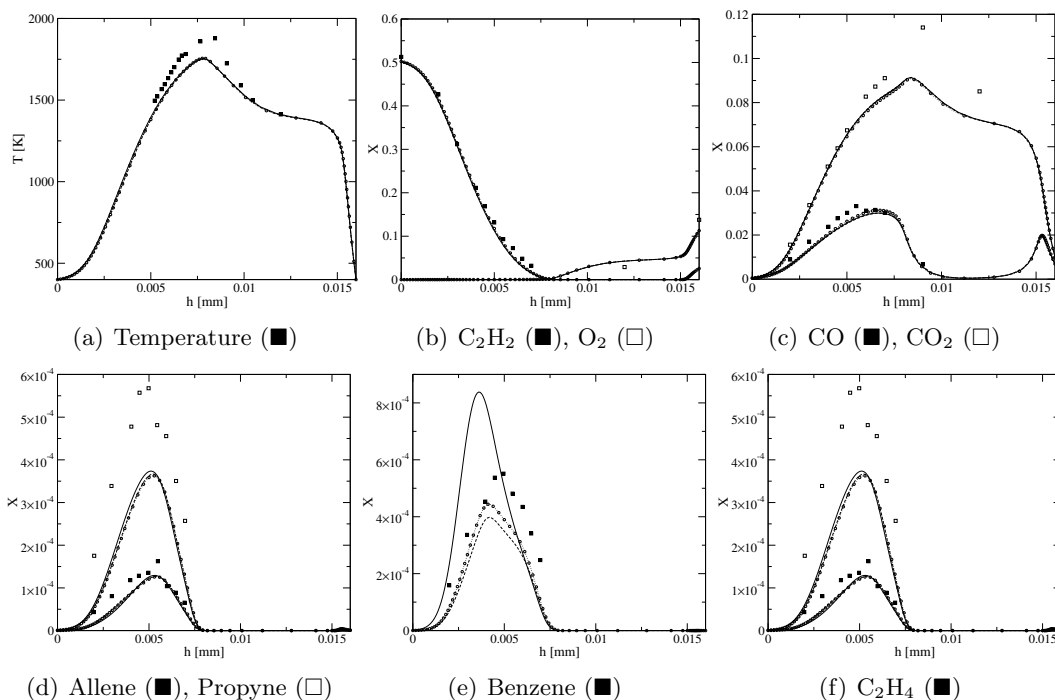
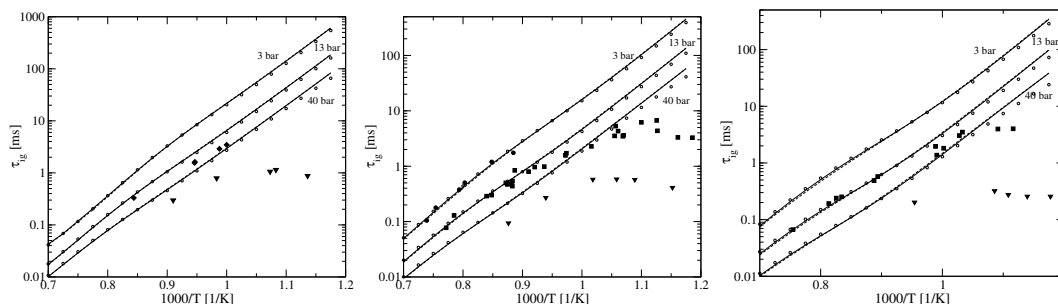


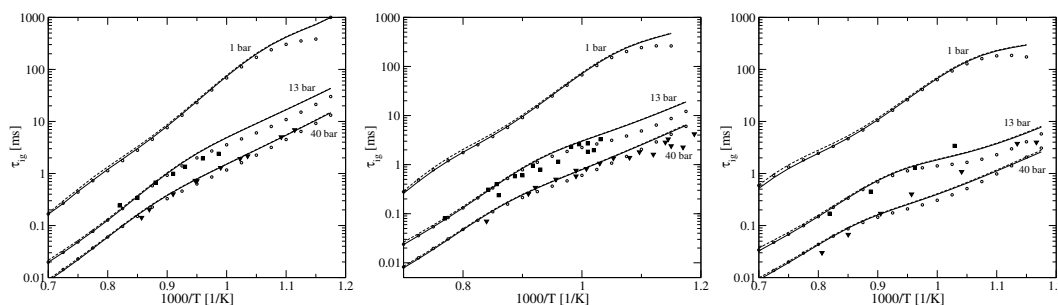
Figure 4.13: Validation of acetylene component in a counter-flow diffusion flame. Comparison between experimental data (symbols, [101, 100]), detailed mechanism (solid line, [9]), single component skeletal mechanism (dashed line) and surrogate skeletal mechanism (dotted line with circles). Thick lines correspond to filled symbols.

***n*-Heptane and Iso-octane** *n*-Heptane and iso-octane detailed mechanisms were reduced and incorporated into the mechanism for soot prediction in Blanquart et al. [9], following the same procedure as described here. Therefore, the prediction of ignition delay times for both alkanes will be compared directly to the predictions obtained using the detailed soot mechanism. Comparisons with the original mechanisms by Curran et al. [25, 26] can be found in [9]. Results are shown in Fig. 4.14 for *n*-heptane and in Fig. 4.15 for iso-octane. The reduction stage has virtually no effect on auto-ignition predictions. However, combining the skeletal soot mechanism with the other component schemes has a non-negligible effect, especially for temperatures below 1000 K. This corresponds to the onset of the ignition timing roll-over due to the NTC behavior. In this temperature region, ignition delay time is extremely sensitive to changes in small radical concentrations, especially the hydroxyl radical  $\dot{\text{O}}\text{H}$ , thus even minor modifications of the base chemistry created



(a)  $C_7H_{16}$  autoignition,  $\Phi = 0.5$  (b)  $C_7H_{16}$  autoignition,  $\Phi = 1.0$  (c)  $C_7H_{16}$  autoignition,  $\Phi = 2.0$

Figure 4.14: Validation of *n*-heptane component for auto-ignition (Figs. 4.14(a), 4.14(b) and 4.14(c)). Comparison between experimental data (filled squares, [21, 49]), detailed mechanism (solid line, [9]), single component skeletal mechanism (dashed line) and surrogate skeletal mechanism (dotted line with circles).



(a)  $C_8H_{18}$  autoignition,  $\Phi = 0.5$  (b)  $C_8H_{18}$  autoignition,  $\Phi = 1.0$  (c)  $C_8H_{18}$  autoignition,  $\Phi = 2.0$

Figure 4.15: Validation of iso-octane component for auto-ignition (Figs. 4.15(a), 4.15(b) and 4.15(c)). Comparison between experimental data (filled squares, [31, 44]), detailed mechanism (solid line, [9]), single component skeletal mechanism (dashed line) and surrogate skeletal mechanism (dotted line with circles).

by the mechanism combination result in significant differences in the prediction. However, these changes remain acceptable when compared to the magnitudes of the discrepancies between experimental data and predictions using the detailed soot mechanism.

**Methyl-Cyclohexane** The next component that needs to be validated is a cyclo-alkane, or naphthene. Comparison with experimental data are shown in Figs. 4.16 and 4.17. Figure 4.16(a) compares ignition delay time measurements at low [98] and higher [111] pressures with predictions using the various mechanisms. As the reduction has been performed for

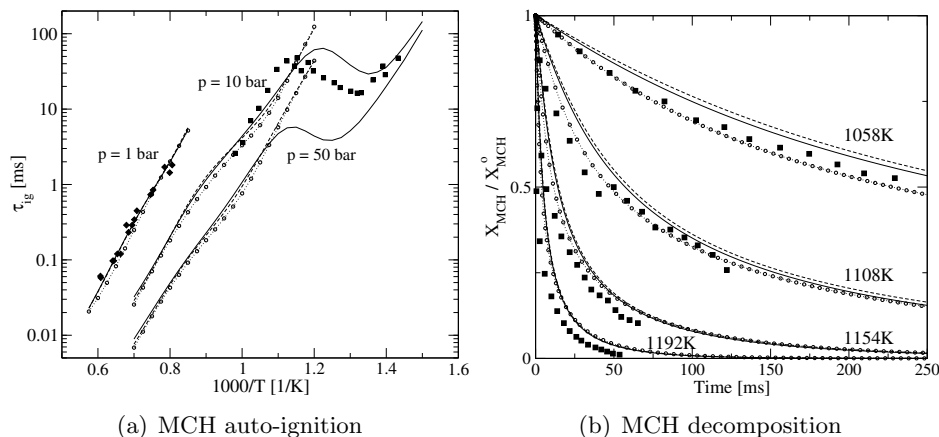


Figure 4.16: Validation of methyl-cyclohexane component for auto-ignition (Fig. 4.16(a)) and fuel decomposition rate in near-pyrolysis conditions (Fig. 4.16(b)). Comparison between experimental data (symbols, [154, 98, 111]), detailed mechanism (solid line, [111]), single component skeletal mechanism (dashed line) and surrogate skeletal mechanism (dotted line with circles).

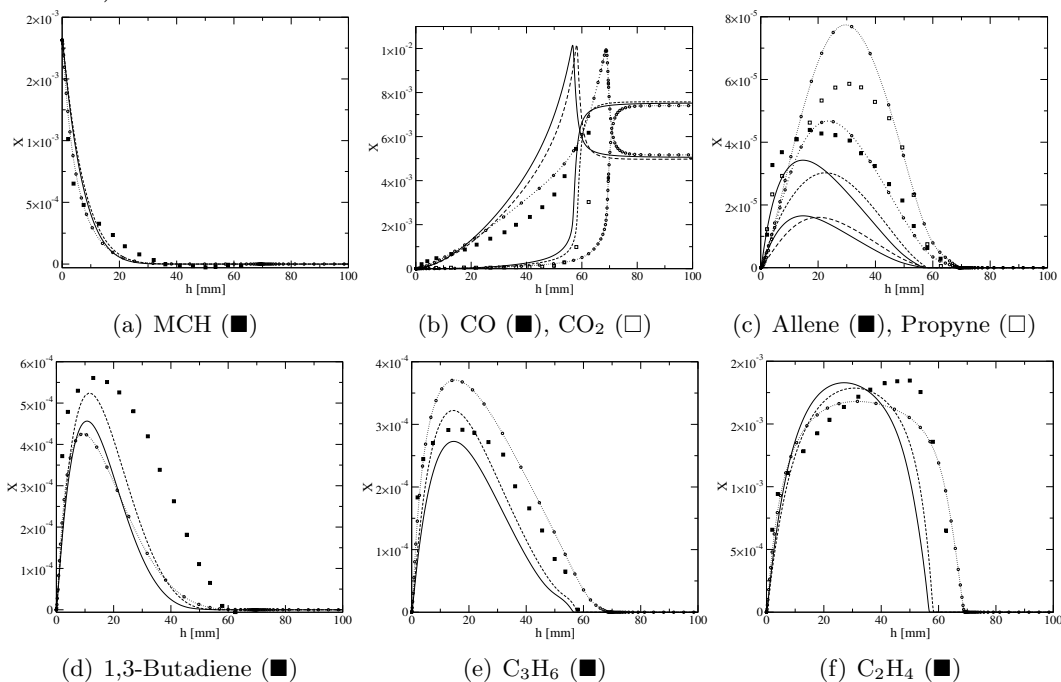


Figure 4.17: Oxidation of methyl-cyclohexane in a plug flow reactor. Comparison between experimental data (symbols, [154]), detailed mechanism (solid line, [111]), single component skeletal mechanism (dashed line) and surrogate skeletal mechanism (dotted line with circles). Thick lines correspond to filled symbols.

temperatures larger than 900 K, the skeletal and combined mechanisms depart significantly from the detailed mechanism when the temperature decreases below this limit. Fuel decomposition rate in near-pyrolysis conditions in a plug flow reactor is shown in Fig. 4.16(b). Although some differences are observed due to the combination process, the experimental data by Zeppieri et al. [154] are very well reproduced. Figure 4.17 displays some species concentrations during the oxidation of methyl-cyclohexane in PFR. Profiles of some species are affected by the reduction and combination. Especially, a 15 ms delay is introduced in the rise of the temperature, which directly impacts the CO and CO<sub>2</sub> concentrations in Fig. 4.17(b). The allene and propyne intermediates are more strongly modified. This is not surprising as the reference soot mechanism is using the latest kinetic data on C<sub>3</sub> species to accurately model these soot precursors. Actually, the combined mechanism predicts allene and propyne concentrations in better agreement with experimental data than the original detailed mechanism by Pitz et al. [111].

***n*-Dodecane.** It was already mentioned that the biggest concern for detailed kinetic modeling of large hydrocarbon species is the lack of appropriate experimental data. The *n*-dodecane mechanism used in this work has been developed by Wang et al. [151] and its oxidation characteristics have been validated using recent measurements of laminar burning velocities [66] and ignition and extinction data in counter-flow configurations [59]. However, the latter phenomena depend much more on transport properties than kinetics, hence were not included in this study that aims to validate the combination of mechanisms from different sources. Although shock tube auto-ignition data will be available in the near future [143], these data were not used in the validation of the mechanism and are not shown here. Instead, ignition delay times over a wide range of temperatures, pressures, and equivalence ratios have been computed and compared between the different mechanisms, and available data for *n*-heptane have been included in the plots for reference. The semi-detailed mechanism for *n*-dodecane represents the low temperature oxidation chemistry using only a few lumped reaction steps. These steps were kept entirely in the skeletal mechanism, as they are necessary to predict the roll-over of the NTC region starting around 1000 K and below.

Results are shown in Figs. 4.18(a), 4.18(b) and 4.18(c) for auto-ignition, and in Fig. 4.18(d) for laminar burning velocities. Merging the mechanisms clearly introduces differences in

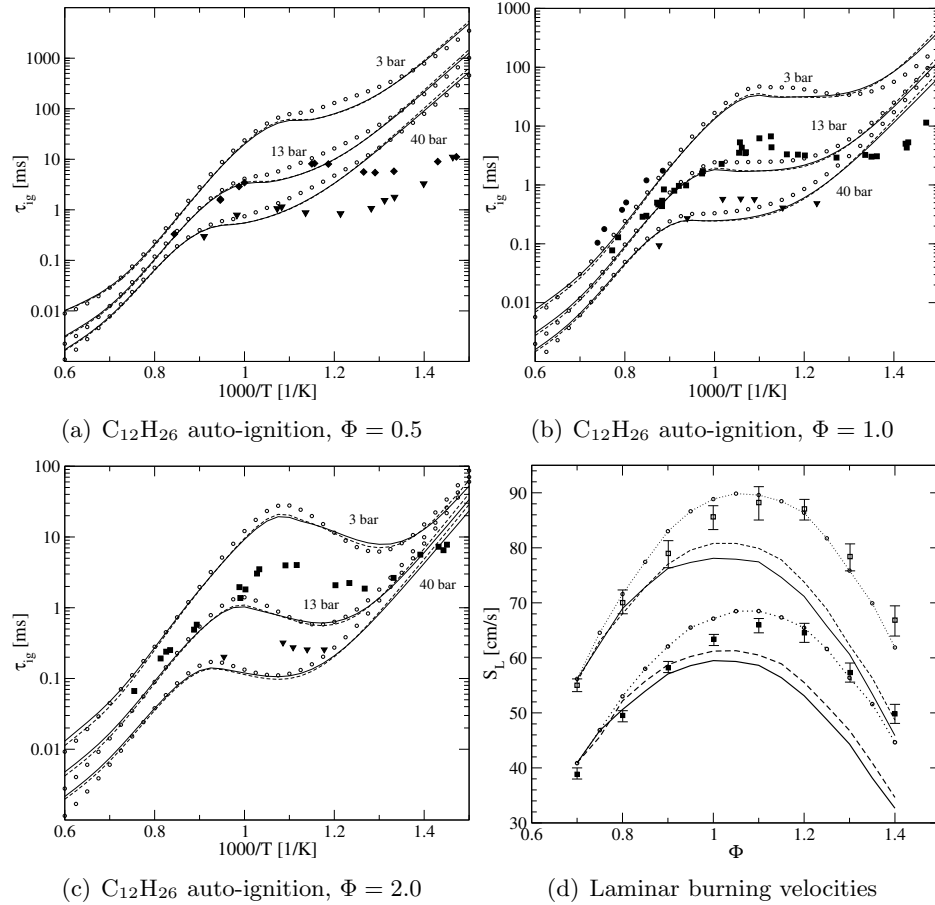


Figure 4.18: Validation of *n*-dodecane component for auto-ignition (Figs. 4.18(a), 4.18(b) and 4.18(c)) and laminar burning velocity (Fig. 4.18(d)). Comparison between experimental data (symbols), detailed mechanism (solid line, [151]), single component skeletal mechanism (dashed line) and surrogate skeletal mechanism (dotted line with circles). Experimental data for auto-ignition are for mixtures of *n*-heptane and air [21, 49], and are shown for reference only. Experimental data for *n*-dodecane laminar burning velocities are taken from Kumar et al. [66].

ignition delay times, mostly in the NTC region due to the high sensitivity of  $\tau_{ig}$  to the hydroxyl radical. However, the biggest impact is observed in the prediction of laminar burning velocities. Indeed, the semi-detailed and skeletal *n*-dodecane mechanisms largely

under-predict  $S_L$  for stoichiometric to rich mixtures, whereas the combined mechanism predicts burning velocities very accurately. An explanation of this significant change is that laminar burning velocities of large hydrocarbons are not sensitive to the fuel decomposition reactions, but depend strongly on an accurate kinetic description of the base chemistry. In the combined mechanism, this base chemistry comes from the soot mechanism, that has been extensively tested for all molecules from  $C_0$  to  $C_4$ , which contributes to explain the improved predictions of  $S_L$ .

### 4.2.3 Comparison with Jet Fuel Experimental Data

In the previous section, the kinetic description of each individual component was thoroughly tested and validated against both experimental data and the predictions of the original detailed mechanisms. The result was a multi-component mechanism containing only 181 species, able to accurately describe the oxidation of *n*-heptane, iso-octane, *n*-dodecane, methyl-cyclohexane, benzene, toluene, and the soot precursor acetylene. Three different surrogate compositions based on these components were chosen in section 4.2.1 to represent jet fuel: neat *n*-dodecane, a surrogate containing a large quantity of *n*-dodecane, plus smaller quantities of iso-octane, methyl-cyclohexane, benzene, and toluene (Surrogate #1, [145]) and a surrogate whose composition has been optimized to match several average properties of jet fuel, consisting of *n*-dodecane, toluene, and methyl-cyclohexane (Surrogate #2). These surrogates will be tested in two different configurations, for which experimental data are available: auto-ignition at high pressure [142] and a burner-stabilized premixed kerosene flame by Doute et al. [34].

**Jet Fuel Auto-ignition.** Simulation results for ignition delay times of jet fuel are shown in Fig. 4.19. Figure 4.19(a) compares two different pressures, 20 and 50 atm, Fig. 4.19(b) compares two levels of dilution for stoichiometric mixtures of jet fuel and air, and Fig. 4.19(c) compares ignition delay times for two different equivalence ratios, 0.5 and 1. The conclusions are similar for all different cases. First, all surrogates over-predict auto-ignition by a factor two to three. New experimental data from Vasu et al. [142] show that *n*-dodecane/air

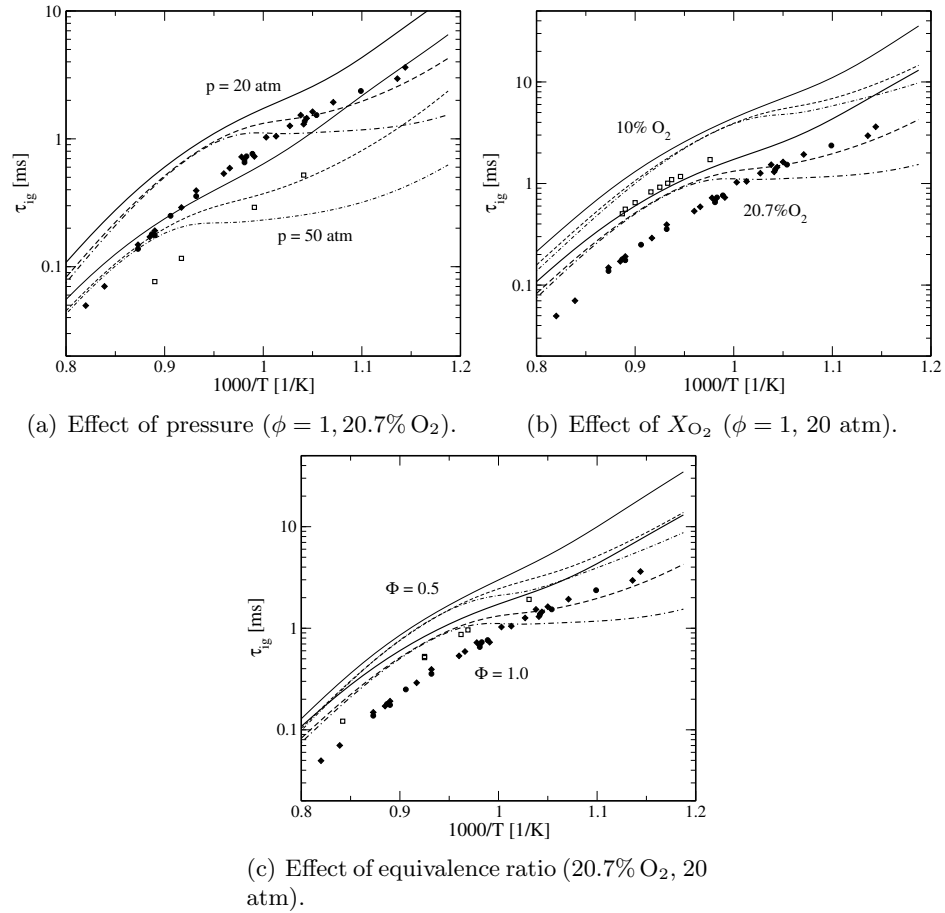


Figure 4.19: Auto-ignition of JetA/JP-8. Comparison between experimental data (squares, [142]), and simulation results obtained with pure dodecane (dash-dotted lines), surrogate #1 (dashed lines) and surrogate #2 (solid lines).

mixtures ignition delay times are close to those of jet fuel. As *n*-dodecane is the major component in all surrogates, this tends to indicate that the *n*-dodecane mechanism does not predicts auto-ignition well. Also, *n*-dodecane is the component that ignites the fastest. As surrogate #2 contains less of the large alkane than the others, it shows the biggest discrepancy compared to experiments at high temperature.

The large errors between experiments and simulation data may be explained by an inappropriate numerical modeling of the shock tube experiments. Indeed, Li et al. [73] recently showed that a gradual pressure rise is present behind the reflected shock as a result

of non-ideal facility-dependent effects. They developed the Chemkin module CHEMSHOCK to modify the constant volume model used to simulate shock tube experiments to include this background pressure gradient. Citing their work, the model consists in two successive suboperations that are performed on a control mass during each infinitesimal time step: (1) first the gas mixture is allowed to combust at constant internal energy and volume (constant U-V model); (2) then the gas is isentropically expanded (or compressed) at frozen composition to the measured pressure:

$$T_{t+dt} = T' \left( \frac{P_{\text{meas}}}{P'} \right)^{\frac{\gamma-1}{\gamma}}, \quad (4.4)$$

where the primes denote quantities obtained at the end of step (1). The density is recomputed from the new values of pressure and temperature.

This two step procedure is equivalent to include directly the pressure gradient in the temperature equation:

$$\frac{\partial T}{\partial t} = -\frac{\dot{\omega}_T}{\rho c_v} + \frac{1}{\rho c_p} \frac{dP}{dt}, \quad (4.5)$$

where

$$\dot{\omega}_T = \sum_{i=1}^{N_S} \left( h_i - \frac{R}{W_i} \right) W_i \dot{\omega}_i \quad (4.6)$$

and  $\dot{\omega}_i$  is the production rate of species  $i$ . The compression term was included in the FlameMaster code used for the simulations. Jet fuel ignition delay times were recomputed with a background pressure gradient of 2%/ms, as recommended in Pang et al. [99] for the shock tube used for the ignition delay measurements. Comparison of the results with and without background pressure gradient is shown in Fig. 4.20. Although the background compression was shown in [99] to have a significant effect for hydrogen mixtures at temperatures as low as 1000K, this effect is not as marked for the heavier molecules included in the surrogates and does not explain the large discrepancies between experiments and simulation data at high temperature. Another possible and most probable explanation for the over-prediction of jet fuel ignition delay times is inaccuracies in the high temperature ignition chemistry and an oversimplified description of the low temperature chemistry in

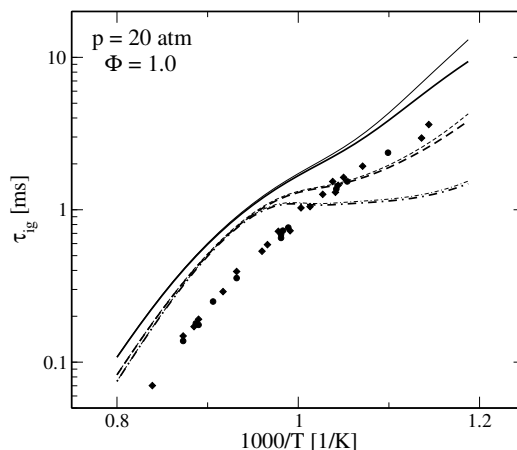


Figure 4.20: Jet fuel ignition delay times. Comparison between experimental data ([142], symbols), simulations using the jet fuel surrogate mechanism with the original constant U-V model (thin lines) and with modified constant U-V model including a background pressure gradient (thick lines). Solid lines correspond to the 3-component surrogate composition, dashed lines to the 5-component surrogate composition and dash-dotted line to pure *n*-dodecane.

the detailed mechanism of You et al. [151].

A second observation concerns the onset of the NTC region. Experimental data show no NTC behavior for temperatures larger than 850 K. However, both pure *n*-dodecane and Surrogate #1 have a strong NTC behavior for temperatures around 1000 K. This NTC is much weaker for Surrogate #2. Disregarding the shift due to the slow ignition of *n*-dodecane in the simulation, Surrogate #2 better represents the jet fuel experimental data.

**Burner-Stabilized Premixed Kerosene Flame.** Experimental and simulated species concentration profiles obtained in a premixed atmospheric kerosene flame, with initial temperature of 473 K [34] are shown in Fig. 4.21. In the simulation, the temperature profile is prescribed from the experimental measurements. The initial conditions in terms of species mole fractions and injection velocity for the premixed kerosene flame need to be adjusted from the experimental data, as none of the surrogates have the correct average formula and molecular weight. The mass fluxes of chemical elements in the simulation are forced to be

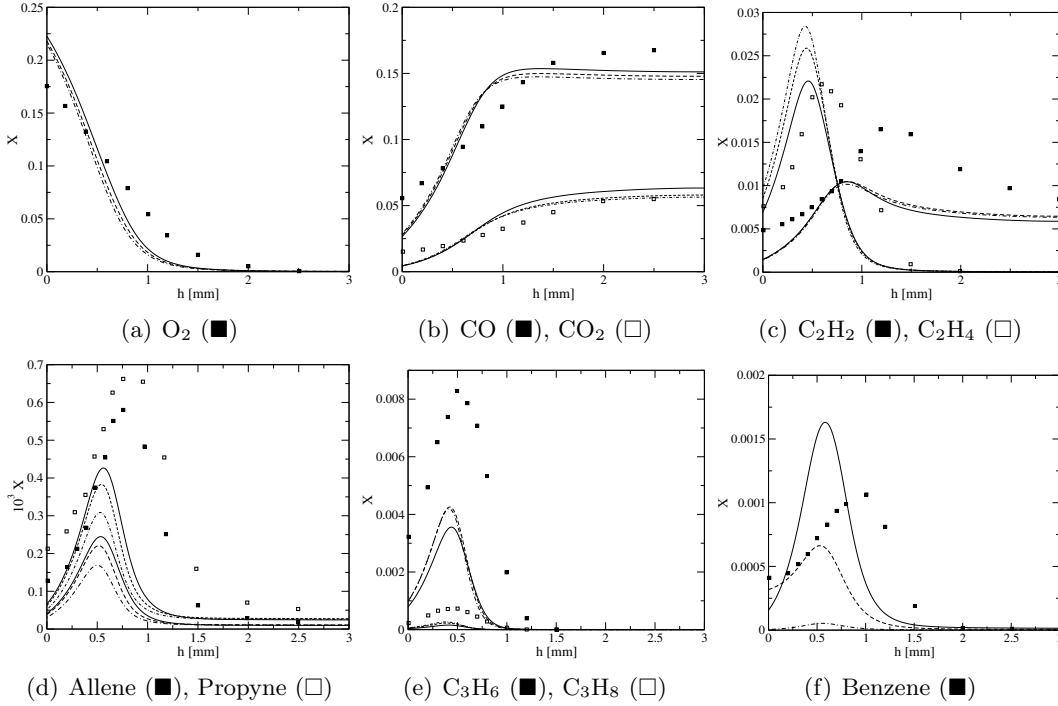


Figure 4.21: Premixed burner-stabilized kerosene flame. Comparison between experimental data (squares, [34]), and simulation results obtained with pure dodecane (dash-dotted lines), surrogate #1 (dashed lines) and surrogate #2 (solid lines).

equal to those prescribed in the experiments, which are evaluated by using an average formula for kerosene of  $C_{11}H_{21}$ . This results in the following constraints on the mass fractions of the injected reactants and the injection velocity:

$$v' = v \left( \frac{n_C}{n'_C} X_F + X_{O_2} + X_{N_2} \right) \quad (4.7)$$

$$X'_F = \frac{n_C}{n'_C} \frac{v}{v'} X_F = \frac{n_H}{n'_H} \frac{v}{v'} X_F \quad (4.8)$$

$$X'_{O_2} = \frac{v}{v'} X_{O_2} \quad (4.9)$$

$$X'_{N_2} = \frac{v}{v'} X_{N_2}, \quad (4.10)$$

where  $X_F$ ,  $X_{O_2}$ , and  $X_{N_2}$  are the mole fractions of kerosene, oxygen, and nitrogen, respectively,  $v$  is the injection velocity,  $n_C$  and  $n_H$  are the number of carbon and hydrogen atoms in the fuel, and the primes refer to quantities imposed in the simulation. Equation 4.8 may

be satisfied only if the surrogate has the same hydrogen-to-carbon ratio. If it is not the case, then only the mass flux of carbon is chosen to be conserved between experiments and simulation.

Prediction of oxygen consumption and major product formation, such as CO and CO<sub>2</sub>, is in acceptable agreement with the measurements. The precise compositions of the surrogates have very little effect on the evolution of the major species. However, the concentration of specific intermediate species are clearly impacted by the initial composition. For example, neat *n*-dodecane tends to produce very little benzene, whereas the presence of toluene and benzene from the inlet increases drastically the maximum concentration of benzene in the flame. Other common intermediates, that are natural decomposition products of any sufficiently large hydrocarbon fuel, are produced in similar quantity by the three surrogates.

The present experimental validation set is not enough to conclude with certitude on the performances of the tested surrogates, except perhaps, for the neat *n*-dodecane case, that is clearly not representative of either jet fuel auto-ignition or flame oxidation. Indeed, too much uncertainty still exists in the detailed kinetic models considered in this study. However, should any of these mechanisms be improved in the near future, only a few steps need to be repeated, namely the reduction of this particular mechanism, combination with the other skeletal schemes, and validation steps for all components. Provided that the reference mechanism is left unchanged, this latter stage should not introduce any problems in the untouched components, and the whole process is expected to be quite fast.

Several jet fuel mechanisms and surrogates of various sizes have been published recently [28, 74, 84, 113, 156], and their ability to predict jet fuel ignition delay times has been assessed by Vasu et al. [142]. None of these mechanisms were able to correctly reproduce the entire set of experimental data. Two mechanisms predict high temperature ignition reasonably well. The first one is the mechanism by Lindstedt et al. [74], that consists of 154 species and 947 reversible reactions (or about twice that number if forward and backward reactions are counted separately, as is done in this work). However, this mechanism does not include low temperature chemistry, and therefore is unable to reproduce the onset of the NTC region at temperatures lower than 1000K. As mentioned before, including

low temperature chemistry for long chain aliphatic fuels requires a significant number of additional species. Ranzi et al. mechanism [113] also reproduces high temperature ignition data quite accurately, but predicts a very strong NTC below 1000K that was not observed experimentally. This mechanism consists of 280 species and 7800 reactions that can be reversible. It has to be compared to the present mechanism containing 181 species and about 1200 reactions, backward and forward counted separately. It should be emphasized again that the latter mechanism was obtained using systematic reduction and combination techniques based on available detailed mechanisms. Any improvement of the detailed scheme can be automatically and quickly included in the skeletal scheme, hence providing a flexibility of use essential when designing surrogate fuels. The skeletal jet fuel mechanisms mentioned here, either the one obtained in this work, or those that can be found in the literature, are still too large to be used directly in CFD codes. Additional modeling assumptions must be introduced, such as QSSA or ILDM, and efficient treatments of the chemistry through tabulation methods such as ISAT or flamelet assumptions are required for complex simulations.

## Chapter 5

# Conclusion and Perspectives

Substantial advances have been made on the topic of chemistry reduction, with the development of a fully automatic, multi-stage reduction strategy that was shown to decrease the computational cost of solving the differential equations associated with large-scale chemical kinetic reaction mechanisms by at least two orders of magnitude. An important characteristic of the resulting small kinetic schemes is that they can be used to predict accurately the entire combustion process, from initial reactants to final products, over a user-defined domain usually parameterized in terms of initial temperature, pressure, equivalence ratio, or reactant composition. For example, only 57 species are necessary to describe the lean-to-rich auto-ignition of iso-octane for temperatures between 600 K and 2000 K and pressures between 1 and 50 bars. As a direct continuation to this work, one could expect a much larger level of reduction if the mechanism was required to be valid only locally, and not over the entire combustion process. In that case, only equations for the locally active species including only active reactions would be solved, the others being discarded temporarily from the set of differential equations and re-introduced as needed. This adaptive chemistry approach, which essentially corresponds to an on-the-fly reduction of the chemical mechanisms can be seen as a logical continuation of this thesis work, and introduces many conceptual challenges that are definitively worth studying in the future.

On the surrogate formulation topic, an interactive framework was developed, that emphasized flexibility and re-use of previously developed kinetic modules. However, this work highlighted two major issues. First, the current lack of both validated experimental and kinetic data for large hydrocarbon molecules relevant to transportation fuels compromises the ability of any surrogate model to correctly represent real fuel. Then, developing an appropriate surrogate for a specific application has to be an iterative process between kinetic modeling and experimental validation. The average global physical and chemical properties of transportation fuels might not be sufficient to guarantee the success of a surrogate formulation. However, the proposed component library approach greatly facilitates the process and could be included in an optimization procedure to produce the best possible surrogate composition.

# Bibliography

- [1] S. S. Ahmed, F. Mauss, G. Moréac, and T. Zeuch. A Comprehensive and Compact *n*-Heptane Oxidation Model Derived Using Chemical Lumping. *Phys. Chem. Chem. Phys.*, 9:1107–1126, 2007.
- [2] A. Arvidsson, T. Lovas, and F. Mauss. An Automatic Sparse Matrix Solver for Reduced Reaction Kinetics, 2007.
- [3] F. Battin-Leclerc. Detailed Chemical Kinetic Models for the Low-Temperature Combustion of Hydrocarbons with Application to Gasoline and Diesel Fuel Surrogates. *Prog. Energy Combust. Sci.*, 2007, in press.
- [4] C Baumgarten. *Mixture Formation in Internal Combustion Engines*. Springer, March 14, 2006.
- [5] A.B. Bendtsen, P. Glarborg, and K. Dam-Johansen. Visualization Methods in Analysis of Detailed Chemical Kinetics Modelling. *Computers and Chemistry*, 25:161-170, 2001.
- [6] S. W. Benson. *Thermochemical Kinetics : Methods for the Estimation of Thermochemical Data and Rate Parameters*. Wiley, New York, 1976.
- [7] B. Bhattacharjee, D.A. Schwer, P.I. Barton, and W.H. Green. Optimally-Reduced Kinetic Models: Reaction Elimination in Large-Scale Kinetic Mechanisms. *Combust. Flame*, 135:191–208, 2003.

- [8] C. M. Bishop. *Neural Networks for Pattern Recognition*. Oxford University Press, Oxford, 1995.
- [9] G. Blanquart, P. Pepiot-Desjardins, and H. Pitsch. Chemical Mechanism for High Temperature Combustion of Engine Relevant Fuels with Emphasis on Soot Precursors. *Combust. Flame*, 2008, submitted.
- [10] R. Bounaceur, V. Warth, P. A. Glaude, F. Battin-Leclerc, G. Scacchi, G. M. Côme, T. Faravelli, and E. Ranzi. Chemical Lumping of Mechanisms Generated by Computer. Application to the Modelling of Normal Butane Oxidation. *J. Chem. Phys.*, 93:1472–1491, 1996.
- [11] D. Bradley, R. A. Hicks, R. A. Lawes, C.G.W. Sheppard, and R. Wolley. Measurement of Laminar Burning Velocities and Markstein Numbers for Iso-octane-Air and Iso-Octane-*n*-Heptane-Air Mixtures at Elevated Temperatures and Pressures in an Explosion Bomb. *Combust. Flame*, 115:126–144, 1998.
- [12] N. J. Brown, G. Li, and Koszykowski. Mechanism Reduction via Principal Component Analysis. *Int. J. Chem. Kin.*, 29:393–414, 1997.
- [13] A. Burcat, C. Snyder, and T. Brabbs. Ignition Delay Times of Benzene and Toluene with Oxygen in Argon Mixtures. Technical Report TM-87312, NASA, 1986.
- [14] B. V. Buxton, C. L. Greenstock, W. P. Helman, A. B. Ross, and W. Tsang. Critical Review of Rate Constants for Reactions of Hydrated Electrons: Chemical Kinetic Data Base for Combustion Chemistry. Part 3: Propane. *J. Phys. Chem. Ref. Data*, 17:513–886, 1988.
- [15] H. F. Calcote and D. M. Manos. Effect of Molecular Structure on Incipient Soot Formation. *Combust. Flame*, 49:289–304, 1983.
- [16] C. V. Callahan, T. J. Held, F. L. Dryer, R. Minetti, M. Ribaucour, L. R. Sochet, T. Faravelli, P. Gaffuri, and E. Ranzi. Experimental Data and Kinetic Modeling of Primary Reference Fuel Mixtures. *Proc. Combust. Inst.*, 26:739–746, 1996.

- [17] M. Chaos, A. Kazakov, Z. Zhao, and F. L. Dryer. A High-Temperature Chemical Kinetic Model for Primary Reference Fuels. *Int. J. Chem. Kinet.*, 39:399–414, 2007.
- [18] J.-S. Chen, T. A. Litzinger, and H. J. Curran. The Lean Oxidation of Iso-octane in the Intermediate Temperature Regime at Elevated Pressures. *Combust. Sci. Tech.*, 156:49–79, 2000.
- [19] J.-Y. Chen. Automatic Generation of Reduced Mechanisms and their Applications to Combustion Modeling. *Trans. Aero. Astro. Soc. Rep. China*, 33:59–67, 2001.
- [20] J.-Y. Chen and Y. F. Tham. Speedy Solution of Quasi-Steady State Species by Combination of Fixed-Point Iteration and Matrix Inversion. *Combust. Flame*, in press, 2008.
- [21] H. K. Ciezki and G. Adomeit. Shock-Tube Investigation of Self-Ignition of *n*-Heptane - Air Mixtures Under Engine Relevant Conditions. *Combust. Flame*, 93:421–433, 1993.
- [22] M. Colket, T. Edwards, S. Williams, N.P. Cernansky, D.L. Miller, F. Egolfopoulos, P. Lindstedt, K. Seshadri, F.L. Dryer, C.K. Law, D. Friend, D.B. Lenhert, H. Pitsch, A.F. Sarofim, M. Smooke, and W. Tsang. Development of an Experimental Database and Kinetic Models for Surrogate Jet Fuels, AIAA 2007-770, 2007.
- [23] D. J. Cook, H. Pitsch, J. H. Chen, and E. R. Hawkes. Flamelet-Based Modeling of Auto-Ignition with Thermal Inhomogeneities for Application to HCCI Engines. *Proc. Combust. Inst.*, 31:2903–2911, 2007.
- [24] J. A. Cooke, M. Bellucci, M. D. Smooke, A. Gomez, A. Violi, T. Faravelli, and E. Ranzi. Computational and Experimental Study of JP-8, a Surrogate, and its Components in Counterflow Diffusion Flame. *Proc. Combust. Inst.*, 30:439–446, 2005.
- [25] H. J. Curran, P. Gaffuri, W. J. Pitz, and C. K. Westbrook. A Comprehensive Modeling Study of *n*-Heptane Oxidation. *Combust. Flame*, 114:149–177, 1998.
- [26] H. J. Curran, P. Gaffuri, W. J. Pitz, and C. K. Westbrook. A Comprehensive Modeling Study of Iso-Octane Oxidation. *Combust. Flame*, 129:253–280, 2002.

- [27] H. J. Curran, W. J. Pitz, C. K. Westbrook, C. V. Callahan, and F. L. Dryer. Oxidation of Automotive Primary Reference Fuels at Elevated Pressures. *Proc. Combust. Inst.*, 27:379–387, 1998.
- [28] P. Dagaut and M. Cathonnet. The Ignition, Oxidation, and Combustion of Kerosene: A Review of Experimental and Kinetic Modeling. *Prog. Energy Combust. Sci.*, 32:48–92, 2006.
- [29] P. Dagaut, M. Cathonnet, J. P. Rounan, R. Foulatier, A. Quilgars, J. C. Boettner, F. Gaillard, and H. James. Jet-Stirred Reactor for Kinetic Studies of Homogeneous Gas-Phase Reactions at Pressures up to Ten Atmospheres (Approx. 1 MPa). *J. Phys. E (Sci. Instrum.)*, 19:207–209, 1986.
- [30] P. Dagaut, A. El Bakali, and A. Ristori. The Combustion of Kerosene: Experimental Results and Kinetic Modeling Using 1- and 3- Component Surrogate Model Fuels. *Fuel*, 85:944–956, 2006.
- [31] D.F. Davidson, B.M. Gauthier, and R.K. Hanson. Shock Tube Ignition Measurements of Iso-Octane/Air and Toluene/Air at High Pressures. *Proc. Combust. Inst.*, 30:1175–1182, 2005.
- [32] S. G. Davis and C. K. Law. Determination of Fuel Structure Effects on Laminar Flame Speeds of C<sub>1</sub> to C<sub>8</sub> Hydrocarbons. *Combust. Sci. Tech.*, 140:427–450, 1998.
- [33] A. M. Dean. Predictions of Pressure and Temperature Effects Upon Radical Addition and Recombination Reactions. *J. Phys. Chem.*, 89:4600–4608, 1985.
- [34] C. Dout, J. L. Delfau, R. Akrich, and C. Vovelle. Chemical Structure of Atmospheric Pressure Premixed n-Decane and Kerosene Flames. *Combust. Sci. Tech.*, 106:327–344, 1995.
- [35] E.G. Eddings, S. Yan, W. Ciro, and A.F. Sarofim. Formulation of a Surrogate for the Simulation of Jet Fuel Pool Fires. *Combust. Sci. Tech.*, 177:715–739, 2005.

- [36] T. Edwards and L. Q. Maurice. Surrogate Mixtures to Represent Complex Aviation and Rocket Fuels. *J. Prop. Power*, 17:461–466, 2000.
- [37] F.N. Egolfopoulos, D.L. Zhu, and C.K. Law. Experimental and Numerical Determination of Laminar Flame Speeds: Mixtures of C<sub>2</sub>-Hydrocarbons with Oxygen and Nitrogen. In *Twenty-third Symposium (International) on Combustion*, pages 471–478, Pittsburgh, PA, 1991.
- [38] ChevronTexaco employees and contractors. Motor Gasoline Technical Review. Technical report, Chevron Corporation, 2004.
- [39] ChevronTexaco employees, contractors, J. Bacha, F. Barnes, M. Franklin, L. Gibbs, G. Hemighaus, N. Hogue, D. Lesnini, J. Lind, J. Maybury, and J. Morris. Aviations Fuels Technical Review. Technical report, Chevron Corporation, 2005.
- [40] ChevronTexaco employees, contractors, J. Bacha, J. Freel, A. Gibbs, L. Gibbs, G. Hemighaus, K. Hoekman, J. Horn, M. Ingham, L. Jossens, D. Kohler, D. Lesnini, J. McGeehan, N. Nikanjam, E. Olsen, R. Organ, B. Scott, M. Sztenderowicz, A. Tiedemann, C. Walker, J. Lind, J. Jones, D. Scott, , and J. Mills. Diesel Fuels Technical Review. Technical report, Chevron Corporation, 2007.
- [41] J. Ewald and N. Peters. On Unsteady Premixed Turbulent Burning Velocity Prediction in Internal Combustion Engines. *Proc. Combust. Inst.*, 31:3051–3058, 2007.
- [42] D. M. Fake, A. Nigam, and M. T. Klein. Mechanism Based Lumping of Pyrolysis Reactions: Lumping by Reactive Intermediates. *App. Cat. A: Gen.*, 160:191–221, 1997.
- [43] J. T. Farrell, N. P. Cernansky, F. L. Dryer, D. G. Friend, C. A. Hergart, C. K. Law, R. M. McDavid, C. J. Mueller, A.K. Patel, and H. Pitsch. Development of an Experimental Database and Kinetic Models for Surrogate Diesel Fuels, SAE 2007-01-0201, 2007.

- [44] K. Fieweger, R. Blumenthal, and G. Adomeit. Self-Ignition of S.I. Engine Model Fuels: a Shock Tube Investigation at High Pressure. *Combust. Flame*, 109:599–619, 1997.
- [45] R. Fournet, V. Warth, P. A. Glaude, F. Battin-Leclerc, G. Scacchi, and Côme. Automatic Reduction of Detailed Mechanisms of Combustion of Alkanes by Chemical Lumping. *Int. J. Chem. Kinet.*, 32:36–51, 2000.
- [46] S. J. Fraser. The Steady State and Equilibrium Approximations: A Geometrical Picture. *J. Chem. Phys.*, 88:4732–4738, 1988.
- [47] M. Frenklach. Computer Modeling of Infinite Reaction Sequences: A Chemical Lumping. *Chem. Eng. Sci.*, 10:1843–1849, 1985.
- [48] M. Frenklach. *Reduction of Chemical Reaction Models*, chapter 5, pages 129–154. American Institute of Aeronautics and Astronautics, Inc., Washington, DC, 1991.
- [49] B. M. Gauthier, D. F. Davidson, and R. K. Hanson. Shock Tube Determination of Ignition Delay Times in Full-Blend and Surrogate Fuel Mixtures. *Combust. Flame*, 139:300–311, 2004.
- [50] G. R. Gavalas. The Long Chain Approximation in Free Radical Reaction Systems. *Chem. Eng. Sci.*, 21:133–141, 1966.
- [51] A. G. Gaydon and I. R. Hurle. *The Shock Tube in High Temperature Chemical Physics*. Reinhold Publishing Corp, New York, 1963.
- [52] R. J. Gill and D. B. Olson. Estimation of Soot Thresholds for Fuel Mixtures. *Comb. Sci. Tech.*, 40:307–315, 1984.
- [53] A. Gomez, G. Sidebotham, and I. Glassman. Sooting Behavior in Temperature-Controlled Laminar Diffusion Flames. *Comb. Flame*, 58:45–57, 1984.
- [54] O. L. Gülder. Correlations of Laminar Combustion Data for Alternative S.I. Engine Fuel, SAE 841000, 1984.

- [55] M. I. Hassan, K. T. Aung, and G.M. Faeth. Measured and Predicted Properties of Laminar Premixed Methane/Air Flames at Various Pressures. *Combust. Flame*, 115:539–550, 1998.
- [56] Y. Hidaka, K. Hattori, T. Okuno, K. Inami, and T. Koike. Shock-Tube and Modeling Study of Acetylene Pyrolysis and Oxidation. *Comb. Flame*, 107:401–417, 1996.
- [57] H. Huang, M. Fairweather, J. F. Griffiths, A. S. Tomlin, and R. B. Brad. A Systematic Lumping Approach for the Reduction of Comprehensive Kinetic Models. *Proc. Combust. Inst.*, 30:1309–1316, 2005.
- [58] Y. Huang, C. J. Sung, and Eng J. A. Laminar Flame Speeds of Primary Reference Fuels and Reformer Gas Mixtures. *Combust. Flame*, 139:239–251, 2004.
- [59] S. Humer, A. Frassoldati, S. Granata, T. Faravelli, E. Ranzi, R. Seiser, and K. Seshadri. Experimental and Kinetic Modeling Study of Combustion of JP-8, its Surrogates and Reference Components in Laminar Non-Premixed Flows. *Proc. Combust. Inst.*, 31:393–400, 2007.
- [60] S. Jerzembeck, N. Peters, P. Pepiot-Desjardins, and H. Pitsch. Laminar Burning Velocities at High Pressure for Primary Reference Fuels and Gasoline: Experimental and Numerical Investigation. *Combust. Flame*, *submitted*, 2008.
- [61] G. Jomaas, X. Zheng, D. L. Zhu, and C. K. Law. Experimental Determination of Counterflow Ignition Temperatures and Laminar Flame Speeds of C<sub>2</sub>C<sub>3</sub> Hydrocarbons at Atmospheric and Elevated Pressures. *Proc. Combust. Inst.*, 30:193–200, 2005.
- [62] W. P. Jones and S. Rigopoulos. Rate-Controlled Constrained Equilibrium: Formulation and Application to Nonpremixed Laminar Flames. *Combust. Flame*, 142:223–234, 2005.
- [63] T. J. Kim, R. A. Yetter, , and F. L. Dryer. New Results on Moist CO Oxidation: High Pressure, High Temperature Experiments and Comprehensive Kinetic Modeling. *Proc. Combust. Inst.*, 25:759–766, 1994.

- [64] S. D. Klotz, K. Brezinsky, and I. Glassman. Modeling the Combustion of Toluene-Butane Blends. *Proc. Combust. Inst.*, 27:337–344, 1998.
- [65] K. Kumar, J. E. Freeh, C. J. Sung, and Y. Huang. Laminar Flame Speeds of Preheated Iso-Octane/O<sub>2</sub>/N<sub>2</sub> and *n*-Heptane/O<sub>2</sub>/N<sub>2</sub> Mixtures. *J. Prop. Power*, 23:428–436, 2007.
- [66] K. Kumar and C.-J. Sung. Laminar Flame Speeds and Extinction Limits of Preheated *n*-Decane/O<sub>2</sub>/N<sub>2</sub> and *n*-Dodecane/O<sub>2</sub>/N<sub>2</sub> Mixtures. *Combust. Flame*, 151:209–224, 2007.
- [67] J. C. W. Kuo and J. Wei. Lumping Analysis in Monomolecular Reaction Systems. Analysis of Approximately Lumpable System. *Ind. Eng. Chem. Fund.*, 8:124–133, 1969.
- [68] O. C. Kwon, M. I. Hassan, and G. M. Faeth. Flame/Stretch Interactions of Premixed Fuel-Vapor/O/N Flames. *J. Prop. Power*, 16:513–522, 2000.
- [69] S.H. Lam and D.A. Goussis. The CSP Method for Simplifying Kinetics. *Int. J. Chem. Kin.*, 26:461–486, 1994.
- [70] G. Li and H. Rabitz. A General Analysis of Exact Lumping in Chemical Kinetics. *Chem. Eng. Sci.*, 44:1413–1430, 1989.
- [71] G. Li and H. Rabitz. A General Analysis of Approximate Lumping in Chemical Kinetics. *Chem. Eng. Sci.*, 45:977–1002, 1990.
- [72] G. Li and H. Rabitz. Combined Symbolic and Numerical Approach to Constrained Nonlinear Lumping With Application to an H<sub>2</sub>/O<sub>2</sub> Oxidation Model. *Chem. Eng. Sci.*, 51:4801–4816, 1996.
- [73] H. Li, Z. C. Owens, D. F. Davidson, and R. K. Hanson. A Simple Reactive Gasdynamic Model for the Computation of Gas Temperature and Species Concentrations behind Reflected Shock Waves. *Int. J. Chem. Kin.*, 40:189–198, 2008.

- [74] R. P. Lindstedt and L. Q. Maurice. Detailed Chemical-Kinetic Model for Aviation Fuels. *J. Prop. Pow.*, 16, 2000.
- [75] T. Lovas, P. Amneus, F. Mauss, and E. Mastorakos. Comparison of Automatic Reduction Procedures for Ignition Chemistry. *Proc. Combust. Inst.*, 29:1387–1393, 2002.
- [76] T. Lovas, D. Nilsson, and F. Mauss. Automatic Reduction Procedure for Chemical Mechanisms Applied to Premixed Methane/Air Flames. *Proc. Combust. Inst.*, 28:1809–1815, 2000.
- [77] T. Lu and C.K. Law. A Directed Relation Graph Method for Mechanism Reduction. *Proc. Combust. Inst.*, 30:1333–1341, 2005.
- [78] T. Lu and C.K. Law. Linear Time Reduction of Large Kinetic Mechanisms With Directed Relation Graph: *n*-Heptane and Iso-octane. *Combust. Flame*, 144:24–36, 2006.
- [79] T. Lu and C.K. Law. On the Applicability of Directed Relation Graphs to the Reduction of Reaction Mechanisms. *Combust. Flame*, 146:472–483, 2006.
- [80] T. Lu and C.K. Law. Systematic Approach to Obtain Analytic Solutions of Quasi-Steady State Species in Reduced Mechanisms. *J. Phys. Chem. A*, 110:13202–13208, 2006.
- [81] T. Lu and C.K. Law. Strategies for mechanism reduction for large hydrocarbons: *n*-heptane. *Comb. Flame*, in press, 2008.
- [82] J. Luche, M. Reuillon, J.-C. Boettner, and M. Cathonnet. Reduction of Large Detailed Kinetic Mechanisms: Application to Kerosene/Air Combustion. *Combust. Sci. Tech.*, 176:1935–1963, 2004.
- [83] U. Maas and S.B. Pope. Simplifying Chemical Kinetics: Intrinsic Low-Dimensional Manifolds in Composition Space. *Combust. Flame*, 88:239–264, 1992.
- [84] M. A. Mawid and B. Sekar. Proc. ASME Turbo Expo, Paper GT2006-904778, 2006.

- [85] M. Metghalchi and J. C. Keck. Burning Velocities of Mixtures of Air with Methanol, Iso-octane, and Indolene at High Pressure and Temperature. *Combust. Flame*, 48:191–210, 1982.
- [86] R. Minetti, M. Carlier, M. Ribaucour, E. Therssen, and L. R. Sochet. A Rapid Compression Machine Investigation of Oxidation and Auto-Ignition of *n*-Heptane: Measurements and Modeling. *Combust. Flame*, 102:298–309, 1995.
- [87] G. Mittal. *A Rapid Compression Machine: Design, Characterization and Auto-ignition Investigation*. PhD thesis, Case Western Reserve University, 2006.
- [88] C. J. Montgomery, M. A. Cremer, J.-Y. Chen, C. K. Westbrook, and L. Q. Maurice. Reduced Chemical Kinetic Mechanisms for Hydrocarbon Fuels. *J. Prop. Power*, 18, 2002.
- [89] C. J. Montgomery, C. Yang, A. R. Parkinson, and J.-Y. Chen. Selecting the Optimum Quasi-Steady State Species for Reduced Chemical Kinetic Mechanisms using a Genetic Algorithm. *Combust. Flame*, 144:37–52, 2006.
- [90] A. Moreau, O. Teytaud, and J. P. Bertoglio. Optimal Estimation for Large-Eddy Simulation of Turbulence and Application to the Analysis of Subgrid Models. *Phys. Fluids*, 18:105101, 2006.
- [91] U.C. Müller. *Reduzierte Reaktionsmechanismen für die Zündung von n-Heptan und Iso-oktan Under Motorrelevanten Bedingungen*. PhD thesis, RWTH Aachen, Germany, 1993.
- [92] M. J. Murphy, J. D. Taylor, and R. L. McCormick. Compendium of Experimental Cetane Number Data, National Renewable Energy Laboratory, 2004.
- [93] National Institute of Standards and Technology. <http://kinetics.nist.gov/>.
- [94] A. Nigam and M. T. Klein. A Mechanism-Oriented Lumping Strategy for Heavy Hydrocarbon Pyrolysis: Imposition of Quantitative Structure-Reactivity Relationships for Pure Components. *Ind. Eng. Chem. Res.*, 32:1297–1303, 1993.

- [95] T. Ohashi, X. Yang, T. Takabayashi, Y. Urata, S. Kubota, and H. Katsuyama. Ignition and Combustion Simulation in HCCI Engines, SAE 2006-01-1522, 2006.
- [96] O. O. Oluwole, P. I. Barton, and W. H. Green. Obtaining Accurate Solutions Using Reduced Chemical Kinetic Models: A New Model Reduction Method for Models Rigorously Validated over Ranges. *Combust. Th. and Model.*, 11:127–146, 2007.
- [97] O. O. Oluwole, B. Bhattacharjee, J. E. Tolsma, P. I. Barton, and W. H. Green. Rigorous Valid Ranges for Optimally Reduced Kinetic Models. *Combust. Flame*, 146:348–365, 2006.
- [98] J. P. Orme, H. J. Curran, and J. M. Simmie. Experimental and Modeling Study of Methyl Cyclohexane Pyrolysis and Oxidation. *J. Phys. Chem. A*, 110:114–131, 2006.
- [99] G. A. Pang, D. F. Davidson, and R. K. Hanson. Shock Tube Ignition Delay Times for Hydrogen-Oxygen-Argon Mixtures at Low Temperatures and Elevated Pressures. Fall Meeting of the Western States Section of the Combustion Institute, Livermore, CA, 2007.
- [100] C. Pels Leusden. *Experimentelle und Theoretische Untersuchung der Russbildung in Laminaren Gegenstromdiffusionsflammen*. PhD thesis, RWTH Aachen, 2001.
- [101] C. Pels Leusden and N. Peters. Experimental and Numerical Analysis of the Influence of Oxygen on Soot Formation in Laminar Counter-flow Flames of Acetylene. *Proc. Comb. Inst.*, 28:2619–2625, 2000.
- [102] G. Pengloan. *A Kinetic Study of Several Aromatic Coumpounds Oxidation : Applied to Pollutants Formation in Car Engines*. PhD thesis, 2001.
- [103] P. Pepiot and H. Pitsch. Systematic Reduction of Large Chemical Kinetic Mechanisms, 4th Joint Meeting of the U.S. Sections of the Combustion Institute, 2005.
- [104] P. Pepiot-Desjardins and H. Pitsch. An Automatic Chemical Lumping Method for the Reduction of Large Chemical Kinetic Mechanisms. *Combust. Th. Model.*, submitted, 2008.

- [105] P. Pepiot-Desjardins and H. Pitsch. An Efficient Error Propagation Based Reduction Method for Large Chemical Kinetic Mechanisms. *Combust. Flame*, in press, 2008.
- [106] N. Peters. Fifteen Lectures on Laminar and Turbulent Combustion, Ercoftac Summer School, 1992.
- [107] N. Peters. *Turbulent Combustion*. Cambridge University Press, 2000.
- [108] N. Peters and B. Roggs. *Reduced Kinetic Mechanisms for Applications in Combustion Systems*. Lecture notes in physics. Springer-Verlag, 1992.
- [109] H. Pitsch and N. Peters. Investigation of the Ignition Process of Sprays Under Diesel Conditions Using Reduced *n*-Heptane Chemistry, SAE 98-2464, 1998.
- [110] W. J. Pitz, N. P. Cernansky, F. L. Dryer, F. N. Egolfopoulos, J. T. Farrell, D. G. Friend, and H. Pitsch. Development of an Experimental Database and Chemical Kinetic Models for Surrogate Gasoline Fuels, SAE 2007-01-0175, 2007.
- [111] W. J. Pitz, C. V. Naik, T. Ni Mhaolduinc, C. K. Westbrook, H. J. Curran, J. P. Orme, and J. M. Simmie. Modeling and Experimental Investigation of Methylcyclohexane Ignition in a Rapid Compression Machine. *Proc. Combust. Inst.*, 31:267–275, 2007.
- [112] S. B. Pope. Computationally Efficient Implementation of Combustion Chemistry Using *in situ* Adaptive Tabulation. *Combust. Th. Model.*, 1:41–63, 1997.
- [113] E. Ranzi, 2006.
- [114] E. Ranzi, M. Dente, A. Goldaniga, G. Bozzano, and T. Faravelli. Lumping Procedures in Detailed Kinetic Modeling of Gasification, Pyrolysis, Partial Oxidation and Combustion of Hydrocarbon Mixtures. *Prog. Energy Combust. Sci.*, 27:99–139, 2001.
- [115] E. Ranzi, T. Faravelli, P. Gaffuri, E. Garavaglia, and A. Goldaniga. Primary Pyrolysis and Oxidation Reactions of Linear and Branched Alkanes. *Ind. Eng. Chem. Res.*, 36:3336–3344, 1997.

- [116] E. Ranzi, T. Faravelli, P. Gaffuri, and A. Sogaro. Low-Temperature Combustion: Automatic Generation of Primary Oxidation Reactions and Lumping Procedures. *Combust. Flame*, 102:179–192, 1995.
- [117] E. Ranzi, A. Frassoldati, S. Granata, and T. Faravelli. Wide-Range Kinetic Modeling Study of the Pyrolysis, Partial Oxidation, and Combustion of Heavy *n*-Alkanes. *Ind. Eng. Chem. Res.*, 44:5170–5183, 2005.
- [118] M. J. A. Rickard, J. M. Hall, and E. L. Petersen. Effect of Silane Addition on Acetylene Ignition Behind Reflected Shock Waves. *Proc. Comb. Inst.*, 30:1915–1923, 2005.
- [119] M. R. Roussel and S. J. Fraser. Geometry of the Steady-State Approximation: Perturbation and Accelerated Convergence Methods. *J. Chem. Phys.*, 93:1072–1081, 1990.
- [120] D. Schmidt, J. Segatz, U. Riedel, J. Warnatz, and U. Maas. Simulation of Laminar Methane-Air Flames using Automatically Simplified Chemical Kinetics. *Combust. Sci. Tech.*, 113–114:3–16, 1996.
- [121] J. M. Simmie. Detailed Chemical Kinetic Models for the Combustion of Hydrocarbon Fuels. *Prog. Energy Combust. Sci.*, 29:599–634, 2003.
- [122] M. A. Singer, S. B. Pope, and H. N. Najm. Operator-Splitting with ISAT to Model Reacting Flow with Detailed Chemistry. *Combust. Th. Model.*, 10:199–217, 2006.
- [123] G.P. Smith, D.M. Golden, M. Frenklach, N.W. Moriarty, B. Eiteneer, M. Goldenberg, C.T. Bowman, R.K. Hanson, S. Song, W.C. Gardiner, V.V. Lissianski, and Z. Qin. [http://www.me.berkeley.edu/gri\\_mech/](http://www.me.berkeley.edu/gri_mech/).
- [124] M. D. Smooke. *Reduced Kinetic Mechanisms and Asymptotic Approximations for Methane-Air Flames*. Lecture Notes in Physics. Springer-Verlag, Berlin, 1991.
- [125] H.S. Soyhan, F. Mauss, and C. Sorousbay. Chemical Kinetic Modeling of Combustion in Internal Combustion Engines Using Reduced Chemistry. *Combust. Sci. Tech.*, 174:73–91, 2002.

- [126] Y.F. Tham and J.Y. Chen. Recent Advancement on Automatic Generation of Simplified Mechanisms, Western States Section of the Combustion Institute, 2002.
- [127] A. Tomlin, T. Turanyi, and M. Pilling. *Mathematical Tools for Construction, Investigation and Reduction of Combustion Mechanisms*. Elsevier, Amsterdam, 1998.
- [128] A. S. Tomlin, G. Li, H. Rabitz, and J. Tóth. The Effect of Lumping and Expanding on Kinetic Differential Equations. *SIAM J. App. Math.*, 57:1531–1556, 1997.
- [129] W. Tsang, Chair and J. W. Hudgens, Editor. Workshop on Combustion Simulation Databases for Real Transportation Fuels, National Institute of Standards and Technology, Gaithersburg, MD, September 2003.
- [130] T. Turányi. Reduction of Large Reaction Mechanisms. *New J. Chem.*, 14:795–803, 1990.
- [131] T. Turányi. Sensitivity Analysis of Complex Kinetic Systems: Tools and Applications. *J. Math. Chem.*, 5:203–248, 1990.
- [132] T. Turányi, A. S. Tomlin, and M. J. Pilling. On the Error of the Quasi-Steady State Approximation. *J. Phys. Chem.*, 97:163–172, 1993.
- [133] C. M. Vagelopoulos and F. N. Egolfopoulos. Direct Experimental Determination of Laminar Flame Speeds. *Proc. Combust. Inst.*, 27:513–520, 1998.
- [134] C.N. Vagelopoulos and F.N. Egolfopoulos. Direct Experimental Determination of Laminar Flame Speeds. In *Twenty-seventh Symposium (International) on Combustion*, pages 513–519, Pittsburgh, PA, 1998.
- [135] S. Vajda, P. Valko, and T. Turányi. Principal Component Analysis of Kinetic Models. *Int. J. Chem. Kin.*, 17:55–81, 1985.
- [136] M. Valorani, F. Creta, F. Donato, , H.N. Najm, and D.A. Goussis. A CSP-Based Skeletal Mechanism Generation Procedure: Autoignition and Premixed Laminar Flames in

- n*-Heptane/Air Mixtures. European Conference on Computational Fluid Dynamics, ECCOMAS CFD, 2006.
- [137] M. Valorani, F. Creta, F. Donato, H.N. Najm, and D.A. Goussis. Skeletal Mechanism Generation and Analysis for *n*-Heptane With CSP. *Proc. Combust. Inst.*, 31:483–490, 2006.
- [138] M. Valorani, F. Creta, D.A. Goussis, J.C. Lee, and H.N. Najm. An Automatic Procedure for the Simplification of Chemical Kinetic Mechanisms Based on CSP. *Combust. Flame*, 146:29–51, 2006.
- [139] M. Valorani, F. Creta, H.N. Najm, and D.A. Goussis. Chemical Kinetics Mechanism Simplification via CSP. *Comp. Fluid and Solid Mech.*, pages 900–904, 2005.
- [140] M. Valorani, D. A. Goussis, F. Creta, and H. N. Najm. Higher Order Corrections in the Approximation of Low-Dimensional Manifolds and the Construction of Simplified Problems With the CSP Method. *J. Comp. Phy.*, 209:754–786, 2005.
- [141] A. Van Maaren, D. S. Thung, and L. P. H. De Goey. Measurement of Flame Temperature and Adiabatic Burning Velocity of Methane/Air Mixtures. *Combust. Sci. Tech.*, 96:327–344, 1994.
- [142] S. S. Vasu, D. F. Davidson, and R. K. Hanson. Jet fuel Ignition Delay Times: Shock Tube Experiments over Wide Conditions and Surrogate Model Predictions. *Combust. Flame*, 152:125–143, 2008.
- [143] S. S. Vasu, D. F. Davidson, Z. Hong, V. Vasudevan, and R. K. Hanson. *n*-Dodecane Oxidation at High Pressures: Measurements of Ignition Delay Times and OH Concentration Time Histories. *Proc. Combust. Inst.*, 32, 2008, submitted.
- [144] M. L. Vermeersch, T. J. Held, Y. Stein, and F. L. Dryer. Auto-Ignition Chemistry Studies of *n*-Butane in a Variable Pressure Flow Reactor, SAE 912316, 1991.

- [145] A. Violi, S. Yan, E. G. Eddings, A. F. Sarofim, S. Granata, T. Faravelli, and E. Ranzi. Experimental Formulation and Kinetic Model for JP-8 Surrogate Mixtures. *Combust. Sci. Tech.*, 174:399–417, 2002.
- [146] H. Wang and M. Frenklach. Detailed Reduction of Reaction Mechanisms for Flame Modeling. *Combust. Flame*, 87:365–370, 1991.
- [147] J. Wei and J. C. W. Kuo. Lumping Analysis in Monomolecular Reaction Systems. Analysis of the Exactly Lumpable System. *Ind. Eng. Chem. Fund.*, 8:114–123, 1969.
- [148] F. A. Williams. *Combustion Theory*. Benjamin/Cummins, Menlo Park, CA, 1985.
- [149] L. E. Withehouse, A. S. Tomlin, and M. J. Pilling. Systematic Lumping of Complex Tropospheric Chemical Mechanisms Using a Time-Scale Based Approach. *Atmos. Chem. Phys. Discuss.*, 4:3785–3834, 2004.
- [150] C. P. Wood, V. G. McDonell, R. A. Smith, and G. S. Samuelsen. Development and Application of a Surrogate Distillate Fuel. *J. Prop.*, 5:399–405, 1989.
- [151] H. Wang X.Q. You, F.N. Egolfopoulos. Detailed and Simplified Kinetic Models of n-Dodecane Oxidation : The role of Fuel Cracking in Aliphatic Hydrocarbon Combustion. *Proc. Combust. Inst.*, 32, 2008, submitted.
- [152] S. Yan, E. G. Eddings, A. B. Palotas, R. J. Pugmire, and A. F. Sarofim. Prediction of Sooting Tendency for Hydrocarbon Liquids in Diffusion Flames. *Energy and Fuels*, 19:2408–2415, 2005.
- [153] Y. Yang, A. L. Boehman, and R.J. Santoro. A Study of Jet Fuel Sooting Tendency using the Threshold Soot Index (TSI) Model. *Combust. Flame*, 149:191–205, 2007.
- [154] S. Zeppieri, K. Brezinsky, and I. Glassman. Pyrolysis Studies of Methylcyclohexane and Oxidation Studies of Methylcyclohexane and Methylcyclohexane/Toluene Blends. *Combust. Flame*, 108:266–286, 1997.

- [155] S. P. Zeppieri, S. D. Klotz, and F. L. Dryer. Modeling Concepts for Larger Carbon Number Alkanes: A Partially Reduced Skeletal Mechanism for *n*-Decane Oxidation and Pyrolysis. *Proc. Combust. Inst.*, 28:1587–1595, 2000.
- [156] R. H. Zhang, E. G. Eddings, and A. F. Sarofim. Criteria for selection of components for surrogates of natural gas and transportation fuels. *Proc. Combust. Inst.*, 31:401–409, 2007.
- [157] Z. Zhao, M. Chaos, A. Kazakov, P. Golkulakrishnan, M. Angioletti, and F. Dryer. Fuel Chemistry Models for Simulating Gasoline Kinetics in Internal Combustion Engines, 31<sup>st</sup> International Symposium on Combustion, Work in progress Poster No. 2C-27, Heidelberg, Germany, 2006.
- [158] X. L. Zheng, H. Y. Sun, and C. K. Law. Thermochemical and Kinetic Analyses on Oxidation of Isobutenyl Radical and 2-Hydroperoxymethyl-2-propenyl Radical. *J. Phys. Chem. A*, 109:9044–9053, 2005.
- [159] I. G. Zsély and T. Turányi. The Influence of Thermal Coupling and Diffusion on the Importance of Reactions: The Case Study of HydrogenAir Combustion. *Phys. Chem. Chem. Phys.*, 5:3622–3631, 2003.